Dynamics of heton-like vortices

Vladimir Gryanik, Mikhail Sokolovskiy, Jacques Verron

V. M. GRYANIK

A. M. Oboukhov Institute of Atmospheric Physics,
Russian Academy of Sciences,
Pyzhevskii per. 3, Moscow 109017 Russia

Alfred Wegener Institute for Polar and Marine Research,
Postfach 12 0161, D-27515 Bremerhaven, Germany,

E-mail: vgryanik@awi-bremerhaven.de

M. A. SOKOLOVSKIY

Water Problems Institute,
Russian Academy of Sciences,
3 Gubkina str., Moscow 117735, Russia

Institute of Mathematics and Mechanics,
Ural Branch of the Russian Academy of Sciences,
16, S. Kovalevskaja str., Ekaterinburg 620219, Russia

E-mail: sokol@aqua.laser.ru

J. VERRON

Laboratoire des Ecoulements Géophysiques et Industriels, CNRS,
BP 53 38041, Grenoble Cedex 9, France
E-mail: jacques.verron@inpg.fr

DYNAMICS OF HETON-LIKE VORTICES

Studies of the properties of vortex motions in a stably stratified and fast rotating fluid that can be described by the equation for the evolution of a potential vortex in the quasi-geostrophic approximation are reviewed. Special attention is paid to the vortices with zero total intensity (the so-called hetons). The problems considered include self-motion of discrete hetons, the stability of a solitary distributed heton, and the interaction between two finite-core hetons. New solutions to the problems of three or more discrete vortices with a heton structure are proposed. The existence of chaotic regimes is revealed. The range of applications of the heton theory and the prospects for its future application, particularly in respect, to the analysis of the dynamic stage in the development of deep ocean convection, are discussed.

In memory of Professor
Vadim Fedorovich Kozlov

1. Introduction

The theory of the vortex motion of an ideal incompressible fluid [11], [120], [113], [127], [148], [174], going back to the classical works of Helmholtz, Gröbli, Kirchhoff, Rankin, Greenhill, Taylor, Poincaré, (see [20], [168], [8]), has developed mainly due to the need to understand the properties of atmospheric cyclones and anticyclones. Indeed, the simplest two-dimensional hydrodynamic models of discrete vortices provide some insight into the type of interaction occurring between elementary vortices and into the structure of the velocity field they induce. However, many effects intrinsic to motion (especially, vortex motion) in the atmosphere or ocean cannot be explained without allowance being made for the rotation of the medium as a whole and the heterogeneity (stratification) of the density field that forms under the effect of gravity. The solution of some important hydrodynamic problems of a planetary nature has become possible with the development of *Geophysical Hydrodynamics* (*GH*) [102], [151], [167], [176] dealing with this class of problem (an independent branch of hydromechanics which has developed over the last three decades), the establishment of domains of flow parameters dominated

Mathematics Subject Classification: 76U05, 76B47, 76E20
Key words and phrases: heton, point vortex, finite-core vortex, two-layer fluid

by vortex motions [18], [19], [74], [32], [41], [99], and the generalization of methods of Hamiltonian dynamics to the description of geophysical processes [20], [67], [102], [176]. Thus, within the context of the quasi-geostrophic approximation, which is valid for fast rotating stably stratified fluids [102], [167], Gryanik and co-authors successively created the theories of discrete vortices for a two-layer fluid [71], a stratified medium comprising an arbitrary number of uniform-density layers [86], [87], [88], and a continuously stratified fluid [72], [73]. The contour dynamics method (CDM) has been developed by Kozlov et al. [119] for the description of finite-size vortices in a two-layer fluid and generalized later for three layers [183], and for the case of continuous stratification [115], [118]. These works formed the basis for new studies, the results of which are partially reflected in this publication.

This paper focuses mainly (sections 3–6) on the analysis of the dynamics of both discrete and distributed baroclinic vortices with zero total intensity — *hetons*. Unlike classical (barotropic) vortices in an ideal fluid, the baroclinic vortices possess a reserve of not only kinetic but also available potential (thermal) energy. As shown in [71], the baroclinic nature of vortices radically changes both the structure of the velocity fields they induce and the character of vortex interaction. Structures comprising two vortices with zero total intensity feature an important *self-motion* property (a two-layer pair moving without changing in shape or intensity [71]). In particular, in the case of two point vortices concentrated in different layers of a two-layer fluid and having equal intensities with opposite signs, each induces a rectilinear and uniform motion in the other.

The notion of *heton* was introduced by Hogg and Stommel [96] with the aim of emphasizing the ability of a baroclinic vortex pair to transfer heat. The word '*heton*' was derived from '*heat*'. Indeed, when the geostrophic and hydrostatic approximations [102], [167], conventional for GH, are valid, any vortex of the top (bottom) layer, which has negative (positive) intensity, induces a downward local distortion of the interface between the layers. When the vorticity sign of each vortex changes, the sign of the curvature of the interface also changes. Since, under conditions of stable stratification, the bottom layer should be denser and (under the assumption of isopycnicity) colder, the integral amount of heat in the domain containing vortices of this type will clearly be anomalous to that in any domain with the same volume. It is therefore obvious that the motion of hetons consisting of combinations of oppositely rotating vortices has a greater effect on the redistribution of heat (heat and salts, in the case of the ocean) than the motion of any other vortex structures. The notion of 'heton' is also used to refer to vortices with finite horizontal dimensions (vortical patches, i. e., domains with constant values of potential vorticity Π_1 and Π_2 in the top and bottom layer, respectively). When the centres of the vortex patches in different layers are vertically aligned, the heton is said to have a *vertical* axis, otherwise the axis is said to be *tilted* (Fig. 1).

Hetons can be generated in a laboratory by sources and sinks of mass [69], [70], by mechanically and locally spinning the top-layer fluid [64], [200], [201], or by heat or buoyancy sources [58], [60], [92]. Such vortices naturally form when baroclinic currents, associated with the phenomenon of deep convection in the ocean, become unstable [1], [26], [27], [28], [30], [42], [43], [44], [47], [48], [49], [50], [55], [79], [84], [111], [112], [126], [128], [129], [130], [136], [131], [132], [133], [135], [141], [143], [160], [193], [194], [206], [207], [218]. The heton idealization is also used when analysing the dynamics of tropical cyclones and hurricanes in the atmosphere [150], [149], [166], [199], [61], [170], surface temperature anomalies [37], [38], [39], [40], Mediterranean intra-thermocline lenses (meddy) [98], [164], [198] in the ocean, and instability of boundary currents [177].

Sections 3–4 focus on studying hetons in a two-layer medium (with constant density values in equal-thickness layers), since the two-layer model [102], [167] is known to exhibit the major features of the large-scale (mesoscale)[1] dynamics of the atmosphere and ocean. Section 5 presents generalizations of the model to the cases of multi-layer (mostly three-layer) and continuously stratified media. Section 6 is devoted to the analysis of specific features, the degree of universality of the heton theory, and its range of its applications. Consideration is given in particular to its future application in describing the dynamic phase of the development of deep ocean convection and in contributing to the solution of the parameterization problem of vortical heat transport in atmospheric and oceanographical mesoscale processes.

The present paper is a translation of an extended version of the paper published in Russian [85].

[1] According to meteorological and oceanographical terminology.

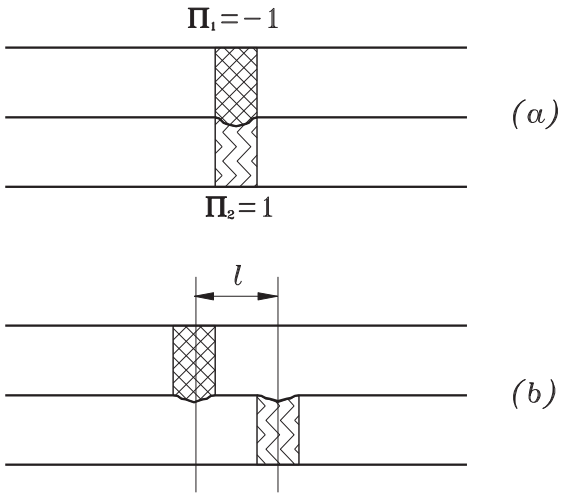

Fig. 1. Schematic representation of a distributed heton with a vertical *(a)* and a tilted axis *(b)*.

2. Basic model equations

We consider the quasi-2D motion of a two-layer ideal, incompressible fluid rotating with an angular velocity of Ω and having constant densities of ρ_1, ρ_2 ($\rho_1 \leqslant \rho_2$), and undisturbed depths of h_1 and h_2 for the top and bottom layers, respectively. In the case where adiabatic motion takes place in the absence of external forces and under conditions allowing the quasi-static and Boussinesq approximation, the asymptotic theory [102], [167], [67] is widely used. This theory is based on the conservation law of the quasi-geostrophic potential vorticity Π_j:

$$\frac{D_j \Pi_j}{Dt} = 0, \tag{2.1}$$

where

$$\Pi_j = \nabla^2 p_j + F_j \left(p_{3-j} - p_j\right), \qquad j = 1, 2. \tag{2.2}$$

Here $D_j()/Dt \equiv \dot{()} + u_j \left(\partial()/\partial x\right) + v_j \left(\partial()/\partial y\right)$ and $\nabla^2() \equiv \partial^2()/\partial x^2 + \partial^2()/\partial y^2$ are two-dimensional operators of the total derivative with respect to time and the Laplacian operator; a dot above a variable means a partial derivative with respect to time; u_j, v_j are components of the velocity vector of fluid particles of the jth layer along the axes x and y of the orthogonal coordinate system, respectively; $F_j = 4\rho_* \Omega^2 D^2 h_j / g(h_1 + h_2)\Delta\rho$, ρ_* — is the mean density, $\Delta\rho = \rho_2 - \rho_1$, D — is a characteristic horizontal linear scale, g is the acceleration of gravity, p_1 and p_2 are anomalies (with respect to the equilibrium hydrostatic state) of hydrodynamic pressure in the layers, related to the velocity components by geostrophic relationships

$$u_j = -\frac{\partial p_j}{\partial y}, \qquad v_j = \frac{\partial p_j}{\partial x}. \tag{2.3}$$

In (2.3) and hereafter it is assumed, without special mention, that subscript j takes on values 1 and 2. From (2.3) it follows that introducing denotation $J\left(z, w\right) \equiv \left(\partial z/\partial x\right)\left(\partial w/\partial y\right) - \left(\partial z/\partial y\right)\left(\partial w/\partial x\right)$ (Poisson brackets for the Jacobian) allows equations (2.1) to be written as

$$\dot{\Pi}_j + J\left(p_j, \Pi_j\right) = 0. \tag{2.4}$$

The structure of equations (2.4) suggests an analogy with the equation of a vortex in classical two-dimensional hydrodynamics; here the potential vortex corresponds to the vorticity[2]. Equa-

[2]The analogy here and below is understood as the formal identity of the equations for the evolution of vorticity and potential vorticity. The physical essence of the problems is different, as can be seen in the difference between the equations relating stream function and pressure in the classical two-dimensional hydrodynamics and in quasi-geostrophic GH-approximation.

tions (2.1)–(2.4) are given in a dimensionless form. Conversion to dimensional variables can be made by using the relationships

$$(x', y') = D\,(x, y)\,; \quad (u', v') = D\,(u, v)\,; \quad t' = (D/U)\,t; \quad \Pi'_j = (U/D)\,\Pi_j;$$
$$p'_1 = 2\Omega\rho_* UD\tilde{p_1} - \rho_1 gz; \quad p'_2 = 2\Omega\rho_* UD\tilde{p_2} - \rho_1 gh_1 - \rho_2 g(z - h_1), \tag{2.5}$$

where $\tilde{p}_j$ is the complete (dimensionless) pressure in the jth layer, primed letters are dimensional values, capital letters, as before, denote the scales of the respective variables, and variable z is measured from the undisturbed surface of the upper layer toward the gravity centre. Equations (2.1)–(2.3) were derived based on the assumption that $U/(2\Omega D) = \varepsilon \ll 1$ and $(p_2^{'} - p_1^{'})/[g\Delta\rho(h_1 + h_2)] = \varepsilon$.

Let as assume that the potential vorticity, which is an unknown function, is nonzero only in a multiply connected two-layer domain $S = S_1 \cup S_2$ (subscripts indicate layer numbers). Now the inversion of operators in the reduced (after separation of variables) right-hand parts of equations (2.2) yields formal integral relationships for pressure values in the layers as follows:

$$p_j = \iint\limits_{S_j} \left[h_j G(r) + h_{3-j} G_0(r)\right] \Pi_j\left(x', y', t\right) dx'dy' +$$
$$\iint\limits_{S_{3-j}} h_{3-j}\left[G(r) - G_0(r)\right] \Pi_{3-j}\left(x', y', t\right) dx'dy' \tag{2.6}$$

where $r = \sqrt{(x - x')^2 + (y - y')^2}$, $G(r) = (1/2\pi)\ln\gamma_* r$, $\gamma_* = 1/L_{reg}$ (L_{reg} is a regularizing scale of length)[3], $G_0(r) = -(1/2\pi)K_0(\gamma r)$, $K_n(x)$ is a modified Bessel function of the nth order, and

$$\gamma = \sqrt{F_j / h_{3-j}} = D/\lambda, \tag{2.7}$$

where $\lambda = \sqrt{4\,g\,\Delta\rho\,h_1\,h_2\,/\rho_*\,\Omega^2\,(h_1 + h_2)}$ — is the Rossby scale [167].

Integral invariants can be readily seen to exist (total potential vorticity, components of momentum, and angular momentum):

$$Q = \sum_{j=1}^{2} h_j \iint\limits_{S_j} \Pi_j\, dx'dy', \qquad P_x = \sum_{j=1}^{2} h_j \iint\limits_{S_j} x'\Pi_j\, dx'dy',$$
$$P_y = \sum_{j=1}^{2} h_j \iint\limits_{S_j} y'\Pi_j\, dx'dy', \qquad M = \sum_{j=1}^{2} h_j \iint\limits_{S_j} \left[(x')^2 + (y')^2\right]\Pi_j\, dx'dy'. \tag{2.8}$$

Expressions (2.6) can be simplified based on the assumption that functions Π_j are piecewise constant. Thus, let us assume that $\Pi_j = \Pi_j^1 \cup \Pi_j^2 \cup \ldots \cup \Pi_j^{N_j}$, where all Π_j^α are constants on finite supports S_j^α: $S_j = S_j^1 \cup S_j^2 \cup \ldots \cup S_j^{N_j}$, $j = 1, 2$; $\alpha = 1, 2, \ldots, N_j$. Here N_j is the number of vortices in the jth layer. Hereafter, Greek letters are used to number vortices within each layer. Now, instead of (2.6) we have

$$p_j(x, y) = \sum_{\alpha=1}^{N_j} \Pi_j^\alpha \iint\limits_{S_j^\alpha} \left[h_j G(r) + h_{3-j} G_0(r)\right]\, dx'dy' +$$
$$\sum_{\alpha=1}^{N_{3-j}} h_{3-j}\Pi_{3-j}^\alpha \iint\limits_{S_{3-j}^\alpha} \left[G(r) - G_0(r)\right]\, dx'dy'. \tag{2.9}$$

[3]For example, in the problems of vortex dynamics on a sphere, L_{reg} is proportional to its radius [18], [19]; in problems taking into account the effects of the two-dimensional compressibility of the medium or free surface, it is proportional to the Oboukhov–Rossby scale [71].

Expressions (2.8) can be simplified in a similar manner. Equations (2.9) show that when constants Π_j^α are known, the pressure anomalies (and, according to (2.3), the velocities in the layers as well) are completely determined by only the geometry of the evolving domains $S_j^\alpha(x,y,t)$. This fact forms the basis of the contour dynamics method [220], developed for the case of a two-layer fluid in [119]. Thus, the Stokes theorem allows the passage in (2.9) from surface integrals to contour integrals:

$$p_j(x,y) = \sum_{\alpha=1}^{N_j} h_j \Pi_j^\alpha \oint\limits_{C_j^\alpha} w \left[W(r) + \frac{h_{3-j}}{h_j} W_0(r) \right] d\nu +$$

$$+ \sum_{\alpha=1}^{N_{3-j}} h_{3-j} \Pi_{3-j}^\alpha \oint\limits_{C_{3-j}^\alpha} w \left[W(r) - W_0(r) \right] d\nu. \tag{2.10}$$

Here, C_j^α are the contours of domains S_j^α, and notations

$$w = \frac{(x'-x)(\partial y'/\partial \nu) - (y'-y)(\partial x'/\partial \nu)}{r^2}, \quad W = \frac{r^2}{4\pi}\left(\ln \gamma_* r - \frac{1}{2} \right),$$

$$W_0 = \frac{1}{2\pi\gamma^2} \left[\gamma r K_1(\gamma r) - 1 \right]$$

are introduced; here ν is a linear parameter measured counterclockwise along each contour C_j^α.

Formulas (2.3) and (2.10) can also be used to express the equations for the velocity components of fluid particles in terms of contour integrals. Without going into the details of the algorithm, we note that, within the context of CDM, the problem is reduced to the numerical solution of equations of motion of marker particles belonging to contours C_j^α of domains S_j^α.

The case of discrete vortices with intensities of κ_j^α will be obtained as the limit

$$\lim_{\substack{S_j^\alpha \to 0 \\ \Pi_j^\alpha \to \infty}} \Pi_j^\alpha \, S_j^\alpha = \kappa_j^\alpha,$$

where S_j^α is an undisturbed circular domain. Now

$$\Pi_j^\alpha = \kappa_j^\alpha \delta\big(x - x_j^\alpha\big)\, \delta\big(y - y_j^\alpha\big), \tag{2.11}$$

and (2.9) transforms to

$$p_j\,(x,y) = \frac{h_j}{2\pi} \left\{ \sum_{\alpha=1}^{N_j} \kappa_j^\alpha \left[\ln \gamma_* r - \frac{h_{3-j}}{h_j} K_0(\gamma r) \right] + \sum_{\alpha=1}^{N_j} \frac{h_{3-j}}{h_j} \kappa_{3-j}^\alpha \left[\ln \gamma_* r + K_0(\gamma r) \right] \right\}, \tag{2.12}$$

where $r = \sqrt{\big(x - x_j^\alpha\big)^2 + \big(y - y_j^\alpha\big)^2}$; $\alpha = 1, 2, \ldots, N_j$; $j = 1, 2$, and, since now we have only one linear scale (Rossby radius), we have to take $D = 1$ in (2.7). From (2.3) and (2.12), we can obtain the equations of motion for the vortices:

$$\dot{x}_j^\alpha = -\frac{h_j}{2\pi} \Bigg\{ \sum_{\substack{\beta=1 \\ \beta \neq \alpha}}^{N_j} \kappa_j^\alpha \frac{y_j^\alpha - y_j^\beta}{\left(r_{jj}^{\alpha\beta} \right)^2} \left[1 + \frac{h_{3-j}}{h_j} \gamma r_{jj}^{\alpha\beta} K_1\left(\gamma r_{jj}^{\alpha\beta} \right) \right] +$$

$$+ \sum_{\beta=1}^{N_{3-j}} \kappa_{3-j}^\alpha \frac{h_{3-j}}{h_j} \frac{y_j^\alpha - y_{3-j}^\beta}{\left(r_{j(3-j)}^{\alpha\beta} \right)^2} \left[1 - \gamma r_{j(3-j)}^{\alpha\beta} K_1\left(\gamma r_{j(3-j)}^{\alpha\beta} \right) \right] \Bigg\}, \tag{2.13}$$

$$\dot{y}_j^\alpha = \frac{h_j}{2\pi}\left\{\sum_{\substack{\beta=1\\ \beta\neq\alpha}}^{N_j}\kappa_j^\alpha\frac{x_j^\alpha - x_j^\beta}{\left(r_{jj}^{\alpha\beta}\right)^2}\left[1+\frac{h_{3-j}}{h_j}\gamma r_{jj}^{\alpha\beta}K_1\left(\gamma r_{jj}^{\alpha\beta}\right)\right]+\right.$$

$$\left.+\sum_{\beta=1}^{N_{3-j}}\kappa_{3-j}^\alpha\frac{h_{3-j}}{h_j}\frac{x_j^\alpha - x_{3-j}^\beta}{\left(r_{j(3-j)}^{\alpha\beta}\right)^2}\left[1-\gamma r_{j(3-j)}^{\alpha\beta}K_1\left(\gamma r_{j(3-j)}^{\alpha\beta}\right)\right]\right\}. \tag{2.14}$$

Here, $r_{ij}^{\alpha\beta}=\sqrt{\left(x_i^\alpha-x_j^\beta\right)^2+\left(y_i^\alpha-y_j^\beta\right)^2}$.

Equations for integral invariants (2.8) take the form

$$Q=\sum_{j=1}^{2}h_j\sum_{\alpha=1}^{N_j}\kappa_j^\alpha,\qquad P_x=\sum_{j=1}^{2}h_j\sum_{\alpha=1}^{N_j}x_j^\alpha\kappa_j^\alpha,$$

$$P_y=\sum_{j=1}^{2}h_j\sum_{\alpha=1}^{N_j}y_j^\alpha\kappa_j^\alpha,\quad M=\sum_{j=1}^{2}h_j\sum_{\alpha=1}^{N_j}\left[\left(x_j^\alpha\right)^2+\left(y_j^\alpha\right)^2\right]\kappa_j^\alpha.$$

System (2.13)–(2.14) can be rewritten in the Hamiltonian form

$$\dot{q}_j^\alpha=\frac{\partial\mathcal{H}}{\partial p_j^\alpha}\equiv J\left(q_j^\alpha,\mathcal{H}\right),\qquad \dot{p}_j^\alpha=-\frac{\partial\mathcal{H}}{\partial q_j^\alpha}\equiv J\left(p_j^\alpha,\mathcal{H}\right), \tag{2.15}$$

where $q_j^\alpha = x_j^\alpha$ — are generalized coordinates, $p_j^\alpha = y_j^\alpha\kappa_j^\alpha/2$ are generalized momenta, and the Hamiltonian

$$\mathcal{H}=-\frac{1}{2\pi}\sum_{j=1}^{2}h_j\left\{\sum_{\substack{\alpha,\beta=1\\ \alpha\neq\beta}}^{N_j}\kappa_j^\alpha\kappa_j^\beta\left[\ln\gamma_* r_{jj}^{\alpha\beta}-\frac{h_{3-j}}{h_j}K_0\left(\gamma r_{jj}^{\alpha\beta}\right)\right]+\right.$$

$$\left.+\sum_{\alpha,\,\beta=1}^{N_j,\,N_{3-j}}\frac{h_{3-j}}{h_j}\kappa_j^\alpha\kappa_{3-j}^\beta\left[\ln\gamma_* r_{j(3-j)}^{\alpha\beta}+K_0\left(\gamma r_{j(3-j)}^{\alpha\beta}\right)\right]\right\}, \tag{2.16}$$

coincides with the energy of interaction of the vortices.

Problems for both discrete and finite-core two-layer vortices with equal layer thicknesses $h_1 = = h_2 = 1/2$ are considered in (Sections 3, 4) below, and the effects of the non-equivalence of the layers are discussed in Section 5.

3. Dynamics of discrete hetons

Let us denote the total number of vortices by N (i. e., $N = N_1 + N_2$). It can be readily shown that invariants M, H, and the combination $(P_x^2 + P_y^2)$ are pairwise involutory. Hence, in the case of three vortices in a two-layer fluid, as in the case of a homogeneous medium [20], [120], [2], [4], [5], [7], [22], [23], [24], [25], the problem will always have a regular solution. In a barotropic fluid where $N = 4$, the problem is non-integrable in the general case [225], [120], [148], [158], [159]. As shown in [20], [9], [56], at

$$Q = P_x = P_y = 0 \tag{3.1}$$

the problem can be reduced to one of three vortices. Hence the problem of four vortices under conditions (3.1) is always integrable. This result does not depend on the specific form of the Hamiltonian and hence holds for the two-layer case as well. In contrast to the case of a homogeneous fluid, where

a large number of special cases of integrability of the vortex problem are known at $N > 3$ [20], [120], [148], [147], few results are available for layered media [84], [96], [97], [186], [187].

Some results from studying the motion of four vortices in a two-layer fluid are given below in 3.3.

Let us now consider certain problems regarding the motion of two-layer heton-type vortices (i. e., at $Q = 0$).

3.1. The case of two vortices: $N = 2$

This class of motion has been examined in numerous studies [71], [96], [186], [187], [219]. The possible variants include a) $N_1 = 2$, $N_2 = 0$ or $N_1 = 0$, $N_2 = 2$,[4] and b) $N_1 = N_2 = 1$. Equations (2.13)–(2.14) yield:

a)

$$u_1^1 = -\frac{\kappa_1^2}{4\pi}\frac{y_1^1 - y_1^2}{\left(r_{11}^{12}\right)^2}\left[1 + \gamma r_{11}^{12} K_1\left(\gamma r_{11}^{12}\right)\right], \qquad u_1^2 = -\frac{\kappa_1^1}{4\pi}\frac{y_1^2 - y_1^1}{\left(r_{11}^{12}\right)^2}\left[1 + \gamma r_{11}^{12} K_1\left(\gamma r_{11}^{12}\right)\right];$$

$$v_1^1 = \frac{\kappa_1^2}{4\pi}\frac{x_1^1 - x_1^2}{\left(r_{11}^{12}\right)^2}\left[1 + \gamma r_{11}^{12} K_1\left(\gamma r_{11}^{12}\right)\right], \qquad v_1^2 = \frac{\kappa_1^1}{4\pi}\frac{x_1^2 - x_1^1}{\left(r_{11}^{12}\right)^2}\left[1 + \gamma r_{11}^{12} K_1\left(\gamma r_{11}^{12}\right)\right]; \tag{3.2}$$

b)

$$u_1^1 = -\frac{\kappa_2^1}{4\pi}\frac{y_1^1 - y_2^1}{\left(r_{12}^{11}\right)^2}\left[1 - \gamma r_{12}^{11} K_1\left(\gamma r_{12}^{11}\right)\right], \qquad u_2^1 = -\frac{\kappa_1^1}{4\pi}\frac{y_2^1 - y_1^1}{\left(r_{12}^{11}\right)^2}\left[1 - \gamma r_{12}^{11} K_1\left(\gamma r_{12}^{11}\right)\right];$$

$$v_1^1 = \frac{\kappa_2^1}{4\pi}\frac{x_1^1 - x_2^1}{\left(r_{12}^{11}\right)^2}\left[1 - \gamma r_{12}^{11} K_1\left(\gamma r_{12}^{11}\right)\right], \qquad v_2^1 = \frac{\kappa_1^1}{4\pi}\frac{x_2^1 - x_1^1}{\left(r_{12}^{11}\right)^2}\left[1 - \gamma r_{12}^{11} K_1\left(\gamma r_{12}^{11}\right)\right], \tag{3.3}$$

respectively. In the general case, the vortices execute circular motions with angular velocities of

a)

$$\omega = \frac{\kappa_1^1 + \kappa_1^2}{4\pi\left(r_{11}^{12}\right)^2}\left[1 + \gamma r_{11}^{12} K_1\left(\gamma r_{11}^{12}\right)\right], \tag{3.4}$$

b)

$$\omega = \frac{\kappa_1^1 + \kappa_2^1}{4\pi\left(r_{12}^{11}\right)^2}\left[1 - \gamma r_{12}^{11} K_1\left(\gamma r_{12}^{11}\right)\right] \tag{3.5}$$

relative to the centres of vorticity with coordinates

a)

$$\left(x_c,\, y_c\right) = \frac{\kappa_1^1\left(x_1^1,\, y_1^1\right) + \kappa_1^2\left(x_1^2,\, y_1^2\right)}{\kappa_1^1 + \kappa_1^2}, \tag{3.6}$$

b)

$$\left(x_c,\, y_c\right) = \frac{\kappa_1^1\left(x_1^1,\, y_1^1\right) + \kappa_2^1\left(x_2^1,\, y_2^1\right)}{\kappa_1^1 + \kappa_2^1}. \tag{3.7}$$

[4] Formulas (2.13) and (2.14) show that, under the above assumption that the layers are of equal thickness, these variants yield identical results, which implies that only one may be considered, e.g., the first.

A combination of two vortices belonging to different layers and rotating (3.5) around a centre (3.7) at $\kappa_1^1 + \kappa_2^1 \neq 0$ will be referred to as a *two-tier top.*

Formulas (3.2)–(3.7) indicate a specific feature of the two-layer model: *vortices in the same layer and vortices in different layers interact according to different laws* [71]. This can be seen most distinctly in the cases of one-layer and two-layer vortex pairs, when we have $\kappa_1^1 = -\kappa_1^2 \equiv \kappa$ in case a) and $\kappa_1^1 = -\kappa_2^1 \equiv \kappa$ in case b), and clearly the centre of vorticity lies at the infinite point, and angular velocities (3.4) and (3.5) are zero.

Suppose that at the initial moment of time, both vortices lie on the x-axis at a distance of l from one another. Now formulas (3.2)–(3.3) yield equations for the velocities of vortex pairs as follows:
a)

$$u_1^1 = u_1^2 = 0;$$
$$v_1^1 = v_1^2 = \pm\frac{\gamma\kappa}{4\pi L}\left[1 + LK_1(L)\right] \equiv \pm\frac{\gamma\kappa}{4\pi} f_1(L); \tag{3.8}$$

b)

$$u_1^1 = u_2^1 = 0;$$
$$v_1^1 = v_2^1 = \pm\frac{\gamma\kappa}{4\pi L}\left[1 - LK_1(L)\right] \equiv \pm\frac{\gamma\kappa}{4\pi} f_2(L), \tag{3.9}$$

where $L = \gamma l$. Here at $\kappa > 0$, the upper (lower) sign refers to the case where the vortex with positive intensity occupies the left (right) location; at $\kappa < 0$, the pair of vortices inverse their direction of motion.

Formulas (3.8)–(3.9) and figure 2 illustrate the behaviour of functions $f_1(L)$ and $f_2(L)$ (note how they are different from function $f(L) = 1/L$). It should be mentioned that heton velocity (3.9) exhibits a nonmonotonic dependence on the distance between vortices, and

$$f_2(L) \sim -L\ln L \to 0 \quad \text{at} \quad L \ll 1, \qquad f_2(L) \sim 1/L \to 0 \quad \text{at} \quad L \gg 1$$

and $f_2(L^*) = \max f_2(L)$, where $L^* = 1.114$ is the solution of the equation

$$f_2'(L) = K_0(L) + \frac{1}{L}K_1(L) - \frac{1}{L^2} = 0.$$

Thus, a heton that has a *vertical axis* is always immobile, while a heton with a *tilted axis* moves translationally with a velocity attaining its maximum at $l = L^*/\gamma$.

3.2. The case of three vortices: $N = 3$

Let us consider variants 1) $N_1 = 3$ and 2) $N_1 = 1$, $N_2 = 2$ (the cases of $N_2 = 3$ and $N_1 = 2$, $N_2 = 1$, respectively, are equivalent to these due to symmetry). Equations (2.13), (2.14) yield:
1)

$$u_1^\alpha = -\frac{1}{4\pi}\sum_{\substack{\beta=1\\ \beta\neq\alpha}}^{3} \kappa_1^\beta \frac{y_1^\alpha - y_1^\beta}{\left(r_{11}^{\alpha\beta}\right)^2}\left[1 + \gamma r_{11}^{\alpha\beta} K_1\left(\gamma r_{11}^{\alpha\beta}\right)\right], \tag{3.10}$$

$$v_1^\alpha = \frac{1}{4\pi}\sum_{\substack{\beta=1\\ \beta\neq\alpha}}^{3} \kappa_1^\beta \frac{x_1^\alpha - x_1^\beta}{\left(r_{11}^{\alpha\beta}\right)^2}\left[1 + \gamma r_{11}^{\alpha\beta} K_1\left(\gamma r_{11}^{\alpha\beta}\right)\right], \tag{3.11}$$

$\alpha = 1, 2, 3.$

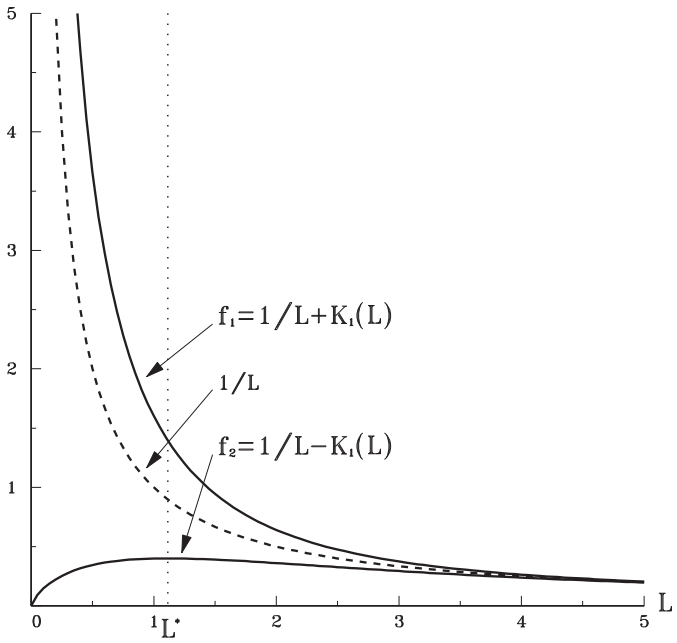

Fig. 2. Relationships (3.8) and (3.9) for $f_1(L)$ and $f_2(L)$.

2)

$$u_1^1 = -\frac{1}{4\pi}\sum_{\alpha=1}^{2}\kappa_2^\alpha \frac{y_1^1 - y_2^\alpha}{\left(r_{12}^{1\alpha}\right)^2}\left[1-\gamma r_{12}^{1\alpha}K_1\left(\gamma r_{12}^{1\alpha}\right)\right],$$

$$u_2^\alpha = -\frac{1}{4\pi}\left\{\kappa_2^{3-\alpha}\frac{y_2^\alpha - y_2^{3-\alpha}}{\left(r_{22}^{\alpha(3-\alpha)}\right)^2}\left[1+\gamma r_{22}^{\alpha(3-\alpha)}K_1\left(\gamma r_{22}^{\alpha(3-\alpha)}\right)\right]+\right.$$

$$\left.+\kappa_1^1\frac{y_2^\alpha - y_1^1}{\left(r_{21}^{\alpha1}\right)^2}\left[1-\gamma r_{21}^{\alpha1}K_1\left(\gamma r_{21}^{\alpha1}\right)\right]\right\}, \tag{3.12}$$

$$v_1^1 = \frac{1}{4\pi}\sum_{\alpha=1}^{2}\kappa_2^\alpha \frac{x_1^1 - x_2^\alpha}{\left(r_{12}^{1\alpha}\right)^2}\left[1-\gamma r_{12}^{1\alpha}K_1\left(\gamma r_{12}^{1\alpha}\right)\right],$$

$$v_2^\alpha = \frac{1}{4\pi}\left\{\kappa_2^{3-\alpha}\frac{x_2^\alpha - x_2^{3-\alpha}}{\left(r_{22}^{\alpha(3-\alpha)}\right)^2}\left[1+\gamma r_{22}^{\alpha(3-\alpha)}K_1\left(\gamma r_{22}^{\alpha(3-\alpha)}\right)\right]+\right.$$

$$\left.+\kappa_1^1\frac{x_2^\alpha - x_1^1}{\left(r_{21}^{\alpha1}\right)^2}\left[1-\gamma r_{21}^{\alpha1}K_1\left(\gamma r_{21}^{\alpha1}\right)\right]\right\}, \tag{3.13}$$

In (3.12) and (3.13), $\alpha = 1, 2$.

We assume that $\kappa_1^1 = -2\kappa$, $\kappa_1^2 = \kappa_1^3 = \kappa$ for variant 1), while for variant 2), following [188, 189], we have restricted our consideration to two cases: 2a) $\kappa_1^1 = -2\kappa$, $\kappa_2^1 = \kappa_2^2 = \kappa$; 2b) $\kappa_1^1 = \kappa_2^2 = -\kappa$, $\kappa_2^1 = 2\kappa$, with the assumption that $\kappa > 0$.

3.2.1. Zero total momentum: $P_x = P_y = 0$

Under these conditions, the three vortices have to lie on a straight line, the two vortices with the same sign lying symmetrically on both sides of a strong central core with opposite-sign intensity.

1) In this case, the centre of rotation coincides with the central vortex. Analogous symmetrical vortical structures of this type in a homogeneous fluid are widely known as *tripolar vortices* (or *tripoles*) [116], [117], [138], [31], [32], [33], [34], [35], [57], [95], [89], [90], [91], [109], [110], [137], [147], [152], [161], [162], [163], [165], [202], [208], [211], [212], [213], [214], [215], [216] rotating with a constant angular velocity around the central vortex in the direction determined by the sign of its vorticity. In this case, (3.10)–(3.11) yield the following expression for the angular velocity of peripheral vortices

$$\omega = -\frac{\kappa\gamma^2}{4\pi L^2}\left\{L\left[K_1(2L) + 2K_1(L)\right] + \frac{3}{2}\right\}. \tag{3.14}$$

This expression differs from the formula for the angular velocity of a tripole in a barotropic medium (under the rigid-lid condition for the surface) by a factor of 1/2, equal to layer thickness, and by members containing McDonald functions. The latter characterize the effect of the lower (for the upper layer) free interface between layers.

2a) In this case, the central core, which coincides with the centre of rotation, and the peripheral vortices belong to different layers. The latter, as in the barotropic case, rotate along circular orbits with a constant angular velocity. In [185], [189] this structure was referred to as a *roundabout*. From (3.12)–(3.13), we derive the following expression for the angular velocity:

$$\omega = \frac{\kappa\gamma^2}{4\pi L^2}\left\{L\left[K_1(2L) + 2K_1(L)\right] - \frac{3}{2}\right\}. \tag{3.15}$$

Here, $L = \gamma l$, where l — is half the distance between the peripheral vortices.

By equating angular velocity (3.15) to zero, we find the unique solution to this equation $L = L^{**} = 0.8602$. Thus, at $L > L^{**}$, the vortices in the lower layer, as in the barotropic case, rotate in an anticyclonic direction, induced by the upper-layer vortex, and we have an *ordinary roundabout*. At $L < L^{**}$, the interaction between the cyclonic vortices becomes predominant and, notwithstanding the anticyclonic spin-up due to the central vortex, they move counterclockwise along a circular trajectory (*inverse roundabout*). At $L = L^{**}$, we have an unstable steady state, in which the bottom-layer vortices are immobile.

Figure 3a gives the initial locations of vortices, and figure 3b shows the trajectories of vortices within a short time interval for the cases with $L > L^{**}$, $L = L^{**}$, and $L < L^{**}$ (left to right). Here, and in Figs. 4, 6 and 7, a triangle-shaped marker denotes the upper-layer vortex with an intensity of κ_1^1, while the lower-layer vortices with intensities of κ_2^1 and κ_2^2 are denoted by the circles and boxes, respectively. The sizes of the markers are proportional to the absolute values of the vortex intensities ($|\kappa_1^1| = 2\kappa$, $|\kappa_2^1| = |\kappa_2^2| = \kappa$).

2b) Peripheral vortices belong to different layers and hence experience different influence from the central vortex. The centre of rotation lies in the segment between the top-layer vortex and the central vortex, belonging to the bottom layer at a distance of

$$L_c = L - \frac{2L^2K_1(L)}{LK_1(2L) + 3/2}. \tag{3.16}$$

from the former vortex. This type of solid-state vortical structure will be referred to as *eccentric roundabout*[5]. The angular velocity is

$$\omega = \frac{\kappa\gamma^2}{4\pi L^2}\left[LK_1(2L) + \frac{3}{2}\right], \tag{3.17}$$

and its sign always coincides with that of the vorticity of the strong vortex. Figure 4a gives the initial locations of vortices, and figure 4b shows the trajectories of vortices within a short time interval for

[5] An analogue of a two-vortex *two-tier top*, which, however, has zero total intensity.

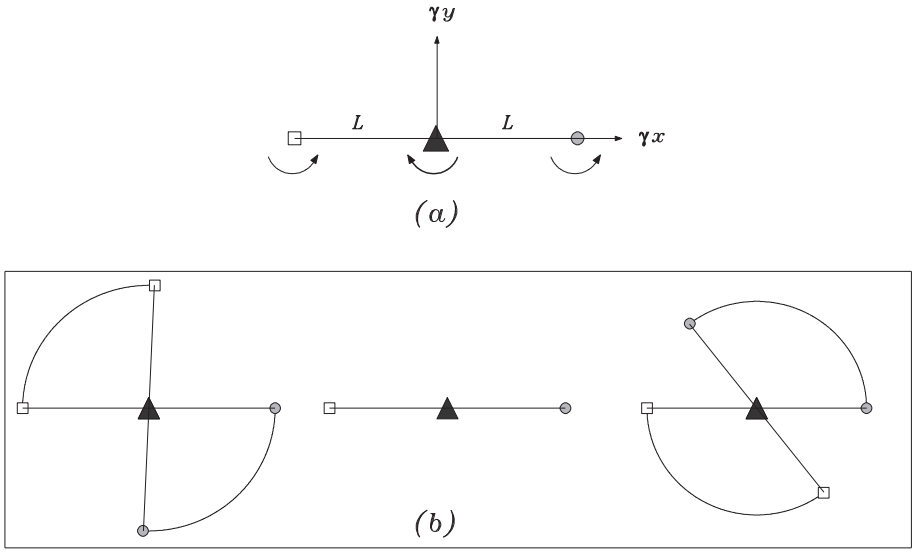

Fig. 3. Case 2a): Diagram of initial vortex locations — *(a)*; initial parts of vortex trajectories — *(b)*. Segments connect the locations of vortices for the initial and final (calculated) time moments.

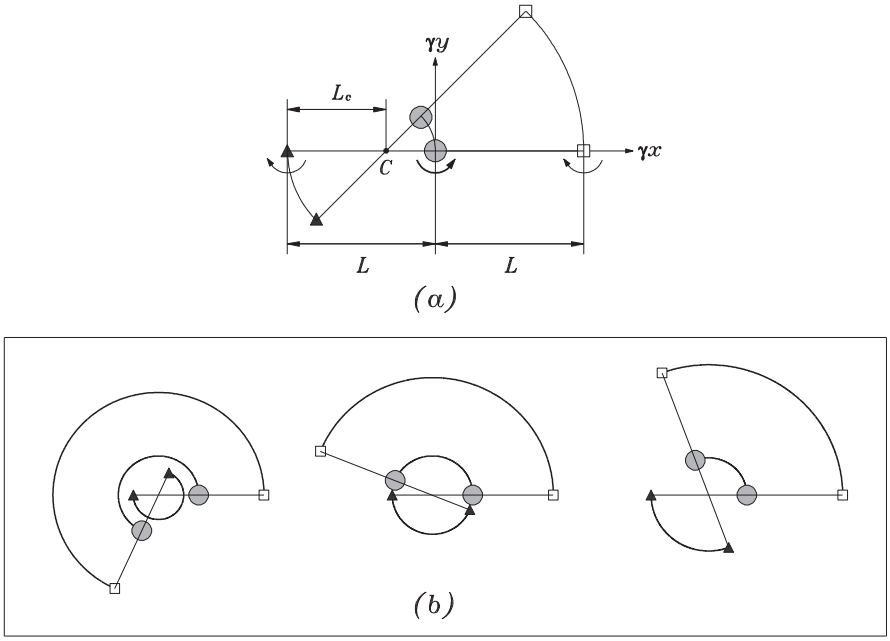

Fig. 4. Case 2b): Schematic representation of vortex motion — *(a)*; initial parts of vortex trajectories — *(b)*.

the cases when the variable L_c, represented by (3.15) satisfies the conditions $L_c < L/2$, $L_c = L/2$ and $L_c > L/2$.

Note on choreographies. The above-mentioned vortical structures of the *roundabout* type with a periodic motion of all vortices along circular trajectories exemplify the so-called *absolutely complex choreographies*. The notion *choreography* was introduced not long ago (2000) by Simó [178] to describe the motion of three bodies with Newtonian interaction potential along closed orbits in celestial mechanics problems.

Choreographies can be

- *absolute* — if the trajectories are closed in a fixed coordinate system;
- *relative* — if the trajectories become closed in a coordinate system that rotates uniformly around the centre of rotation (or moves with a constant translational velocity if the centre of rotation is at infinity);

- *simple* — when all bodies (or vortices) move along the same trajectory;
- *complex* — if at least one body moves along an individual trajectory.

The first attempt to apply the notion of choreography to vortex dynamics in a homogeneous fluid on a plane and a sphere was made by Borisov and Mamaev [21].

The two-layer character of the vortical structures discussed in this work makes the presence of choreographies even more important. As will be shown below, situations are possible where vortices have common trajectories but belong to different layers.

Without going into a systematic study of choreographies, we will, however, indicate each case where this special class of vortex motion exists.

3.2.2. Nonzero total momentum

In this case the relative motion of vortices is conveniently studied in the so-called trilinear coordinates (t_1, t_2, t_3) [2], [5], [172], [173], [188], [189] — see Fig. 5. We restrict our consideration to the example of case 2a), where the trilinear coordinates take the form

$$t_1 = -\frac{3\kappa^2\left(r_{22}^{21}\right)^2}{P^2} \leqslant 0, \quad t_2 = \frac{6\kappa^2\left(r_{21}^{21}\right)^2}{P^2} \geqslant 0, \quad t_3 = \frac{6\kappa^2\left(r_{21}^{11}\right)^2}{P^2} \geqslant 0,$$
$$t_1 + t_2 + t_3 = 3, \qquad P^2 = P_x^2 + P_y^2, \tag{3.18}$$

and the 'physical area' is defined by the expression

$$12t_1 + \left(t_2 - t_3\right)^2 \leqslant 0. \tag{3.19}$$

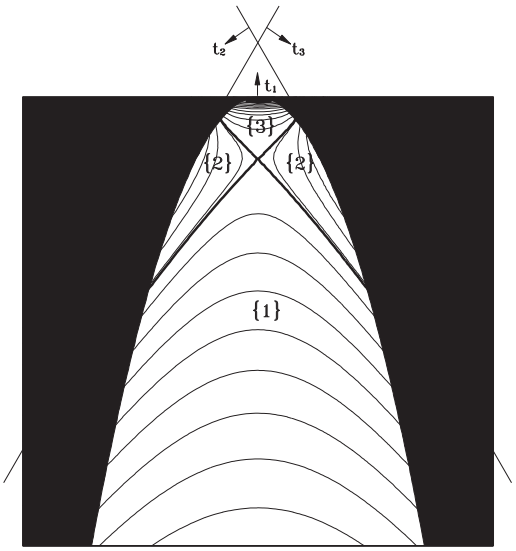

Fig. 5. Scheme of trilinear coordinates (3.18) and the phase portrait for the problem of motion of three vortices in the 'physical area' (3.19): case a). Thick lines represent separatrices dividing subareas {1}, {2} and {3}.

A characteristic phase portrait is shown in figure 5. The black area represents a 'nonphysical area', where the distances between the vortices fail to satisfy the triangle inequalities. During the motion of vortices, the image point in the phase plane executes a periodic motion along the respective trajectory and is periodically reflected from the boundary (at this moment, the vortices are collinear), which reverses its motion. Analysis of the phase portrait yields the following results:

- All relative motions are periodic, and within every period, the system passes twice through collinear states. This means, in particular, that in order to exhaustively study the properties of

absolute motions it is sufficient to consider only the initial conditions with a collinear location of the three vortices (such initial conditions are used in all examples discussed below).

- Relative motions are finite.
- Three types of motion are possible, differing with respect to the interaction between the vortices:
  - Type $\{1\}$ — the interaction between vortices in the lower layer dominates, and the motion can be conventionally defined by the scheme

$$\binom{1}{2}\binom{2}{2}+\binom{1}{1},$$

    where notation $\binom{i}{j}$ refers to a vortex with the intensity of κ_j^i;
  - Type $\{2\}$ — one of the vortices in the lower layer is seized by the vortex in the upper layer, and the situation is described by one of the formulas:

$$\binom{1}{1}\binom{1}{2}+\binom{2}{2} \qquad \text{or} \qquad \binom{1}{1}\binom{2}{2}+\binom{1}{2},$$

  - Type $\{3\}$ — both vortices in the lower layer are involved in an anticyclonic motion induced by vortex $\binom{1}{1}$:

$$\binom{1}{1}\binom{1}{2}\binom{2}{2}.$$

    Examples of absolute motion for the three types are given in figure 6.
- The phase portrait has three elliptic (stable) singular points and one hyperbolic (unstable) singular point. One of the elliptic points (at $t_1 = 0$) corresponds to the case when the vortex system forms a pair (heton) from merged lower-layer cyclones and the upper-layer anticyclone. The other two elliptic points correspond to nontrivial collinear states representing a uniformly moving vortex triplet. Such a structure was called a *triton* in [188], [189], [190], [191]. The existence condition for a triton is specified by the dispersion equation

$$\frac{A^2-2AL+4L^2}{2AL(2L-A)} = K_1(A)+K_1(2L-A)+K_1(2L), \tag{3.20}$$

  and the velocity of its motion by the equality

$$V=\frac{\kappa\gamma}{4\pi}\left\{\frac{1}{A}-K_1(A)-\Big[\frac{1}{2L-A}-K_1(2L-A)\Big]\right\}\equiv\frac{\kappa\gamma}{4\pi}F\big[A(L)\big]. \tag{3.21}$$

  The meaning of the variable A is apparent from figure 7a. Figure 7b shows the dispersion curve $A(L)$, as the solution of (3.20), and the function F from (3.21). Full (dashed) curves represent branches for which $A < L$ ($A > L$). Figure 7 shows, in particular, that no solutions of the *triton* type exist at $L < L^{**}$.

  The hyperbolic point in the phase plane corresponds to the vortex configuration in the form of an isosceles triangle with the upper-layer vortex in the apex. The length of the lateral side and the angles at the base of the triangle are related by the dispersion equation

$$\frac{1+2L|\cos\phi|K_1(2L|\cos\phi|)}{\cos^2\phi} = 4\big[1-LK_1(L)\big], \tag{3.22}$$

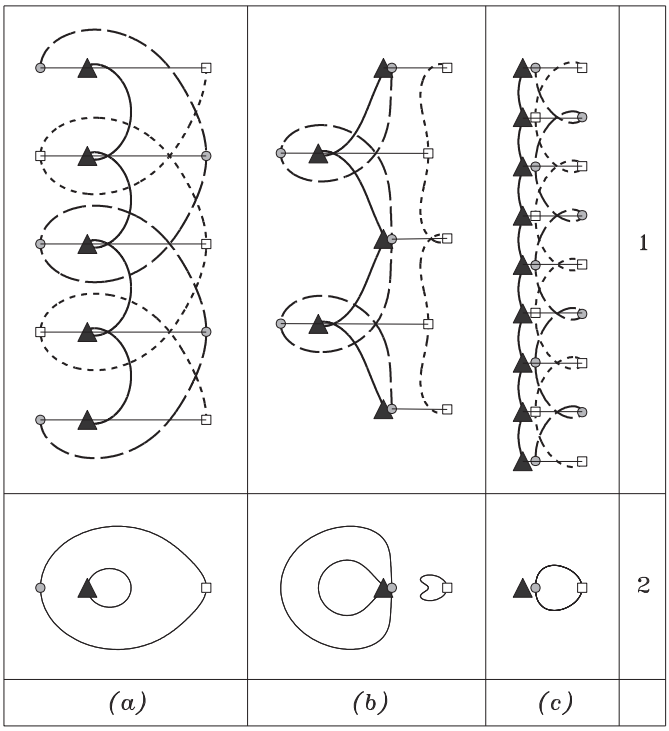

Fig. 6. **1**. Examples of motion types {1} — *(a)*, {2} — *(b)* and {3} — *(c)*. The solid line represents the trajectory of the vortex in the upper layer $\binom{1}{1}$, the long-dash line the trajectory of the first vortex in the lower layer $\binom{1}{2}$, and the short-dash line that of the second vortex in the lower layer $\binom{2}{2}$. Markers, spaced a half period apart, fix the synchronous (collinear) locations of the vortices; **2**. The respective relative choreographies in the coordinate system that moves uniformly in the negative y-direction. Markers show the initial locations of vortices. Vortices in the lower layer have common trajectories in fragments $2a$ and $2c$.

and the velocity of the uniform motion of the vortex structure in the direction parallel to the triangle base is expressed by the formula[6]

$$V = -\frac{\kappa\gamma \sin\phi}{4\pi L}\big[1 - LK_1(L)\big]. \tag{3.23}$$

- All vortex motions are associated with *relative choreographies* in a coordinate system moving with a constant translational velocity.

Trajectories of absolute motion of a stable *triton* configuration and an unstable triangular configuration with dispersion relationships (3.20) and (3.22) holding true are given in Figs. 8.1.a and 8.1.b, respectively. In the first case, the collinearity is permanent and the segments passing through all three vortices are drawn only for the initial and final calculation time moments. In the second case, the vortices form either a collinear configuration or a triangle after every quarter-period, and in both situations, the lower-layer vortices change places after every half-period (if the translational motion of the entire vortex system is not taken into account). Clearly the image point in the phase plane in this experiment 'slips' from the saddle location into area {3}. Obviously the relative choreography for the triton constitutes three fixed points (figure 8.2.a).

[6]In the case of a homogeneous fluid [208], the stationary solution of the (3.22) type is associated with an isosceles triangle with sides of arbitrary length. Expressions (3.20) and (3.22) are a particular case of more general relationships obtained in [73] for continuous stratification conditions and with allowance made for differential (nonuniform) rotation at a triangular configuration of vortices, two of which (with the same signs) are on one horizon, and the third on the other.

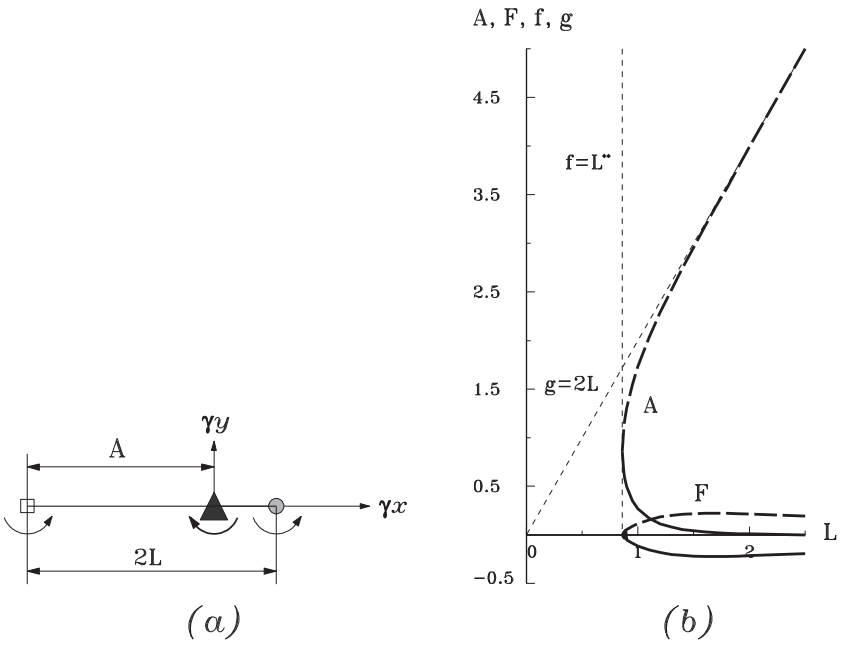

Fig. 7. Diagram of initial vortex location for the collinear structure *triton - (a)*; dispersion curve $A(L)$ and function F (3.21) characterizing the translational velocity of the *triton - (b)*. The sloping short-dash line $g = 2L$ is an asymptote for the dispersion curve ($A \sim 2L$), and the vertical line is determined by the equality $f = L^{**}$, where L^{**} is the solution of equation $\omega = 0$ from (3.15) for the extreme case of zero total momentum ($A = L$).

3.3. The case of four vortices with zero total intensity and momentum

The properties of interaction between four discrete vortices in a two-layer fluid that satisfy conditions (3.1) have been adequately studied [96], [219], [84], [186], [187] for the special case of $N_1 = N_2 = 2$. Here, we present the principal results of these works. Equations of motion (2.13)–(2.14) in this case take the form:

$$u_j^\alpha = -\frac{1}{4\pi}\left\{\kappa_j^{3-\alpha}\frac{y_j^\alpha - y_j^{3-\alpha}}{\left(r_{jj}^{\alpha(3-\alpha)}\right)^2}\left[1+\gamma r_{jj}^{\alpha(3-\alpha)}K_1\left(\gamma r_{jj}^{\alpha(3-\alpha)}\right)\right]+\right.$$
$$\left.+\sum_{\beta=1}^{2}\kappa_{3-j}^{\beta}\frac{y_j^\alpha - y_{3-j}^{\beta}}{\left(r_{j(3-j)}^{\alpha\beta}\right)^2}\left[1-\gamma r_{j(3-j)}^{\alpha\beta}K_1\left(\gamma r_{j(3-j)}^{\alpha\beta}\right)\right]\right\}, \tag{3.24}$$

$$v_j^\alpha = \frac{1}{4\pi}\left\{\kappa_j^{3-\alpha}\frac{x_j^\alpha - x_j^{3-\alpha}}{\left(r_{jj}^{\alpha(3-\alpha)}\right)^2}\left[1+\gamma r_{jj}^{\alpha(3-\alpha)}K_1\left(\gamma r_{jj}^{\alpha(3-\alpha)}\right)\right]+\right.$$
$$\left.+\sum_{\beta=1}^{2}\kappa_{3-j}^{\beta}\frac{x_j^\alpha - x_{3-j}^{\beta}}{\left(r_{j(3-j)}^{\alpha\beta}\right)^2}\left[1-\gamma r_{j(3-j)}^{\alpha\beta}K_1\left(\gamma r_{j(3-j)}^{\alpha\beta}\right)\right]\right\}, \tag{3.25}$$

where j, $\alpha = 1, 2$. Thus, (3.24)–(3.25) constitute a system of eight equations. Now let us suppose that $\kappa_1^1 = \kappa_1^2 = -\kappa_2^1 = -\kappa_2^2 = -\kappa < 0$.

As stated above, when conditions (3.1) are valid, reduction to the three-vortex problem is possible, where the properties of relative motion can be analysed with the use of trilinear coordinates. However, in the particular case of zero total momentum of the four-vortex system, such analyses can be made in the common orthogonal coordinates as well.

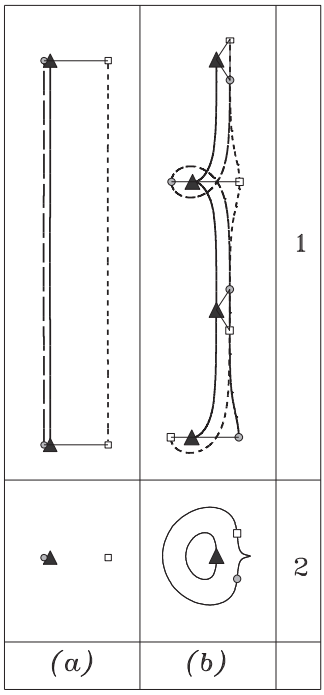

Fig. 8. **1.** Stationary trajectories of three vortices in *(a)* a stable condition (*triton* — an elliptic singular point) and *(b)* unstable condition (in the form of an isosceles triangle — hyperbolic singular point). **2.** Respective relative choreographies in a coordinate system moving uniformly in the negative y-direction. Markers show the initial vortex locations. In the fragment $2b$, lower-layer vortices have common trajectories.

3.3.1. Zero total angular momentum: $M = 0$

Complete analysis of the relative motions yields the phase portrait (isolines of the Hamiltonian on plane $(\gamma x, \gamma y)$) in figure 9a, obtained for the first time in [96]. An equivalent phase portrait in trilinear coordinates is also shown in figure 9b.

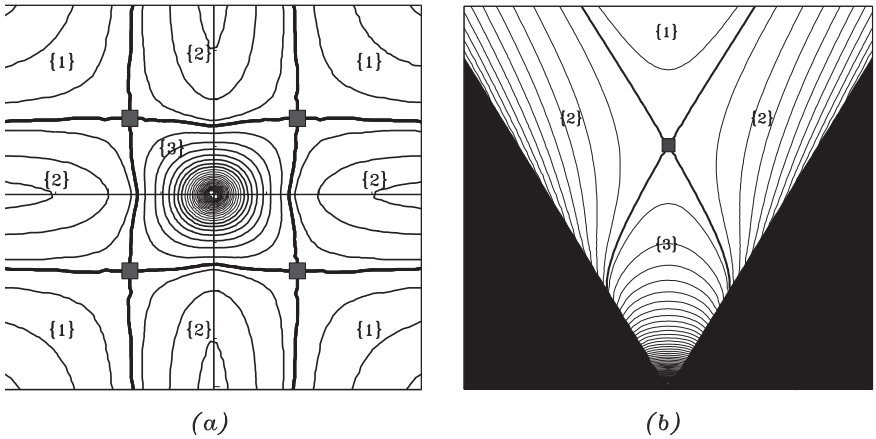

Fig. 9. Phase portraits of the problem of four vortices with zero total momentum in rectangular — *(a)* and triangular — *(b)* coordinates.

In this case, the axes of the trilinear coordinate system

$$t_1 = 3\kappa^2\big(r_{22}^{12}\big)^2 \geqslant 0, \qquad t_2 = 3\kappa^2\big(r_{21}^{11}\big)^2 \leqslant 0, \qquad t_3 = -3\kappa^2\big(r_{21}^{22}\big)^2 \leqslant 0, \quad \text{at} \quad t_1 + t_2 + t_3 = 0, \tag{3.26}$$

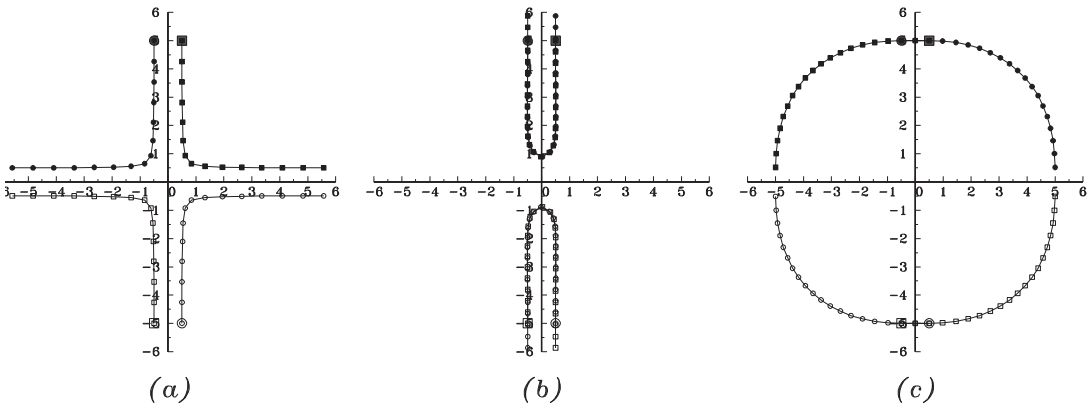

Fig. 10. Trajectories of motion of types {1}, {2} and {3} of four vortices (two hetons with tilted axes) with zero total momentum.

having the same orientation as in figure 5, cross at point (0, 0, 0), and the "physical area" is specified by inequalities (3.26).

In addition to the areas {1}[7], which exist also for vortex interactions in a homogeneous fluid [11, 127], areas {2} and {3} also appear in the two-layer case. Geometrically, areas {1} and {2} represent infinite relative motions, while areas {3} represent finite ones. From the dynamic viewpoint, interaction between vortices from different layers dominates in motions of types {1} and {2}, and interaction between vortices in the same layer dominates for motions of type {3}. If the locations of vortices at the initial time moment allow the hetons to move towards one another, the mutual approach of two-layer pairs in area {2} is accompanied by a continuous decrease in the tilt of their axes (i. e., the distances between the upper and lower vortices) down to zero; after that, the vortices in each heton exchange places (in the view from above), and the pairs start a reverse motion: the heton behaviour resembles an elastic collision at a distance, with the subsequent movement of the hetons in opposite directions. Otherwise, i. e., if the hetons have vertical axes at the initial time moment, only the second part of this scenario will be observed. In this case, area {2} will only correspond to those locations for which the distance c between the vertical axes satisfies the inequality $c > C^*/\gamma$, where $C^* = 1.4332$. In the case of inverse inequality, we find ourselves in area {3}. In area {3}, the upper and lower vortices move in opposite directions along finite O-shaped (according to the terminology used in [96]) overlapping trajectories. Clearly, motions of type {3} in this case correspond to *absolutely simple choreographies*. In virtue of the invariance of M, both axial and mirror symmetry of vortex locations will take place at any moment (this means that at any time moment, the two vortices in each layer are situated at the ends of an imaginary segment with a centre in the origin of coordinates). The trajectories are quasi-circular near the origin, and away from it they assume the form of a four-point star with stagnation points in its acute angles (these are the intersection points of separatrixes shown in the figure by boxes).

Assuming for these points

$$x_j^\alpha = x_{3-j}^{3-\alpha} = -x_j^{3-\alpha} = -x_{3-j}^\alpha = y_j^\alpha = y_{3-j}^{3-\alpha} = -y_j^{3-\alpha} = -y_{3-j}^\alpha = b/2,$$

we obtain from (3.24)–(3.25) a transcendent equation in $B = \gamma b$

$$\frac{1}{B} = 2\left[K_1(B) + \frac{1}{\sqrt{2}B} K_1\big(\sqrt{2}B\big)\right] \tag{3.27}$$

which has the solution $B = B^* = 1.5947$.

[7]These domains correspond to the opposite motion of pairs with subsequent exchange of partners. The only difference from the barotropic case is that each pair has a two-layer structure, i. e., represents a heton with a tilted axis.

It should be mentioned that, unlike in the case of three vortices, where the consideration of only collinear initial states was sufficient for the complete analysis of all possible motions, this is not sufficient in this case (since some phase trajectories do not reach the boundary of the 'physical area'). Therefore, in addition to the collinear conditions, it is necessary to consider, for example, the initial locations of vortices in the vertices of squares with a side greater than B^*.

Examples of motions of types {1}, {2} and {3} are given in Figs. 10a, 10b and 10c, respectively. Here, circular (square) markers denote anticyclonic (cyclonic) vortices of the upper (lower) layer. Shaded (hollow) markers denote the vortices that were located in the upper (lower) part of the figure at the initial time moment. Larger markers correspond to the initial locations of vortices. The calculation time intervals are chosen so as to allow the demonstration in 10b of the process of the motion of each vortex along the straight line coinciding with the initial trajectory of its partner from the other layer, and in 10c, its motion up to the moment that the trajectories overlap.

3.3.2. Nonzero total angular momentum: $M \neq 0$

In this case, the characteristic phase portrait in trilinear coordinates

$$t_1 = \frac{3\kappa\left(d_{21}^{22}\right)^2}{M} \geqslant 0 \ (\leqslant 0), \qquad t_2 = -\frac{3\kappa\left(d_{21}^{11}\right)^2}{M} \leqslant 0 \ (\geqslant 0), \qquad t_3 = -\frac{3\kappa\left(d_{21}^{21}\right)^2}{M} \leqslant 0 \ (\geqslant 0),$$
$$\text{where} \quad M > 0 \ (M < 0), \quad \text{and} \quad t_1 + t_2 + t_3 = 3 \tag{3.28}$$

in the 'physical area'

$$t_1 t_2 \leqslant \frac{9}{4} \tag{3.29}$$

is determined by figure 11, whence it can be seen that the relative motions, as in the previous case, can be divided into three qualitatively different types. However, in contrast to the case of $M = 0$, all vortex trajectories now have only central symmetry.

Trajectories of four vortices for cases {1}, {2} and {3} are shown in Figs. 12a, 12b and 12c, respectively (to avoid overloading the diagram, markers in the latter figure denote only the initial locations of vortices). Clearly, motions of types {1} and {2} represent the cases of noncentral, head-on collision of hetons. In the first case, the pairs of vortices exchange partners, while in the second, each heton remains an indivisible two-layer pair in the process of interaction.

Let us now consider in more detail the properties of finite captured motions of type {3} which are the richest in content within the context of this problem. These motions consist of the anticyclonic rotation of the upper vortices and cyclonic (or anticyclonic) rotations of the lower ones, depending on the degree of asymmetry in the initial construction of vortices. Moreover, it turns out that all trajectories of this type in the system of coordinates, rotating in the same direction as the lower vortices, are associated with *relative choreographies*. The transition boundary from one regime to the other is associated with an *absolute choreography* — see figure 13.

The structure of the obtained choreographies suggests the following general properties of the motions associated with them:

- Upper vortices rotate along quasi-elliptic orbits in an anticyclonic direction and always remain at the opposite ends of the same diameter of the figure.

- The two lower vortices execute synchronous cyclonic rotations with respect to two centrally symmetrical peripheral fixed points.

- After every quarter period, the vortices form alternating collinear and rhomb-shaped configurations (the latter is observed in the moments when the respective image point in the phase plane crosses the axis of symmetry of the 'physical area').

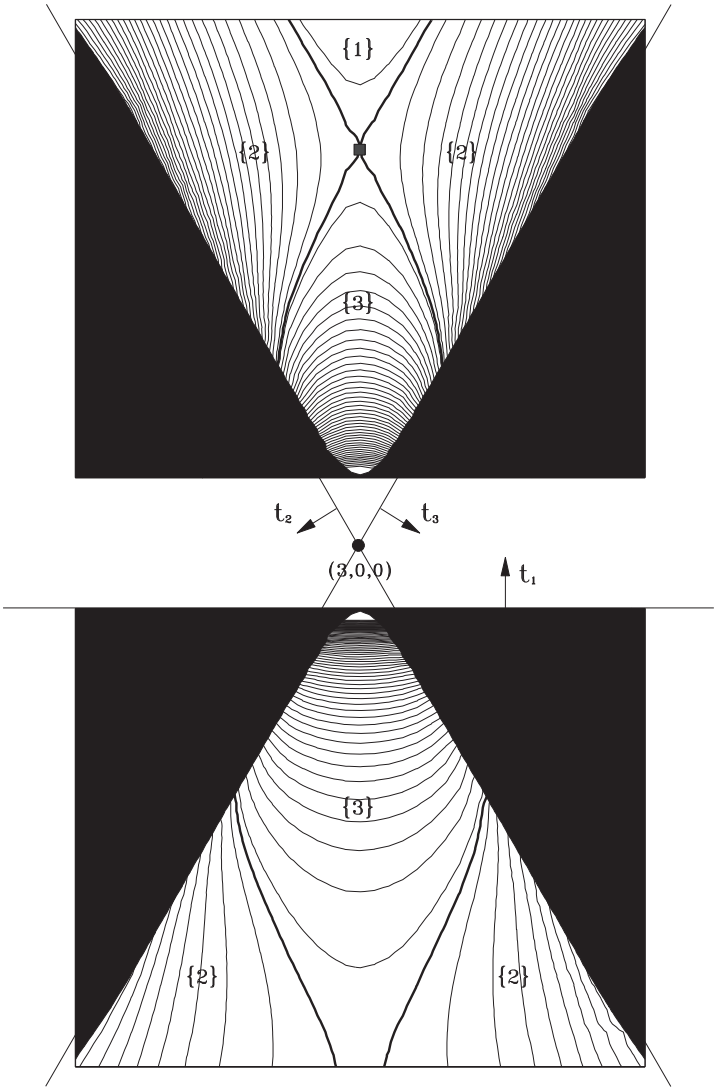

Fig. 11. Phase portraits in trilinear coordinates for the problem at $M > 0$ (top) and $M < 0$ (bottom). Orientation of axes and the coordinates of the singled-out point are shown.

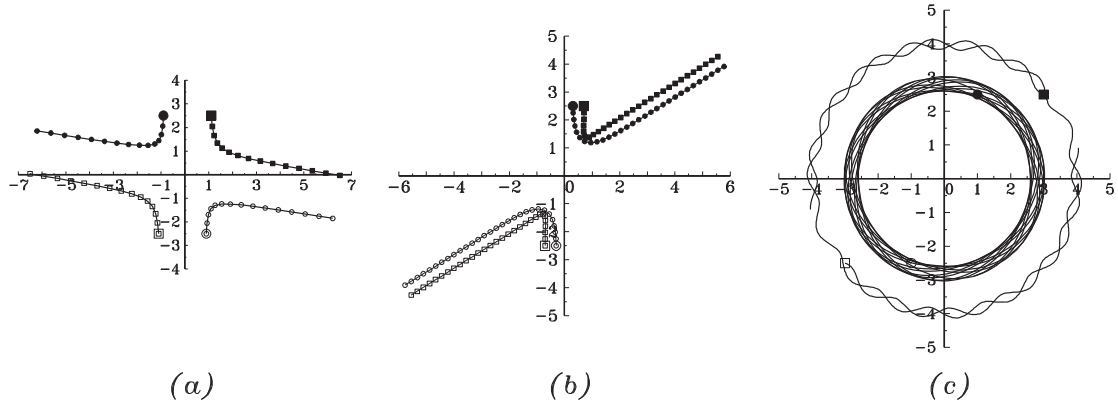

Fig. 12. Trajectories of motion of types {1} — *(a)*, {2} — *(b)* and {3} — *(c)* of four vortices with nonzero total angular momentum.

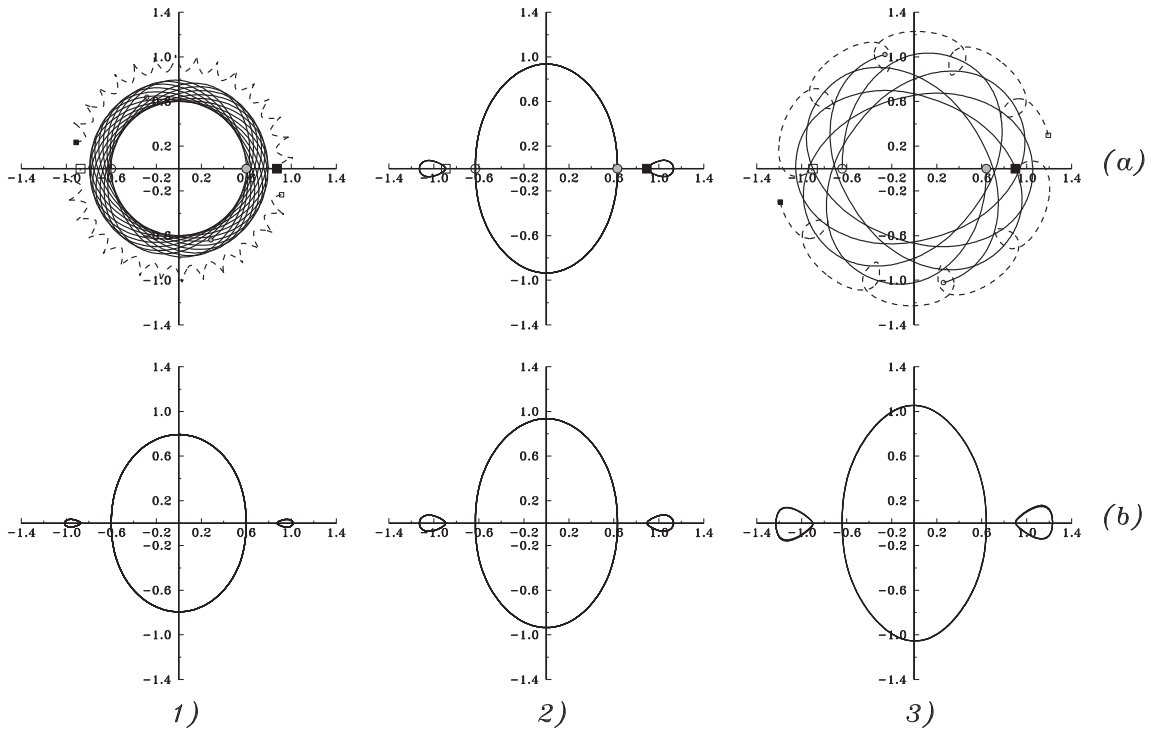

Fig. 13. Trajectory of motions of type {3} for four vortices with a nonzero total angular momentum — *(a)* and the respective choreographies — *(b)*. 1) refers to relative motions in system of coordinates rotating in a cyclonic direction; 2) refers to absolute motion; 3) refers to relative motions in system of coordinates rotating in a anticyclonic direction.

- The ratio of the revolution periods of upper and lower vortices is 1:2.
- The choreographies characterize the stationary (and presumably stable) solution of system (3.24)–(3.25).
- The properties mentioned above refer to *relative* motions in cases 1) and 3) and to *absolute* motions in case 2) — figure13.

The hyperbolic stationary point marked by a box in the upper part of figure 11 in this case corresponds to four vortices located in the four vertices of the rhomb, which rotates with an angular velocity of

$$\omega = \frac{\kappa\gamma^2}{2\pi B^2}\left[1 - BK_1(B) - \frac{1 + 2B|\sin\phi| K_1\big(2B|\sin\phi|\big)}{4\cos^2\phi}\right], \tag{3.30}$$

where B now is half the rhomb side, and ϕ is half its acute angle. Instead of (3.27) we have

$$8\big[1 - BK_1(B)\big] = \frac{1 + 2B|\sin\phi| K_1\big(2B|\sin\phi|\big)}{\sin^2\phi} + \frac{1 + 2B|\cos\phi| K_1\big(2B|\cos\phi|\big)}{\cos^2\phi}. \tag{3.31}$$

In the particular case of a rhomb degenerated into a square ($\phi = \pi/4$), (3.31) reduces to (3.27), by virtue of which (3.30) yields $\omega = 0$.

3.4. Case $N > 4$

3.4.1. Integrable cases

A system of vortices with $N > 4$ allows integration when it has additional symmetries [155], [12], [3], [148], [114]. For example, if $N_1 = N_2 = n$, and hetons in the initial moment are located in the vertices

of a regular n-polygon, the equations of relative motion can be reduced to equations describing the evolution of an equivalent heton. The method reducing Hamiltonian systems in this way is described in [3], [148] within the context of a model of two-dimensional vortices.

Following [3], we will search the solution of (2.13)–(2.14) in the form

$$x_j^\alpha = r(t)\cos\left(\phi_j + \frac{2\pi(\alpha-1)}{n}\right), \qquad y_j^\alpha = r(t)\sin\left(\phi_j + \frac{2\pi(\alpha-1)}{n}\right), \tag{3.32}$$

where $(r,\, \phi_j)$ are polar coordinates, $j = 1, 2$ is the number of the layer, $\alpha = 1, 2, \ldots, n$ is the number of the heton. Now, assuming that $\kappa_j^\alpha = -\kappa_{3-j}^\alpha$, we obtain reduced equations

$$\dot r = -\frac{\kappa_j}{4\pi r}\left\{\frac{n}{2}\, s\,(0,\, n\phi) - \gamma r\left[\sum_{\alpha=1}^{n-1} s\,(\alpha,\, 0)\, S\,(\alpha,\, 0) + \sum_{\alpha=0}^{n-1} s\,(\alpha,\, \phi)\, S\,(\alpha,\, \phi)\right]\right\}, \tag{3.33}$$

$$\dot\phi = \quad \frac{\kappa_j}{4\pi r^2}\left\{-\frac{1}{2} + \gamma r\left[\sum_{\alpha=1}^{n-1} S\,(\alpha,\, 0) + \sum_{\alpha=0}^{n-1} S\,(\alpha,\, \phi)\right]\right\}, \tag{3.34}$$

for an equivalent heton. Here $\phi = \phi_{3-j} - \phi_j$ and

$$s\big(a,\, b\big) = \frac{\sin\left(\frac{2\pi a}{n} + b\right)}{1 - \cos\left(\frac{2\pi a}{n} + b\right)}, \quad S\big(a,\, b\big) = \left|\sin\left(\frac{\pi a}{n} + \frac{b}{2}\right)\right| K_1\left(2\gamma r\left|\sin\left(\frac{\pi a}{n} + \frac{b}{2}\right)\right|\right).$$

The condition for the Hamiltonian invariance takes the form

$$\Phi\,(r,\, \phi,\, n) = \ln\left[r\prod_{\alpha=1}^{n-1}\left|\sin\left(\frac{\pi\alpha}{n} + \frac{\phi}{2}\right)\right|\right] + K_0\left(2\gamma r\left|\sin\frac{\phi}{2}\right|\right) -$$
$$\sum_{\alpha=1}^{n-1}\left\{K_0\left(2\gamma r\left|\sin\frac{\pi\alpha}{n}\right|\right) - K_0\left[2\gamma r\left|\sin\left(\frac{\pi\alpha}{n} + \frac{\phi}{2}\right)\right|\right]\right\} = \text{const}. \tag{3.35}$$

Figure 14 gives examples of phase portraits (level lines of function (3.35)) for the relative motion of three and six hetons, which have three and six radial axes of symmetry, respectively. In this case, areas $\{3\}$ take the form of hexagonal stars in the former case and dodecagonal stars in the second (this is analogous to the case of two hetons, where such an area has the form of a four-point star — figure 9a). It should be mentioned that in this case, the phase curves are constructed in the axes $(x,\, y)$ at different values of γ (see the figure caption), and changing to coordinates $(\gamma x,\, \gamma y)$ will double the linear scale in figure 14b.

Solutions of type $\{1\}$ are still represented by motions in which hetons 'collide at a distance' and then move in opposite directions. Solutions of type $\{2\}$ imply pairwise exchange of partners between hetons that originally moved along adjacent axes of symmetry. Examples of these two types of motion for $n = 6$ are given in figure 15. The calculation time intervals in this case are chosen so that the final coordinates of each vortex in figure 15a coincide with the initial coordinates of its partner, and in figure 15b represent its own mirror image with respect to an axis of symmetry that is individual for each heton. Stable solutions of type $\{3\}$ are associated with the rotation of vortices (in the anticyclonic direction in the upper layer and cyclonic direction in the lower layer). At any moment, the vortices in both layers lie in the vertices of regular n-polygons with periodically varying side lengths. The side lengths are minimum at the moments when the respective polygons coincide in the planar view (in this case we observe n hetons with vertical axes), and maximum when the vortices form a regular $2n$-point structure (that is, one of the polygons is turned through $\pi/2n$ with respect to the other). The angular velocity of each n-polygon, conversely, attains its maximum in the first case and minimum in

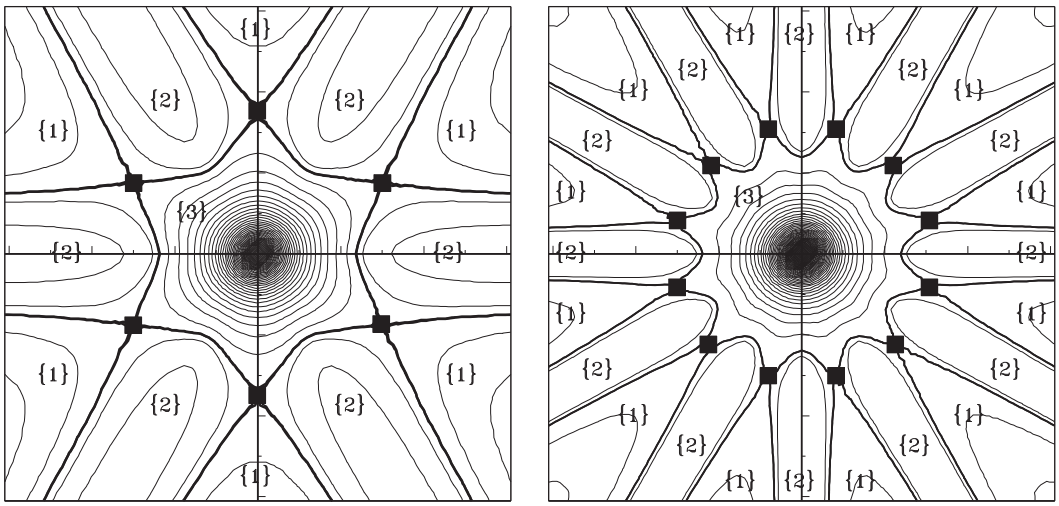

Fig. 14. Phase portraits (contours of the Hamiltonian) in axis (x, y) for a system of three ($\gamma = 1$) — *(a)* and six ($\gamma = 2$) — *(b)* hetons uniformly distributed over a circumference. Notations {1}, {2} and {3} are the same as in figure 8. Box markers denote the intersection points of separatrices.

the second. However, purely periodic solutions of this type exist only for $n = 2$ (i. e., at $N = 4$, when, with the condition of zero total intensity of vortices, the system is integrable); only *quasi-periodicity* is possible at $n > 2$. Moreover, as will be shown in section 3.4.2, solutions of type {3} can even be unstable.

Saddle-type unstable stationary states of the vortex system are shown in figure 14 by points marked by shaded squares. The polar coordinates of the saddles can be found by equating the right-hand parts of equations (3.33)–(3.34). Thus, from (3.33), we have

$$\phi = \pi/n,$$

and (3.34) can be reduced to a transcendent equation

$$\frac{1}{2R} = S\Big(0,\, \frac{\pi}{n}\Big) + \sum_{\alpha=1}^{n-1}\Big[S\big(\alpha,\, 0\big) + S\Big(\alpha,\, \frac{\pi}{n}\Big)\Big], \tag{3.36}$$

where $R = \gamma r$. Let the solution of (3.36) for any fixed n be denoted by R^S_{max}; then an equation for R^S_{min} (the distance from the centre to the nearest point of the separatrix) can be derived from the condition that the respective image points should lie in the same phase curve, i. e., equating the values of function Φ from (3.32) at $R = R^S_{max}$ and $R = R^S_{min}$. In figure 16 the values $R^S_{max}(n)$ and $R^S_{min}(n)$ are represented by hollow circles and triangles, respectively. It is worth mentioning that both R^S_{max} and R^S_{min} are virtually linear functions of n. Shaded dots and triangles show the locations of $R^N_{max}(n)$ and $R^N_{min}(n)$, respectively (the maximum and minimum distance from the centre to the *instability domain* boundaries). The region of 'regular splitting' in this figure relates to type {1} and {2} motions, while the region of 'confinement', to finite quasi-stable solutions of type {3}. This figure will be discussed in more detail in section 3.4.2 below.

The heton analogies of von Kármán streets [79], [80], [84] (see figure 17) provide an example of an integrable heton system comprising an infinite number of vortices. The streets consist of two parallel vortex rows with a period of a. One row is in the upper layer, and the other in the lower. The vortices belonging to different layers have opposite signs. The rows are separated by b. In the antisymmetric street (figure 17b), vortices from the lower layer are off set by a half period relative to those from the upper layer. The accurate integrability of equations in this case is due to the invariance with respect

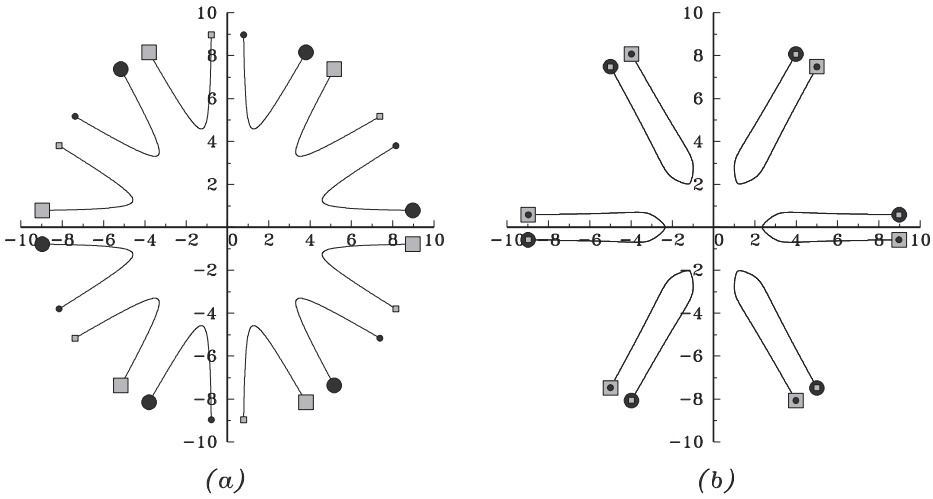

Fig. 15. Trajectories of motion of types {1} — *(a)*, and {2} — *(b)* for a heton system with initial coordinates specified by formulas (3.29) at $n = 6$, $r = 9$, $\phi = \pi/24$ — *(a)* and $\phi = \pi/18$ — *(b)*. The initial locations of vortices are specified by large markers (the circle is for the upper layer, and the box for the lower), and the final locations by small markers.

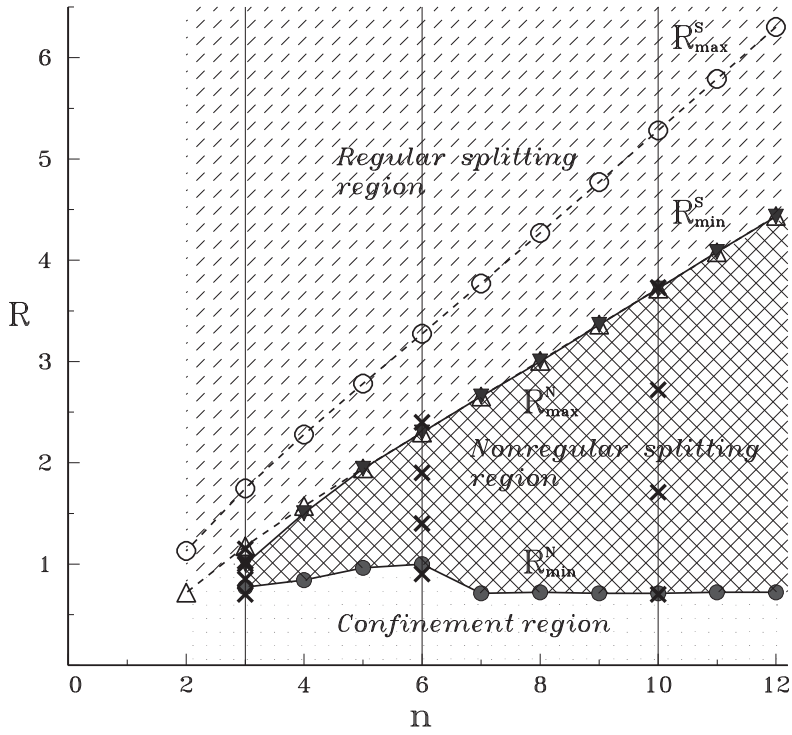

Fig. 16. The state diagram of an n-symmetrical heton configuration with initially vertical axes for $n =$ $= 2, 3, \ldots, 12$. The inclined dashed lines are 'continuations', into the origin of coordinates, of imaginary curves that pass through $R^S_{min}(n)$ and $R^S_{max}(n)$. The locations of crosses correspond to the calculation parameters presented in figure 19. Other explanations for the figure are given in the text.

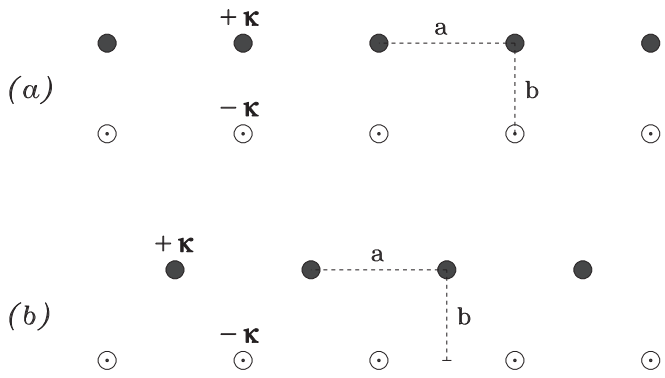

Fig. 17. Schematic representation of the geometry of vortical heton paths: *(a)* — symmetrical; *(b)* — antisymmetrical paths.

to a shift in the period along the street. As shown in [79], [80], von Kármán heton streets move with a constant velocity in the direction of the street axis. The velocity of a symmetrical street for models with equal layer thickness is given by the equation

$$u = \frac{\kappa}{4a}\coth\frac{\pi b}{a} - \frac{\kappa\gamma}{4\pi}\left[K_1(\gamma b) + 2\sum_{\alpha=1}^{\infty}\frac{b}{\sqrt{(\alpha a)^2+b^2}}K_1\left(\gamma\sqrt{(\alpha a)^2+b^2}\right)\right], \tag{3.37}$$

and the velocity for an antisymmetric streets, by:

$$u = \frac{\kappa}{4a}\tanh\frac{\pi b}{a} - \frac{\kappa\gamma}{4\pi}\sum_{\alpha=1}^{\infty}\frac{2b}{\sqrt{(a/2+\alpha a)^2+b^2}}K_1\left(\gamma\sqrt{(a/2+\alpha a)^2+b^2}\right). \tag{3.38}$$

The streets move without changing their shape because the velocity induced by other vortices in the point of location of each vortex is equal to the translation velocity of the street as a whole. The first term in (3.37)–(3.38) accounts for the barotropic interaction between vortices, and the second term for the baroclinic interaction. The barotropic term dominates at large distances between the rows, and street velocity coincides with that of classical von Kármán streets for this limit. As the period a tends to infinity, the velocity of the symmetrical street tends to that of an individual heton (3.9). Figure 18 demonstrates the dependence of stratification $\sigma = \gamma a$ and the relative thickness of the layers on asymmetry parameters $k = b/a$. A diagram of state which classifies the existence domains of heton streets at different values of k, as well as a complete analysis of limiting cases, is given in [79], [80].

In the barotropic limit $\sigma \to \infty$, the conditions of street linear stability are similar to the classical [127]. Screening of vortices (finite values of σ) increases the stability of streets. This effect, within the context of approximation based on the equivalent-barotropic model, was studied in [139]. The stability of solutions of (3.37)–(3.38) in a complete formulation has not been studied.

Although the range of problems that allow exact integration, is clearly not exhausted by the examples considered, it is limited and fails to give a comprehensive notion of the behaviour of heton systems.

3.4.2. Quasi-regular and chaotic heton dynamics

Systems with $n > 2$ hetons in a general location are not integrable, since they do not have a sufficient number of integrals of motion (the total number of vortices that form hetons is $N > 4$). The dynamics of heton populations reflects a complex coexistence of regular and chaotic regimes [97], [129], [55], [43], [44], [84]. The realization of one or another regime depends on the problem parameters and boundary conditions. The simplest examples of nonintegrable situations arise even with a stochastic disturbance of the initial heton locations in the case of the n-symmetric heton configurations discussed

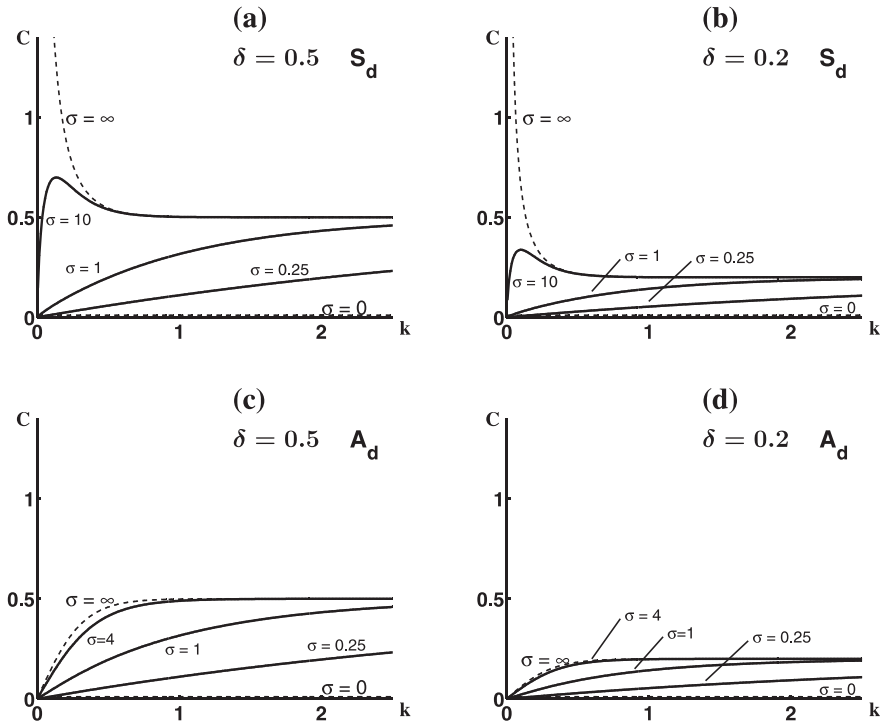

Fig. 18. Velocity C of symmetrical (S_d) and asymmetrical (A_d) von Kármán heton vortex streets, standardized by $\kappa/2a$, as a function of parameter k at different values of parameters $\sigma = \gamma a$ and $\delta = h_1/(h_1 + h_2)$.

above. Indeed, numerical experiments show that the introduction of small random disturbances (white noise) ε^α ($\max \varepsilon^\alpha \leqslant 0.01$) in the coordinates of vortices

$$R_j^\alpha\big|_{t=0} = \bar{R} + \varepsilon^\alpha \tag{3.39}$$

results in an instability of the symmetric solution of (3.32) within interval $\bar{R} \in \left[R^N_{min}, R^N_{max}\right]$, where $R^N_{max} \leqslant R^S_{min}$ (see 'nonregular splitting' region in figure 16).

Analysis of numerical experiments shows that instabilities of two types occur:

- At $n \in [3; 5]$, the instability is due to the baroclinic interaction between vortices from *different* layers (the equivalent-barotropic subsystem of vortices in each layer is stable [74]). In this case, the instability zones in the phase plane belong to area {3} — their external boundaries are located at a finite distance from separatrices - and hence the layer of stochasticity, which forms near the points of separatrix intersection, has almost no effect on the behaviour of the vortex system.

- With an increase in n (at $n \geqslant 6$), in addition to the interaction between layers, the role of barotropic instability increases, associated with the interaction between vortices within a layer. As shown in figure 16, the outer boundaries of the instability areas belong to a circumference, which reaches as far as the points of separatrices with the minimal distance of R^S_{min} from the centre. The internal boundary of the irregular scattering domain at $n \geqslant 7$ runs along an asymptote (shown by the horizontal dashed line in the figure), determined by the value of R^S_{min} for $n = 2$.

Note that the coexistence of the chaotic and quasi-regular motions in a problem with an analogous formulation was mentioned in [97] at $n = 6$. The boundaries of the instability domains established in [97] coincide up to ε with those shown in figure 16.

Some results of calculations for $n = 3$, $n = 6$ and $n = 10$ are given in figure 19. It should be mentioned that, as stated in the list of features of instability types, at $n = 3$, motions of finite character (figure 19.4.a) are observed at $\bar{R} \in \left[R^N_{max};\, R^S_{min}\right]$, i. e., beyond the local region of nonregular splitting. However, the motion instabilities are quasi-ordered within the region (figure 19.2.a, 19.3.a). The upper part of figure 20 shows a segment of vortex trajectories for the second of these cases, for a short stage of the passage the splitting regime after all vortices have made two complete revolutions around the closed star-shaped trajectories. The initial and final moments of this time interval are denoted by T_1 and T_2, respectively. The lower part of the figure gives more detailed configurations of the vortex triplets in both layers in the initial, intermediate, and final moments. The future motion of the vortex pair in the upper part of the figure will be virtually rectilinear, while the two two-layer pairs in the lower part will move in the opposite direction, taking part in the 'reshuffle' of vortices.

The analysis of behaviour of an n-symmetrical heton configuration in the instability domain is, in general, a problem that has not been solved yet[8].

Numerical experiments [97] with 37 hetons ($N = 74$), which originally are uniformly distributed over a hexagonal domain, at different values of γ, also suggest the possible formation of both chaotic and quasi-ordered (at least in the initial stage of evolution) two-layer structures.

The evolution of a heton population uniformly distributed within a circle or an ellipse has been studied by Legg and Marshall [129] while Danilov et al. [43], [44] have studied its evolution within a fixed-width band, and Doronina, Gryanik, et al., [55], [84] on a circle.

It should be emphasized that the behaviour of sufficiently complex heton-type vortex structures (at least for $N \geqslant 4$) may feature both finite and infinite types of motion. In the latter case, interaction results in the splitting of hetons with tilted axes. An individual heton, as shown in section 3.1, moves uniformly along a straight line. Estimates and calculation results show that, in the case of several hetons moving away from one another, their velocities are almost constant (in this case, the interaction between different hetons basically determines the directions in which they split). Thus, with a vortex system that behaves regularly, we can accept with complete confidence that the law of barocline vortex spreading is linear (with respect to time). This law also turns out to be valid in the stochastic regime. Confirmation of this observation was obtained in [43], [44], [55], [84].

4. Finite-core hetons

The model of discrete vortices considered above is extremely idealized. True vortices always have a finite horizontal scale. The next step towards reality can be the model of vortex patches — finite domains with constant vorticity, which where discussed in section 2. Finite-core vortices are distinct from discrete ones in two principal ways. First, they are characterized by instability (even for a solitary heton) [119], [10], [14], [15], [16], [17], [100], [166], [93], [186]; second, a tendency towards merging of like-sign vortex patches that are located close to one another [174], [32], [99], [147], [186], [203], [210], [209].

Generally it is considered that, if several finite-size vortices are far enough away from one another, their interaction would differ only slightly from the interaction of equivalent discrete vortices. Analysis of numerous concrete calculations shows this to be the case. Moreover, it has been found that in many cases, within relatively wide ranges of external parameters, the behaviour of finite-core vortices that are close enough to one another can be quite adequately described within the context of a simple singular model. In fact, there are no general recommendations with respect to the applicability of the discrete approach. However, in each specific case, it may be chosen by using numerical experiments, as was done, in particular, in [186], [189]. The discrete vortex method [13] is widely used and known

[8] In the limit at $\gamma \to 0$, i. e., $\Delta\rho \to \infty$, there is almost no interaction between vortices located in different layers, and we have the problem [127], [113], [148], [74], [12], [155], [121], [122] of the evolution of n-polygonal vortex structures — anticyclonic in the upper layer and cyclonic in the lower layer.

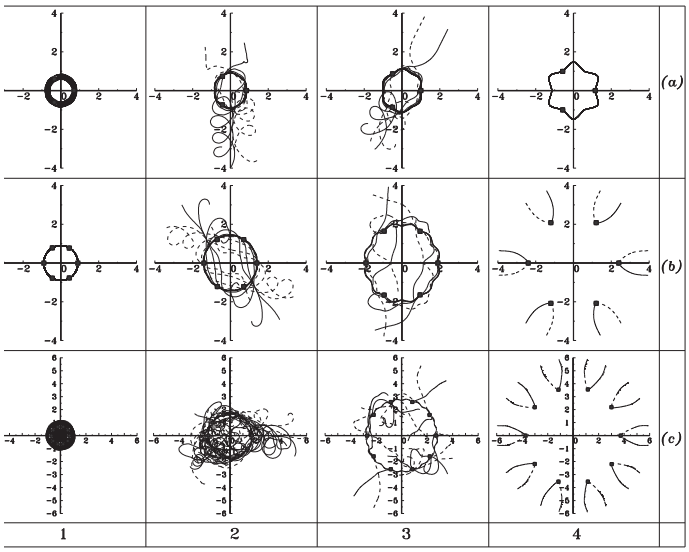

Fig. 19. Trajectories of hetons with initially vertical axes, localized in vicinities of vertices of regular n-polygons with random disturbances in their radial coordinates in accordance with equations (3.39), when their average distance from the centre is $\bar{R} = r + \Delta r(i-1)$, where i is the number of the column in the figure: *(a)* $n = 3$, $r = 0.7$, $\Delta r = 0.15$; *(b)* $n = 6$, $r = 0.9$, $\Delta r = 0.5$; *(c)* $n = 10$, $r = 0.7$, $\Delta r = 1.01$ (these parameters correspond to the locations of crosses in figure 16).

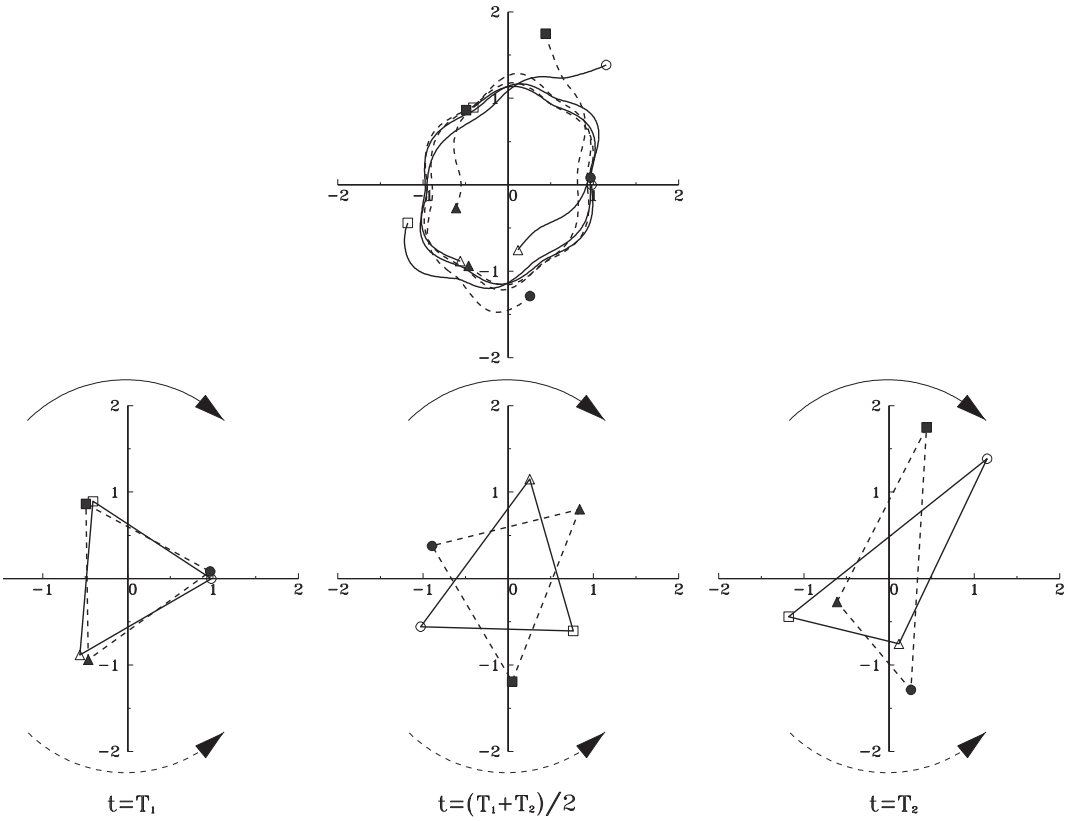

Fig. 20. Top: detailed presentation of the process of passing to the infinite regime for a three-heton system according to the scenario in figure 19.3.a. Bottom: a set of synchronous triangular configurations constructed on vortices from the upper (solid line) and lower (dashed line) layers. Arc arrows show the respective directions of rotation at the stage preceding the scattering of vortices.

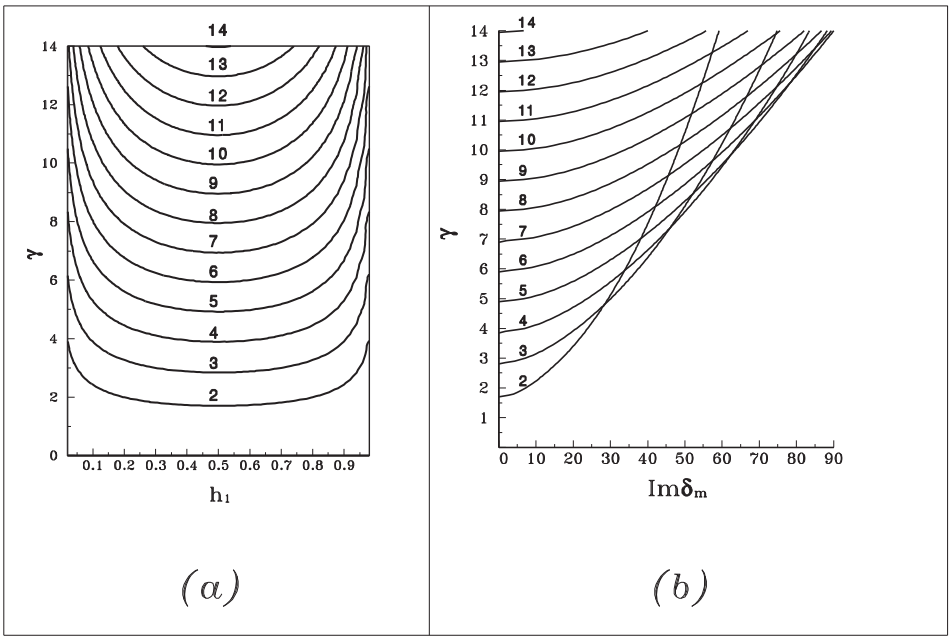

Fig. 21. Neutral stability curves for different modes — *(a)*, and increments in their growth for the case of equal-thickness layers — *(b)*.

to yield applicable results. This approach, in particular, allows modelling the dynamics of an isolated finite-size vortex through the choice of an optimal set of a specified number of discrete vortices.

We will use a more efficient and, in our opinion, more convenient contour dynamics method (CDM). The CDM was used in [181], [182], [186], [187], [189] to consider a series of problems involving heton interaction. Here we will take a quick look at two problems — the stability of an axially symmetric heton (in the context of the problem of splitting two-layer vortices) and interaction between two finite-core hetons which initially had vertical axes.

4.1. Evolution of a solitary heton

Consider a finite-core heton which, in the undisturbed state, has an axially symmetric form: a two-layer structure comprising round vortex patches of unit radius located exactly one under the other. This state is a stationary solution of the conservation equations of potential vorticity (2.1), and the question of the stability of this solution naturally arises.

4.1.1. On the linear analysis of heton stability

Let fluid lines coinciding with the external boundaries of the vortices be described by the parametric relationships

$$r = f_j\big(\theta,\, t;\, \alpha\big), \qquad \alpha = f_j\big(\theta,\, 0;\, \alpha\big), \qquad j = 1,\, 2, \tag{4.1}$$

where parameter α characterizes the radial Lagrangian coordinate of points belonging to contours, and θ is a polar angle. Let us present the function in the form

$$f_j\big(\theta,\, t;\, 1\big) = 1 + \varepsilon_j \exp\big[i\, m\,(\theta - \delta_m t)\big], \qquad |\varepsilon_j| \ll 1, \quad j = 1,\, 2, \quad m \geqslant 1, \tag{4.2}$$

where m is the number of the azimuthal mode, and i is the imaginary unit. Clearly condition $\operatorname{Im}\delta_m > 0$ must hold for unstable modes.

The algorithm for examining stability was described in [119]. In essence, the problem reduces to the analysis of the solution of a system of linear algebraic equations in ε_j.

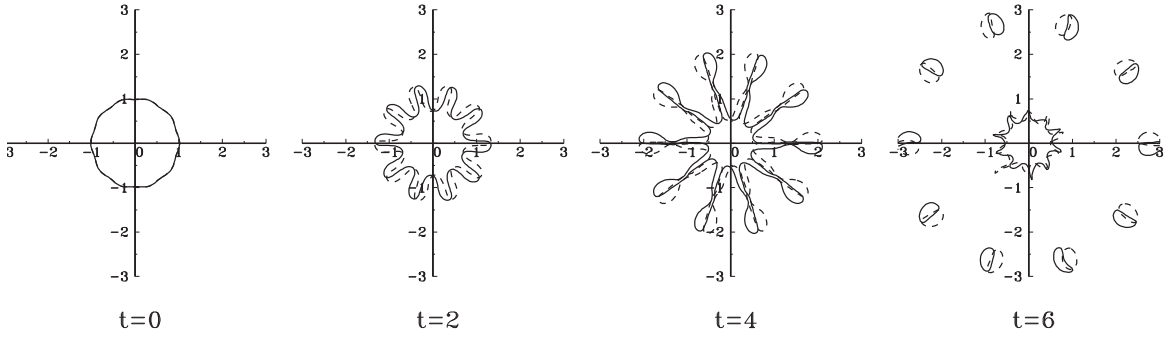

Fig. 22. Evolution of an unstable heton with regular initial disturbances of contours at $\gamma = 14$. The solid line corresponds to the contours of the upper vortex patches, and the dashed line to the lower ones.

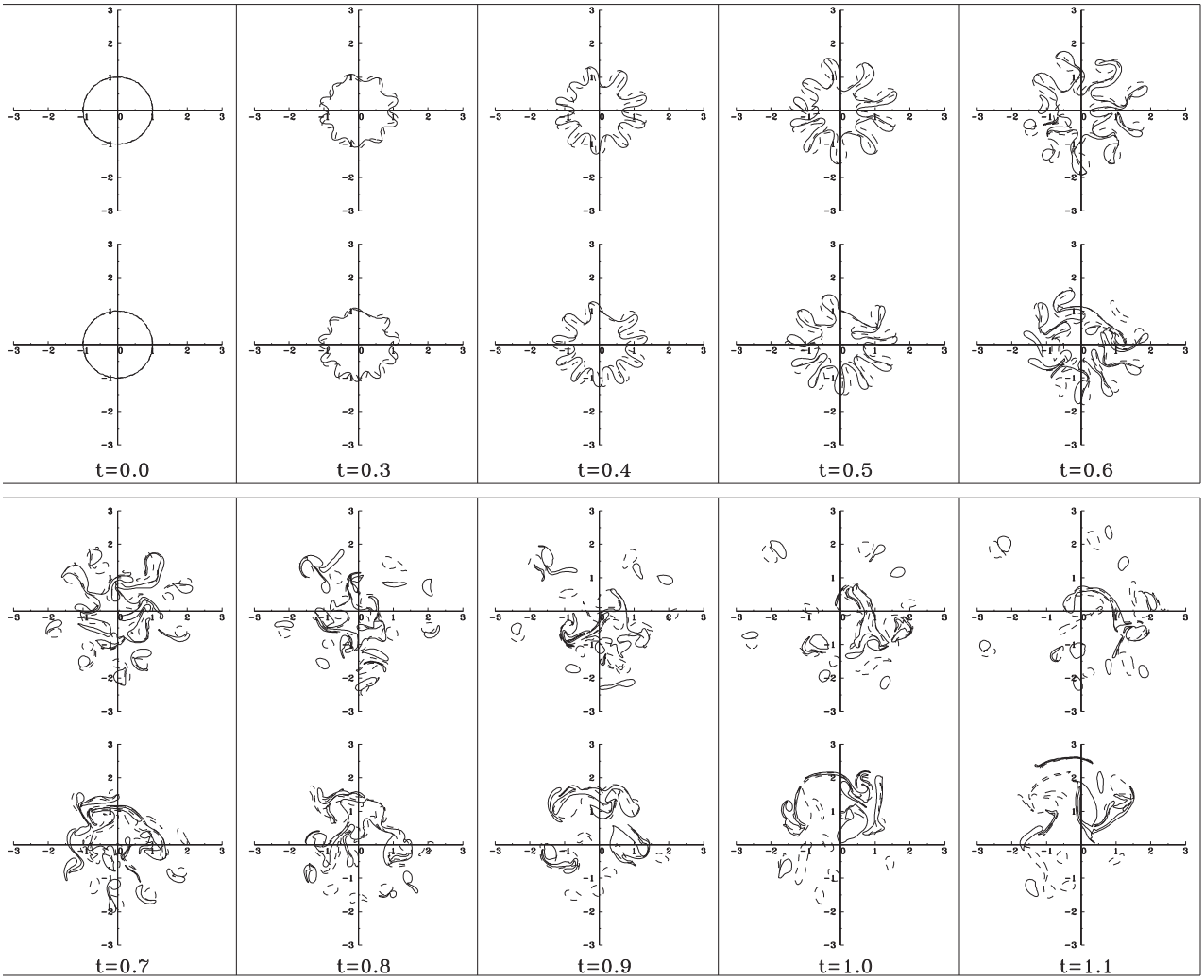

Fig. 23. Evolution of an unstable heton with random initial disturbances of contours at $\gamma = 14$. Synchronous configurations of the vortex patches in the upper and lower layers are shown in the upper and lower lines of the frames, respectively.

Figure 21 shows the of neutral stability curves of unstable modes in the plane (h_1, γ) and the increments in these modes at $h_1 = h_2 = 1/2$ (the calculations discussed below have been made for this case). In figure 21a, the instability domain of each of the modes corresponds to the part of the plane above the respective neutral curve. Obviously, modes with $m \geqslant 2$ can be unstable, and the minimum stability margin is characteristic of the case of equal-thickness layers. The number of unstable modes increases with increasing γ (compare with the example in section 3.4, where an increase in γ for discrete hetons, uniformly distributed over a circumference, was accompanied by a transfer from finite to infinite motions, which is analogous to the decay of an unstable vortex structure).

4.1.2. Modeling the nonlinear phase of heton instability

Calculations made in [119], [186] show that linear analysis of stability correctly predicts the initial phase of instability development, that is, the maximum-instability modes derived from this analysis are, as a rule, those that occur in reality.

If we begin the CDM-based study of the evolution of an unstable vortex from its undisturbed state, the transition to its decay phase will sooner or later take place due to the so-called 'computational noise' caused by errors inevitable in any numerical calculations. The transition to the nonlinear instability stage can be facilitated by introducing small (regular or random) disturbances in the vortex contours. However, if the growth increments of several unstable modes are close to one another, the artificial initial disturbances can bring about the development of instability in a mode other than the most unstable one. Such a case is illustrated by figure 22, where the decay of a heton is shown for a situation where, theoretically, the sixth mode exhibits maximum instability, but where the small disturbances (with an amplitude of 0.02), introduced into the heton contour at the initial time moment, corresponded to $m = 10$ with the result that the tenth mode formed. The time corresponding to each fragment is shown beneath it (the dimensionless time unit is half the rotation period of a fluid particle belonging to the boundary of the undisturbed vortex). Figure 23 gives an example of the evolution of an unstable heton at $\gamma = 14$ for the initial conditions where 120 uniformly distributed marker points were specified at each contour and the fluid particles were subjected to random shifts in radial direction with an amplitude of 0.05. Decay obviously takes place in an essentially asymmetrical regime. To make the figure more comprehensible, the configurations of the vortical patches in the upper and lower layers are artificially offset in relation to one another.

4.2. On the interaction of two finite-core hetons

Different cases of interaction between two finite-core hetons with tilted axes, whose initial locations are symmetrical with respect to one of the axes, have been studied in [181], [182], [186], [187]. However, in order to demonstrate the principal differences with respect to the discrete vortex model we will consider a particular case involving hetons with vertical axes.

Let the vertical axes of two two-layer unit-radius vortices, each consisting of two round vortex patches (in the upper and lower layers), be separated by space b. Figure 24 shows their possible states in this part of the plane of parameters (γ, $b/2$). Here, the dashed line denotes the boundary, defined by the solution of equation (3.27), dividing the plane into parts with finite (on the left) and infinite (on the right) behaviour of discrete vortices. As can be seen, this line matches the case of finite-core vortices between domains S_3 and S_1 quite adequately. It is important to note that this effect was also obtained in [203], where calculations were made with the help of the differential pseudo-spectral code with allowance made for dissipation (biharmonic friction)[9]. It is clear, however, that the interaction of finite-core vortices is far more complicated and has many differences. We will restrict our consideration to three examples, relating to S_2, S_1, and U_1 types, represented in the diagram by circle markers (here

[9]Legras and Dritschel [134] compared the calculation results using the pseudo-spectral method and CDM and found them to be qualitatively similar. However, the authors of [134] believe the CDM to be more convenient for studying the processes of vortex filament formation, and vortex merging and division.

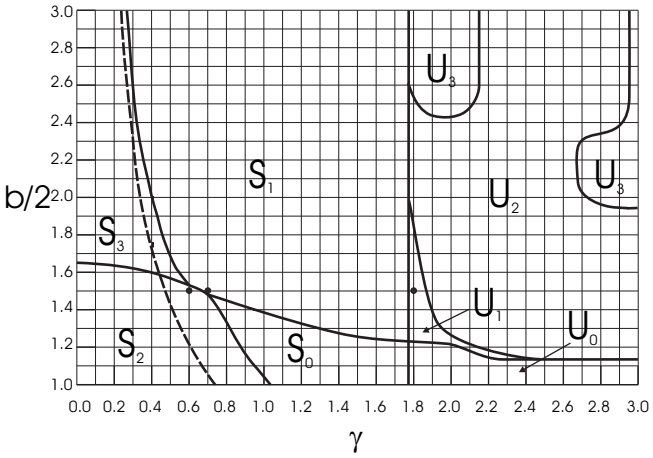

Fig. 24. Diagram of possible regimes of two finite-core hetons consisting of round unit-radius vortex patches, which initially had vertical axes separated by b in the rectangular domain ($\gamma \in (0; 3]$; $b/2 \in [1; 3]$). Denotations for regime subdomains: S_1 corresponds to the motion of hetons in opposite directions along the straight line passing through their centres in the initial time moment (an analogue of type $\{2\}$ motions for discrete vortices); S_0 is the same regime as S_1 but after temporary merging of vortex patches in layers and their subsequent separation; S_2 corresponds to merging of originally round patches into quasi-elliptical vorticity structures rotating in opposite directions; S_3 corresponds to layer-by-layer rotation of vortex patches in opposite directions (an analogue of type $\{3\}$ motions for discrete vortices); U_0 corresponds to heton merging and subsequent division into more than two hetons moving away from one another; U_1 correspond to the moving of two hetons away from one another accompanied by their decay with the formation of four new hetons; U_2 corresponds to the decay of hetons with the formation of non-compensated two-layer vortices, subsequent merging of vortex patches and re-formation of hetons; U_3 corresponds to the decay of hetons into two-layer vortices moving away from one another without subsequent merging.

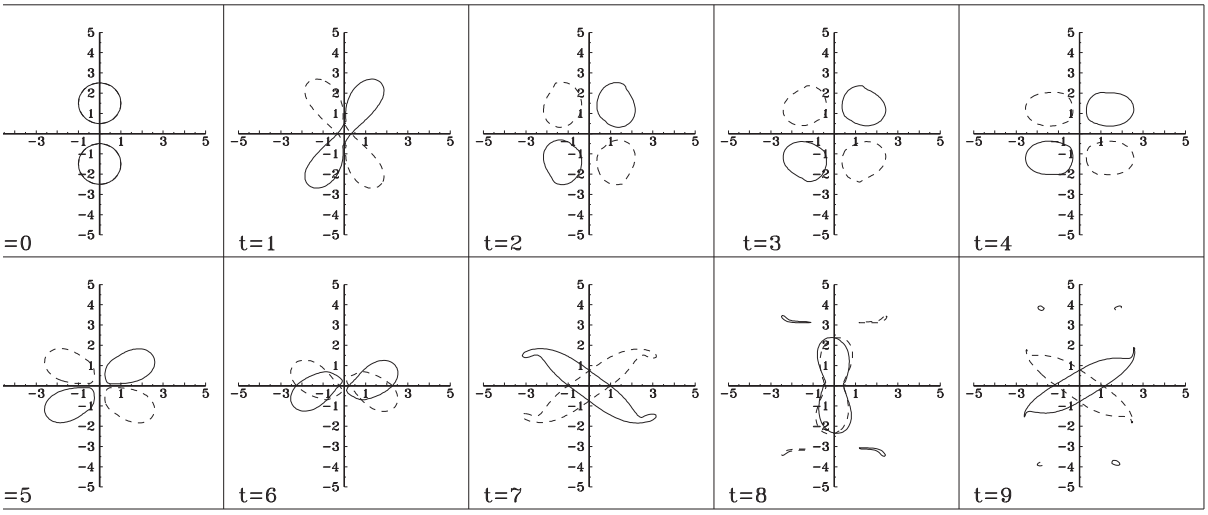

Fig. 25. Example of formation of an S_2 type vortex structure ($\gamma = 0.6$; $b = 1.5$).

the distance between the centres of vortex patches is fixed, and the stratification parameter γ takes of different values).

Figure 25 shows the evolution of a configuration in the case when the vortex patches in both layers merge to form quasi-elliptic vortices while rotating in opposite directions. Note that no evolution takes place in the system within the time interval from 2 to 5 dimensionless time units, when the centre

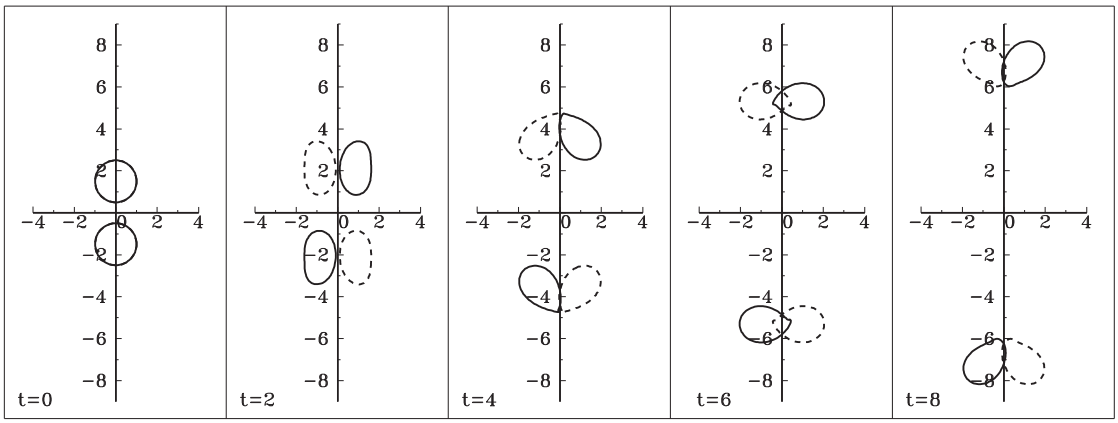

Fig. 26. Example of formation of S_1 type vortex structure ($\gamma = 0.7$; $b = 1.5$)

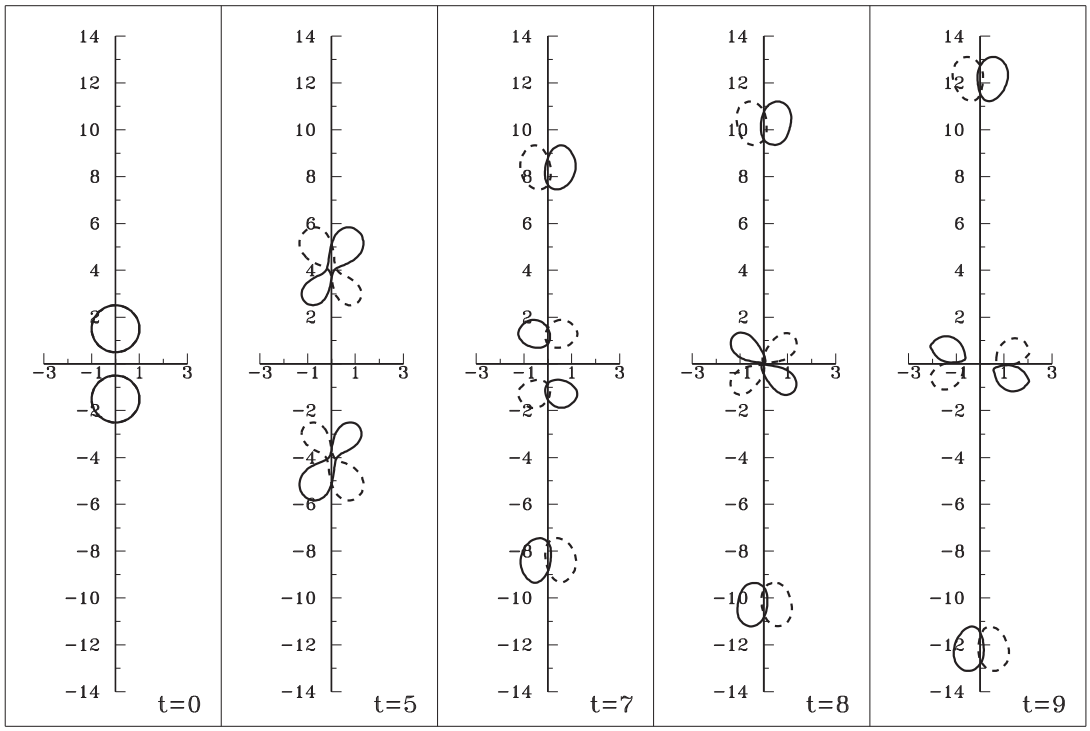

Fig. 27. Example of formation of U_1 type vortex structure ($\gamma = 1.8$; $b = 1.5$)

of each vortex lies in the neighborhood of a fixed saddle point (stagnation point) — the respective marker in figure 24 is very close to the boundary between the finite and infinite motion domains.

Figure 26 shows the formation of hetons with tilted axes and their subsequent divergence. The fact that an insignificant difference in parameter γ between this and the previous experiment makes the results essentially different suggests that the solutions to the respective system of equations are of a 'rigid' nature.

An interesting example of interaction between hetons under the conditions where they are unstable is shown in figure 27 for the case of a relatively weak stratification (or small deformation radius). At the initial stage, the hetons start moving away from one another; however, in doing so, each heton divides into two two-layer pairs, such that one continues moving in the same direction, and the other in the opposite direction. Next, the vortex patches of the hetons involved in the movement towards one another merge temporarily in each layer, then break down, and the newly formed two-layer pairs

move away in the normal direction. If we compare the resultant effects of the interaction of two hetons in this and previous figures, without going into detail regarding intermediate processes, we see that two two-layer pairs moving away from one another form in the first case, and four such pairs form in the second.

The examples considered above, though illustrating only certain features of the interaction between finite-core vortices, demonstrate, in our opinion, the wide diversity of vortex interaction. Different types of interaction between finite-core hetons are discussed in more detail in [181], [182], [186], [203], [204], [205].

5. Other heton theories and the range of applications of the two-layer model with layers of equal thickness

Most of the results in this paper pertain to the case of equal h_1 and h_2. The effect of different layer thicknesses in a two-layer fluid (in particular, for hetons, when $h_1 \sum_{\alpha=1}^{N_1} \Pi_1^\alpha + h_2 \sum_{\alpha=1}^{N_2} \Pi_2^\alpha = 0$) has been studied in [71], [119], [44], [219]. An important effect of layers of different thickness is the increased stability of a solitary axially symmetric heton ($N_1 = N_2 = 1$) with a vertical axis. Thus, it can be seen from figure 21a that a heton where $h_1 = h_2$ has the minimum stability reserve for all unstable modes.

The dynamical consequences of the condition $h_1 \neq h_2$ are similar to those found in multilayer and continuously stratified models, where they are most impressive. We will now consider such models.

5.1. Multilayer model

In multilayer models, the dynamics of discrete vortices, for which the potential vorticity takes the form (2.11) with $j = 1, 2, \ldots, M$ (M is the number of layers), is described by Hamiltonian equations of the form 2.15 with the Hamiltonian

$$\mathcal{H} = -\frac{1}{4\pi} \sum_{\substack{j=1 \\ m=1}}^{M} \sum_{\substack{\alpha=1 \\ \beta=1}}^{N_j, N_m} h_j \left[U_{j1} U_{1m}^{-1} \kappa_j^\alpha \kappa_m^\beta \ln \gamma_* r_{jm}^{\alpha\beta} - \sum_{k=1}^{M-1} U_{jk} U_{km}^{-1} \kappa_j^\alpha \kappa_m^\beta K_0 \left(\gamma_k r_{jm}^{\alpha\beta} \right) \right]. \tag{5.1}$$

Here γ_k are eigenvalues of the potential vortex operator, such that $0 = \gamma_0 < \gamma_1 < \gamma_2 < \ldots < \gamma_{M-1}$, and U_{jm} is a matrix with dimensions of $M \times M$, composed of the respective eigenvectors. The structure of the flow induced by vortices is characterized by several Rossby scales ($L_k = 1/\gamma_k$). The potential vortex can be distributed either uniformly over the thickness of each layer or within several layers.

A hierarchy of hetons exists in the multilayer model [86], [88]. The integral vorticity of each heton is zero. The vertical vorticity distribution follows the structure of the baroclinic modes of the potential vortex operator. Therefore, it is natural to call such baroclinic vortex structures *m-modal hetons* ($m = 1, 2, \ldots, M-1$)[10].

The case of $M = 2$, corresponding to a two-layer model, involves only one baroclinic mode, i. e., a mere heton. At $M > 2$, only the first of m-modal hetons is very close to a two-layer one (figure 28). However, even in this case, the structure of the velocity field induced by the heton, and hence the velocity of its propagation, depend on more than only the first Rossby baroclinic radius. When all the vortices lie along the same vertical, this m-modal heton will be considered, as before, to have a *vertical* axis, whereas when the vortices are offset in relation to the vertical, it will be considered to have an *arc-like* axis.

[10] In our opinion, the term *modon*, which was applied to such vortices in [86], [183], would be more suitable. However, in the oceanographical literature, the term *modon* has already been associated with finite-core dipole vortex structures [195], [107], [103]).

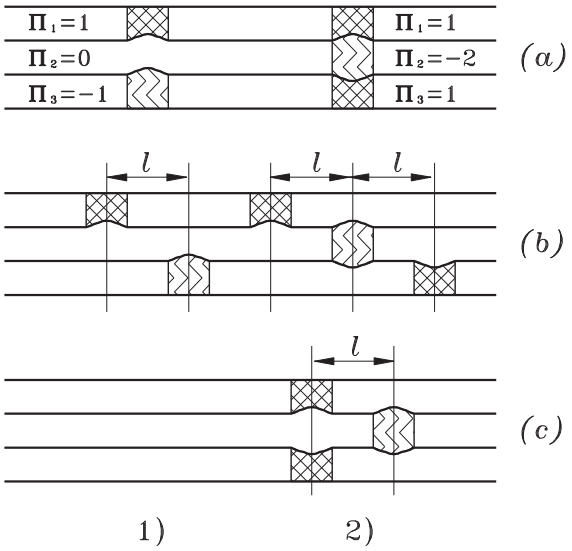

Fig. 28. Schematic representation of a finite-core heton with a *vertical* axis — *(a)*, with *tilted* axis — *(b)*, and with *arc-wise* axis — *(c)* in the case of a three-layer fluid with layers of equal thickness: 1) 1-modal heton; 2) 2-modal heton.

For example, in the case of a model with three equal-thickness layers $h_1 = h_2 = h_3 = h$ and $\Delta\rho_1 = \Delta\rho_2 = \Delta\rho$, we have $\gamma_1 = 0, \gamma_2 = \sqrt{F} = \gamma, \gamma_3 = \sqrt{3F} = \gamma\sqrt{3}$, where $F = \rho_* \Omega^2 / gh\Delta\rho$. If the distance between the vortices is l, then, by introducing the dimensionless distance $L = l\sqrt{F} = l\gamma$, we find that the propagation velocity of a 1-modal heton with $\kappa_1^1 = -\kappa_3^1 = \kappa$, $\kappa_2^1 = 0$ (figure 28.1.b)[11], a non-zero momentum, and zero angular momentum is

$$v = \frac{\gamma\kappa}{3\pi L}\left[1 - \sqrt{3}LK_1\left(\sqrt{3}L\right)\right] \tag{5.2}$$

(compare with (3.9)).

A 2-modal heton with an *arc-like* axis, comprising vortices with intensities of $\kappa_1^1 = \kappa_3^1 = \kappa$, $\kappa_2^1 = -2\kappa$ (see figure 28.2.c), moves with a velocity of

$$v = \frac{\gamma\kappa}{6\pi L}\left[1 - \frac{3L}{2}K_1(L) + \frac{\sqrt{3}L}{2}K_1\left(\sqrt{3}L\right)\right]. \tag{5.3}$$

Comparison of (5.2) and (5.3) shows that the velocity of an m-modal heton decreases with increasing m because of the increasing degree of localization in the horizontal direction.

However, when a 2-modal heton has zero momentum (figure 28.2.b), it has no translational motion, and the angular velocity of its rotation is

$$\omega = \frac{\gamma^2\kappa}{6\pi L^2}\left[\frac{3}{2} - 2\sqrt{3}LK_1\left(\sqrt{3}L\right) + \frac{3}{2}LK_1(2L) - \frac{\sqrt{3}}{2}LK_1\left(2\sqrt{3}L\right)\right]. \tag{5.4}$$

Note that vortex structure (5.4) incorporates the properties of a *heton* (zero total intensity) and an analogue of an *ordinary (two-tier) roundabout*. Therefore, it is natural to call this structure a *three-tier roundabout*.

Let us consider several more examples of solutions describing uniformly rotating vortex structures in a three-layer fluid:

[11] Discrete vortices are meant in this case, and the references to this figure pertain to the locations of the centres of vortex patches.

- A *tripole*, localized in the upper $\left(\kappa_1^1 = -2\kappa,\ \kappa_1^2 = \kappa_1^3 = \kappa\right)$ or lower $\left(\kappa_3^1 = -2\kappa,\ \kappa_3^2 = \kappa_3^3 = \kappa\right)$ layer, the peripheral vortices of which rotate with an angular velocity of

$$\omega = \frac{\gamma^2\kappa}{6\pi L^2}\left[\frac{3}{2} + 3LK_1(L) + \sqrt{3}LK_1\left(\sqrt{3}L\right) - \frac{3}{2}LK_1(2L) - \frac{\sqrt{3}}{2}LK_1\left(2\sqrt{3}L\right)\right]. \tag{5.5}$$

- A *tripole*, localized in the middle layer $\left(\kappa_2^1 = -2\kappa,\ \kappa_2^2 = \kappa_2^3 = \kappa\right)$, with an angular velocity of

$$\omega = \frac{\gamma^2\kappa}{6\pi L^2}\left[\frac{3}{2} + 4\sqrt{3}LK_1\left(\sqrt{3}L\right) - 2\sqrt{3}LK_1\left(2\sqrt{3}L\right)\right]. \tag{5.6}$$

- A *roundabout*, comprising vortices with intensities of $\kappa_1^1 = \kappa_1^2 = \kappa$ in the upper layer (or $\kappa_3^1 = = \kappa_3^2 = \kappa$ in the lower layer) and the central vortex $\kappa_2^1 = -2\kappa$ in the middle layer. The angular velocity is

$$\omega = \frac{\gamma^2\kappa}{6\pi L^2}\left[\frac{3}{2} - 2\sqrt{3}L\left(K_1\left(\sqrt{3}L\right) + K_1\left(2\sqrt{3}L\right)\right)\right]. \tag{5.7}$$

- A symmetric *inverse roundabout*, comprising two vortices in the middle layer $\kappa_2^1 = \kappa_2^2 = \kappa$ and one vortex in the upper $\kappa_1^1 = -2\kappa$ (or lower $\kappa_3^1 = -2\kappa$) layer. In this case the angular velocity is

$$\omega = \frac{\gamma^2\kappa}{6\pi L^2}\left[\frac{3}{2} - 2\sqrt{3}LK_1\left(\sqrt{3}L\right) - \frac{3}{2}LK_1(2L) - \frac{\sqrt{3}}{2}LK_1\left(2\sqrt{3}L\right)\right]. \tag{5.8}$$

- A symmetric *roundabout*, comprising a vortex $\kappa_1^1 = -2\kappa$ in the upper layer (or $\kappa_3^1 = -2\kappa$ in the lower layer) and two vortices with intensities of $\kappa_3^1 = \kappa_3^2 = \kappa$ in the lower layer (or in the second case, $\kappa_1^1 = \kappa_1^2 = \kappa$, two vortices in the upper layer). The angular velocity is

$$\omega = \frac{\gamma^2\kappa}{6\pi L^2}\left[\frac{3}{2} - 3LK_1(L) + \sqrt{3}LK_1\left(\sqrt{3}L\right) + \frac{3}{2}LK_1(2L) - \frac{\sqrt{3}}{2}LK_1\left(2\sqrt{3}L\right)\right]. \tag{5.9}$$

- Vortex structure with tilted axis, complementing (5.2), for which $\kappa_1^1 = \kappa_3^1 = \kappa$, $\kappa_2^1 = 0$, and determining a *top* with an angular velocity of

$$\omega = \frac{\gamma^2\kappa}{3\pi L^2}\left[1 - \frac{3L}{2}K_1(L) + \frac{\sqrt{3}L}{2}K_1\left(\sqrt{3}L\right)\right]. \tag{5.10}$$

We note also the existence of *heton* nonmodal structures with tilted axes, localized either in the two upper layers ($\kappa_1^1 = -\kappa_2^1 = \kappa$, $\kappa_3^1 = 0$) or in the two lower layers ($\kappa_3^1 = -\kappa_2^1 = \kappa$, $\kappa_1^1 = 0$), moving with a velocity of

$$v = \frac{\gamma\kappa}{6\pi L}\left[1 - \sqrt{3}LK_1\left(\sqrt{3}L\right)\right], \tag{5.11}$$

and associated nonmodal structures of the *top* type ($\kappa_1^1 = \kappa_2^1 = \kappa$, $\kappa_3^1 = 0$ and $\kappa_3^1 = \kappa_2^1 = \kappa$, $\kappa_3^1 = 0$), rotating with an angular velocity of

$$\omega = \frac{\gamma^2\kappa}{3\pi L^2}\left[1 - \sqrt{3}LK_1\left(\sqrt{3}L\right)\right]. \tag{5.12}$$

The properties of hetons (5.11) were studied in [88], [46].

Studies condacted in [86] showed the interaction between 1- modal hetons (figure 28a) to be analogous to the heton interaction in the two-layer model (see figures 9 and 10). In the case of the

interaction of 2-modal hetons (figure 28a, right), type {2} trajectories become asymmetrical about the y-axis because of the asymmetry that appears in the inter-layer interaction. However, a 2-modal heton with an arc-wise axis forms asymptotically (at $t \to \infty$), see figures 28c and (5.3). Such a heton is the simplest example of a quasi-stationary vortex cluster, if the vortex centres in the upper and lower layers are offset with respect to one another by a small distance a. At $a \ll l$, the interaction between the upper and lower vortices results in their mutual rotation, i. e., the formation of a vortex top, the interaction of which with an inversely rotating vortex in the middle layer brings about the movement of the vortex system as a whole, i. e., a heton cluster. Heton clusters are typical examples of a vortex structure in multilayer models [86], [88].

The possible existence of four discrete vortices was mentioned by Marshall [139] for the case of a medium comprising four layers of equal thickness. The effects of both stratification and the finite size of the vortex core in the generation of a chaotic state in the case of four and more layers are examined in [139].

The dynamics of *finite-core* vortices within the context of a three-layer CDM-model was studied in [183], [184], [185]. Here the stability of axially symmetric three-layer (and, in particular, modal) vortex structures was examined and the numerical calculation results were shown to be in agreement with the experiment [180]. It was shown also that disturbances of the upper and lower interfaces between the layers with density jumps $\Delta\rho_1$ and $\Delta\rho_2$ such that $\Delta\rho_1 \gg \Delta\rho_2$ (which is typical of the ocean) generate the development of low and high unstable modes, respectively. This corroborates an analogous statement in [179] regarding the stability analysis of a three-layer flow in a channel.

The problem of stability and dynamics of finite-core three-layer modons (vortices with dipole barotropic and axially symmetric baroclinic components) on β-plane is considered in [107].

5.2. Model of a continuously stratified fluid

Adiabatic quasi-geostrophic flows in a continuously stratified fluid are described by the potential vortex equation $\Pi(x,\, y,\, z,\, t)$ [102], [167]

$$\frac{D\Pi}{Dt} = 0, \tag{5.13}$$

$$\Pi = \nabla^2\Psi + \frac{\partial}{\partial z}\left[\frac{f^2}{\tilde{N}^2}\frac{\partial\Psi}{\partial z}\right], \tag{5.14}$$

where Ψ is the stream function and $\tilde{N}$ is the Brunt–Väisälä frequency.

The horizontal $\mathbf{u} = (u,\, v)$ and vertical w velocities, pressure anomalies p, and the density ρ are related to the stream function by equations

$$u = -\frac{\partial\Psi}{\partial y}, \qquad v = \frac{\partial\Psi}{\partial x}, \tag{5.15}$$

$$w = \frac{f}{\tilde{N}^2}\left[\frac{\partial}{\partial t}\frac{\partial\Psi}{\partial z} + \left(\Psi,\, \frac{\partial\Psi}{\partial z}\right)\right], \tag{5.16}$$

$$p = f\rho_0\Psi, \tag{5.17}$$

$$\rho = \frac{f\rho_0}{g}\frac{\partial\Psi}{\partial z}. \tag{5.18}$$

In this case, the potential vorticity is specified as localized along three coordinates

$$\Pi(x, y, z) = \sum_{\alpha=1}^{N} \Gamma_\alpha \delta(x - x_\alpha)\, \delta(y - y_\alpha)\, \delta(z - z_\alpha), \tag{5.19}$$

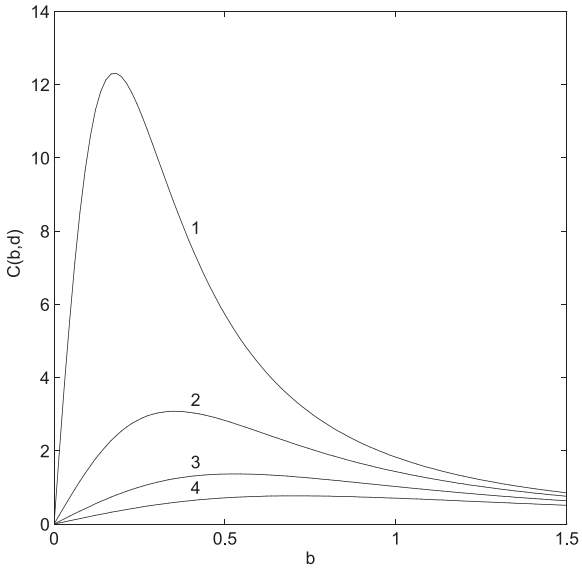

Fig. 29. The velocity of an individual three-dimensional heton $C(b,d)$ vs. the horizontal distance between vortices b at vertical distances of 1) $d = 0.25$, 2) $d = 0.5$, 3) $d = 0.75$, 4) $d = 1$.

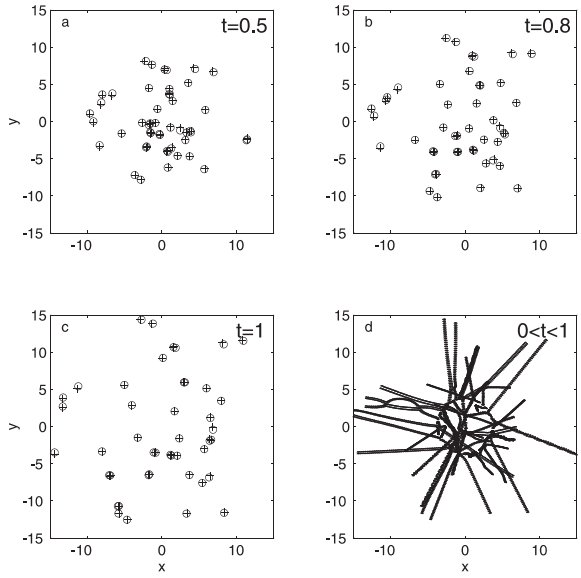

Fig. 30. Results of numerical experiments on the degeneration of a temperature anomaly, which are represented by heton distributions in different time moments *(a)–(c)*. Heton trajectories for a fixed time interval *(d)*.

where Γ_α is the intensity of the vortex with the number α. This distinguishes the continuously stratified models from multilayer models where the potential vorticity is assumed to be uniformly distributed over the layer thickness.

The flow induced by three-dimensional point anomalies of potential vorticity (5.19) in a uniformly stratified fluid with horizontal boundaries and a thickness of H, which can be described by Brunt-Väisälä frequency $\tilde{N}$, is characterized by the stream function

$$\Psi(x,y,z) = \sum_{\alpha=1}^{N} \Gamma_\alpha G(x,y,z;x_\alpha,y_\alpha,z_\alpha). \tag{5.20}$$

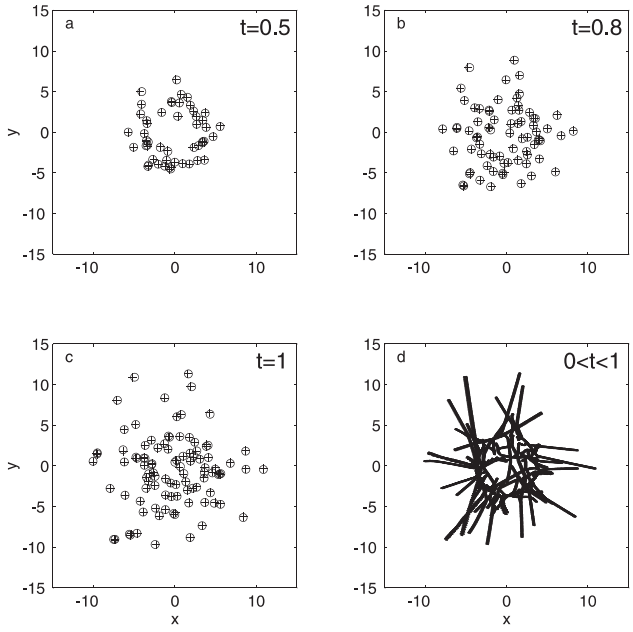

Fig. 31. Numerical experiments with equilibrium temperature anomaly represented by heton distributions in different time moments *(a)–(c)*. Heton trajectories for a fixed time interval *(d)*.

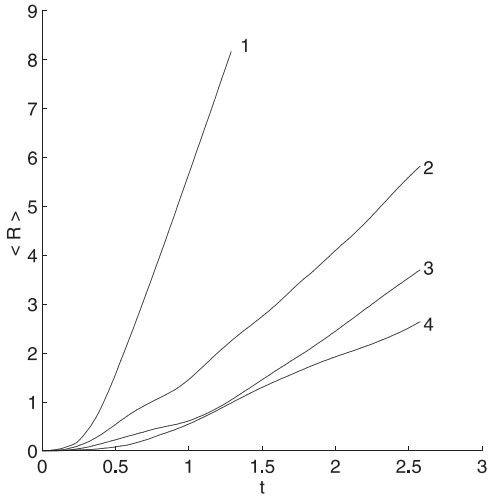

Fig. 32. Time dependence of the mean radius of temperature anomaly at different relative thicknesses of the mixed layer: 1. $h_{mix}/H = 1/4$; 2. $h_{mix}/H = 1/2$; 3. $h_{mix}/H = 3/4$; 4. $h_{mix}/H = 1$, where H is the total depth. The averaging was carried out over 10 realizations.

Green's function $G(x, y, z; x_0, y_0, z_0) = G(r, z, z_0)$ is specified as

$$G(r, z, z_0) = \sum_{m=-\infty}^{+\infty} \Big[G_0(r, z - z_0 + 2Hm) + G_0(r, z + z_0 + 2Hm) \Big], \tag{5.21}$$

$$G_0(r, z) = -\frac{\tilde{N}}{4\pi f} \left(r^2 + \frac{\tilde{N}^2}{f^2} z^2 \right)^{-\frac{1}{2}}, \tag{5.22}$$

where $G_0(r, z)$ is Green's function in an unlimited medium and $r = \sqrt{(x - x_0)^2 + (y - y_0)^2}$.

Calculating the energy of heton interaction $\mathcal{H}$ by using (5.19)–(5.22) and applying the standard procedure for deriving the motion equations [71], we obtain the Hamiltonian equations of motion

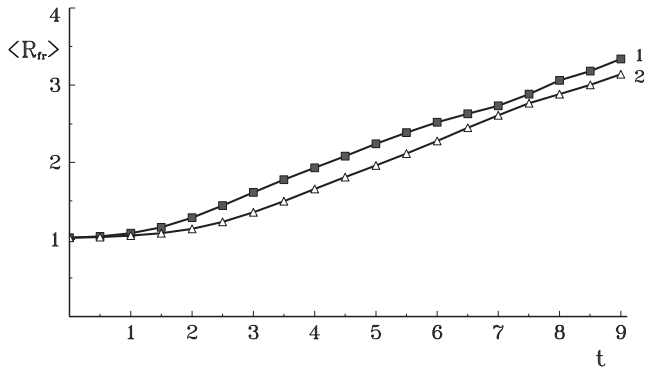

Fig. 33. Time dependence of $\langle R_{fr} \rangle$ for $\gamma = 14$ — 1; $\gamma = 10$ — 2.

for the horizontal coordinates of vortices. These equations coincide with (3.15) with intensities κ replaced by Γ. The dependence of the Hamiltonian on the vertical coordinates z_α in these equations is parametric because the dependence of the evolution equation on the potential vortex in the quasi-geostrophic approximation is also parametric. The system of equations obtained has integrals of motion — momentum and angular momentum — which also coincide with the traditional analogues with intensities κ replaced by the respective intensities Γ.

The closest to the two-layer model with layers of equal thickness (both in terms of kinematic and dynamic properties) is the model of a continuously stratified fluid with a constant Brunt-Väisälä frequency where quasi-three-dimensional hetons are composed of vortices with anticyclonic circulation $\Gamma_{a\alpha} < 0$ and coordinates $x_{a\alpha}$, $y_{a\alpha}$, $z_{a\alpha} = H/4$ and vortices with cyclonic circulation $\Gamma_{c\alpha} > 0$ and coordinates $x_{c\alpha}$, $y_{c\alpha}$, $z_{c\alpha} = 3H/4$ (symmetric model). The Hamiltonian of the heton system in this case takes the form

$$\mathcal{H} = -\sum_{\substack{\alpha,\beta=1 \\ \alpha<\beta}}^{N} \Big[\Gamma_{a\alpha}\Gamma_{a\beta}G\Big(r_{a\alpha,a\beta}, \frac{H}{2}, \frac{H}{2}\Big) + \Gamma_{c\alpha}\Gamma_{c\beta}G\Big(r_{c\alpha,c\beta}, \frac{3H}{2}, \frac{3H}{2}\Big)\Big] + \\ + \sum_{\alpha,\beta=1}^{N} \Gamma_{a\alpha}\Gamma_{c\beta}G\Big(r_{a\alpha,c\beta}, \frac{H}{2}, \frac{3H}{2}\Big). \qquad (5.23)$$

In this model, the vortices are located symmetrically about the middle of the layer and also symmetrically within the equivalent upper $0 < z < H/2$ and lower $H/2 < z < H$ layers. Since the vertical coordinates of the vortices $z_{a\alpha} = H/4$, and $z_{c\alpha} = 3H/4$ do not change during their motion (the dependence of the Hamiltonian (5.23) is only parametric), the kinematic correspondence with the two-layer model with equal-thickness layers holds within any time interval. In the general case, the model of a continuously stratified fluid enables studying flows induced by hetons with an essentially asymmetrical vertical distribution of potential vorticity [84].

In the case of quasi-three-dimensional hetons composed of vortices with a cyclonic circulation $\Gamma_{c\alpha} > 0$ and coordinates $x_{c\alpha}$, $y_{c\alpha}$ on the surface of the fluid $z_{c\alpha} = 0$ and with an anticyclonic circulation $\Gamma_{a\alpha} < 0$ and coordinates $x_{a\alpha}$, $y_{a\alpha}$ within the water volume $z_{a\alpha} = h$, the Hamiltonian takes the form

$$\mathcal{H} = -\sum_{\substack{\alpha,\beta=1 \\ \alpha<\beta}}^{N} \Big[\Gamma_{c\alpha}\Gamma_{c\beta}G\Big(r_{c\alpha,c\beta}, 0, 0\Big) + \Gamma_{a\alpha}\Gamma_{a\beta}G\Big(r_{a\alpha,a\beta}, h, h\Big)\Big] + \\ + \sum_{\alpha,\beta=1}^{N} \Gamma_{c\alpha}\Gamma_{a\beta}G\Big(r_{c\alpha,a\beta}, 0, h\Big). \qquad (5.24)$$

Solution of the equations of motion with the Hamiltonian (5.24) for the case of a single heton shows that the three-dimensional heton moves in the same manner as the two-dimensional heton

(uniformly and rectilinearly) but with a velocity

$$C = -\frac{\partial}{\partial b} G(b, 0, d) = \sum_{m=-\infty}^{+\infty} \frac{2b}{\left[b^2 + (d + 2m)^2\right]^{3/2}}, \tag{5.25}$$

where C is standardized by $\Gamma/2\pi H\tilde{\lambda}$, $b = |r_c - r_a|/\tilde{\lambda}$, and $d = h/H$ are dimensionless distances between the vortices in the horizontal and vertical directions, respectively, and $\tilde{\lambda} = \tilde{N}H/f$ is the Rossby radius in the continuous model.

A notion of the common features of, and distinctions between, the dynamics of vortices in the continuous and two-layer models can be derived from the comparison of expressions for the velocity of motion of an individual three-dimensional heton (5.25) and a two-dimensional heton (3.9), as well as from figures 29 and 2.

The velocity has a solitary maximum, the magnitude of which decreases with increasing distance between the vortices along the vertical coordinate. At $b^2 + d^2 \ll 1$, solution (5.25) has an asymptotic

$$C = \frac{2b}{\left(b^2 + d^2\right)^{3/2}}, \tag{5.26}$$

describing hetons in a semi-infinite medium $H \to \infty$ or in the limit of a small heton vertical dimension $d \to 0$. At $b \ll d$, we have

$$C = b\left[\frac{2}{d^3} + \frac{1}{4}\zeta\left(3, \frac{d}{2}\right) + \frac{1}{4}\zeta\left(3, -\frac{d}{2}\right)\right], \tag{5.27}$$

where $\zeta(q, z)$ is the Riemann function. The heton velocity is maximum at $d \ll 1$:

$$C_{max}(d) = \frac{4}{3\sqrt{3}}\frac{1}{d^2}, \quad b_{max} = \frac{d}{\sqrt{2}}. \tag{5.28}$$

The velocity of hetons increases linearly with distance for small b values, attains its maximum, and then decreases in accordance with the algebraic law $\sim b^{-2}$, if distance b between the vortices is greater than the local Rossby radius $\tilde{N}h/f$ but less than the conventional Rossby radius $\tilde{\lambda} = \tilde{N}H/f$.

Thus, analysis of (5.25) shows that at $r \leqslant \tilde{\lambda}$, the dynamics of vortices in the continuous model essentially differs from the respective dynamics in the two-layer and multi-layer models. To examine the relationship between the continuous and multilayer models at scales $r \gg \tilde{\lambda}$, we write Green's function in an equivalent form

$$G(r, z, z_0) = \frac{1}{H}\left[g_0(r) + \sum_{m=1}^{\infty} g_m(r) Z_m(z) Z_m(z_0)\right], \tag{5.29}$$

$$g_m(r) = \begin{cases} \dfrac{1}{2\pi}\ln\left(\dfrac{re^c}{2L_*}\right), & m = 0, \\ -\dfrac{1}{2\pi}K_0(\lambda_m r), & m = 1, 2, \ldots, \end{cases} \tag{5.30}$$

$$Z_0 = 1, \qquad Z_m = \cos\left(\frac{\pi m}{H} z\right), \qquad m \geqslant 1, \tag{5.31}$$

where $\lambda_m = \pi m/L$, c is Euler's constant.

Although the structure of Green's function in the general case depends on the Brunt–Väisälä frequency profile $\tilde{N}(z)$ and boundary conditions, the asymptotic behaviour of Green's function is universal at both small and large scales and can be adequately approximated by expressions (5.22) and (5.30). At small scales ($r \ll \tilde{\lambda}$), the stratification can always be approximated by a linear velocity profile

(constant Brunt–Väisälä frequency), and hence Green's function is algebraic, see (5.21) and (5.29). At large scales ($r \gg \tilde{\lambda}$), Green's function has a universal barotropic (logarithmic) asymptotic and is insensitive to the details of stratification, see (5.22) and (5.30).

Taking the first two terms ($m = 1, 2$) in expansions (5.22) and (5.30), we find that the vortex interaction in the continuous model at scales $r \gg \tilde{\lambda}$ coincides with that described by the two-layer model with the effective intensity of two-layer vortices $\kappa = \Gamma H$. Thus, for the velocity of a solitary heton at $b > \lambda_1^{-1}$, we have

$$C = \frac{2}{b}\left[1 + \lambda_1 b K_1(\lambda_1 b)\cos(\pi d)\right], \tag{5.32}$$

with an estimate for the maximum velocity

$$C_{max}(1) = 0.8, \quad b_{max} = 1.11\lambda_1^{-1}. \tag{5.33}$$

The velocities of a solitary heton and a heton in a two-layer fluid coincide exactly in the symmetrical model, see (5.24). The expression for the velocity obtained within the context of the same approximation as (5.32) has the form

$$C = \frac{1}{b}\left[1 - \lambda_1 b K_1(\lambda_1 b)\right], \tag{5.34}$$

and after identifying λ_1^{-1} as the Rossby radius of the two-layer model and γ as κH, this equation coincides with (3.9). Incorporating the next N terms $m = 3, ..., N$ in the expansion of Green's function for the model of a continuously stratified fluid (5.29) yields modifications that have analogues only in equivalent N-layer models. The aforementioned asymptotic equivalence of continuous and N-layer models shows that the classification of stationary heton-type vortex structures for N-layer models (reflected in Table 2) also holds in the case of a continuously stratified fluid. The solution for hetons with arc-type axes and for triangular hetons is given in explicit form in [73].

The dynamics of hetons in the continuous model was examined in [72], [73], [79], [136]. A number of exact solutions for a model of a semi-infinite medium were obtained in [72]. In [79], an interpretation is given of the equations of motion for two hetons described by the Hamiltonian (5.29) and the interaction of hetons randomly distributed over a circumference is examined. The dynamics of a heton population is described in more detail in section 6.1 in the context of the problem of simulating heat transfer during the development of deep convection in the ocean. The problem of the formation of heton clusters is discussed in [136]. Lim and Majda [136] suggested a generalization of the theory [72], [79] through the incorporation of surface temperature anomalies. This generalization, however, is merely terminological, since, in according to the Bretherton theorem [29], it does not cause any new effects because the properties of surface temperature anomalies coincide, both kinematically and dynamically, with the properties of potential vorticity anomalies, when the latter are located on the surface. This equivalence is accounted for implicitly in models [72], [79].

The effect of the finite vortex size in the continuous model can be taken into account, for example, within the context of the distributed ellipsoidal vortex approximation. In this case, the potential vorticity is assumed to be uniform within the ellipsoid and zero outside it [221], [222], [223], [224], [146], [197]. The equations of motion for the centres of ellipsoids and their axes form a closed Hamiltonian system of equations [222], [146]. As shown in [222], [197], assuming that the ratio of the ellipsoid size to the distance between ellipsoids is small, the equations of motion of centres coincide with the equations of motion of discrete vortices. The same conclusion also holds for arbitrary localized three-dimensional anomalies of potential vorticity with a finite carrier [73].

An illustrative example of a CDM application within the context of the model of a continuously stratified fluid [115] is provided by Kozlov and Mazur [118], who studied the evolution of an ellipsoidal vortex approximated by a set of infinitely thin fluid disks. The authors examined the process of the breaking down of an unstable strongly elongated elliptic disk, thus demonstrating a possible mechanism for the formation of the quasi-circular intra-thermocline lenses observed in the North Atlantic.

Summarizing the results discussed in sections 5.1-5.2, we can conclude that the two-layer model adequately reproduces the asymptotic dynamics of vortices in a multilayer fluid at scales greater than the first Rossby scale but far smaller than the Oboukhov scale ($L_* \gg \tilde{\lambda} \geqslant L_1$). The same property [84] persists in continuous-stratification models for localized three-dimensional vortices [72], [79], [84], [197], [136]. It should be remembered, however, that both the multilayer and continuously stratified models can have solutions for which there are no direct analogues in the two-layer model, for example, a two-mode heton (5.3) and a three-tier top (5.4).

6. Some applied aspects of heton theories

The heton concept is used in tropical meteorology for studying the mechanisms known to control the dynamics of developed tropical cyclones (hurricanes), for example, their typical trajectories [61], in oceanology for the examination of the mechanisms that characterize typical trajectories of Mediterranean intra-thermocline [98] and deep-seated [197] lenses, and in the investigations of possible scenarios of heat transfer by localized baroclinic vortices that form during the development of deep convection in the ocean [128], [129], [141], [50], [43], [44], [84]. All the geophysical vortex structures mentioned above have a number of features in common, such as their essentially baroclinic nature (since they form in a stratified medium), their local character because of their generation due to the action of local heat (or mass) sources, and, finally, their zero total potential vorticity due to the fact that heat sources do not generate total angular momentum. Thus, the necessary conditions for the applicability of heton theories are met.

6.1. Heton theories and the problem of heat transfer in deep convection

In its purest form, the heton theory is widely used in studying the dynamic phase of the development of deep convection in the ocean [129], [130], [141], [84], [50], [44], [77], [78].

Deep convection develops when the ocean surface cools in a local area with the characteristic dimensions greater than the Rossby radius. The cooling causes convective mixing of the top oceanic layer and brings about the formation of a temperature anomaly. The downwelling of the cooled fluid is controlled by rotation [51], [26], [27], [28], [59], [92], [141], [101], [30], [156], [217] with the resulting formation of an anomaly of potential vorticity with a cyclonic circulation at the surface and an anticyclonic circulation in the main water body, that is, with the formation of a heton [129]. The temperature anomalies with a strong horizontal heterogeneity are approximated by populations of discrete hetons, while quasi-homogenous anomalies are approximated by finite-core hetons, which can be quite adequately described by using CDM. Thus, studying the subsequent evolution of the temperature anomaly reduces to the problem of nonlinear heton dynamics.

With larger potential vorticity anomalies, which satisfy the conditions of the development of baroclinic instability, smaller hetons form at the boundary of the anomaly. These hetons separate from the boundary and freely propagate through the water mass, where they execute horizontal mixing. The heton formation phase can be adequately described by the linear instability theory (see section 4.1.1), whereas the scatter phase is clearly illustrated by the problem of N discrete hetons, uniformly distributed over a circumference (figures in section 3.4.2), and the problem of the breaking down of an unstable finite-core heton (figures 22 and 23).

Examples shown in figures 30 and 31 demonstrate the evolution of a heton population in the context of the model of a continuously stratified fluid with a constant vertical density gradient. The initial distribution of hetons in figure 30 over the circumference is random, and their spreading simulates the degradation of a temperature anomaly. The hetons in figure 31 are randomly generated on a circumference. This model describes a stationary temperature anomaly, where the heat flux from the surface is balanced by the heat flux carried by hetons [129]. The results of a large number of numerical experiments [84] show that the mean radius of a degenerating temperature anomaly (at

different values of the mixed layer thickness h_{mix}) increases linearly with time (figure 32). Calculations for finite-core vortices (see section 3.1.2 in this paper) demonstrate that the degeneration of an anomaly in the case of finite-core vortices, like the discrete vortices, can be described by a linear law. This fact is corroborated by figure 33, which shows time dependencies of the mean front of vortex motion $\langle R_{fr} \rangle$. The averaging was conducted both over the points (over the 10 fluid particles in each layer that are furthest from the initial vortex centre) and over the realizations (10 realizations) for each of the specified values of γ.

6.2. Parametrization problem of vortical heat transfer

Convective temperature anomalies have been shown to play an important part in the heat balance of the ocean [141]. In ocean general circulation models, mesoscale heat transfer is commonly considered to be of the diffusion type (proportional to the local temperature gradient) [217], [65], [160], [140]. In models involving a constant diffusion coefficient, the mean radius of the temperature anomaly increases as $\langle R \rangle \sim t^{1/2}$. In models based on a nonlinear diffusion coefficient proportional to the temperature gradient, the growth of the mean radius is even weaker: $\langle R \rangle \sim t^{1/3}$. As follows from the results discussed in sections 3 and 4, the heton theory and numerical experiments provide convincing evidence of a linear law $\langle R \rangle \sim t$, which leads to more efficient heat transfer than the diffusion law. The problem of constructing a physically based parametrization to take into account the non-diffusive character of heat transport by hetons, has not yet been completely solved [128], [193], [84]. An approach to this problem based on the description of dynamical and statistical processes was proposed in [49], [50] within the context of the equilibrium statistical theory and in [84] within the context of the inequilibrium kinetic theory.

7. Conclusion

The review of publications and the original results given in this paper show that, within a little more than 20 years of its appearance, the theory of localized baroclinic vortices has evolved considerably and contributed to many, sometimes surprising, results. At the same time, this theory has found fields for application in both meteorology and oceanology. The concept of hetons — baroclinic vortices with zero total intensity — has proved to be useful and has enabled the identification of a range of important problems that can be treated completely and coherently within the context of the approximation of quasi-geostrophic discrete and finite-core vortices. This success has been to the physical consistency of the analytical heton theory and the simplicity of its implementation in numerical experiments. The two-layer geostrophic heton model has shown itself to be a basic minimal model that takes into account the baroclinic nature of vortices in a stratified uniformly rotating fluid in its simplest form.

The heton theory provides a basic for the classification of the types of stationary vortex structures in a baroclinic fluid. Tables 1 and 2 synthesize the principal stationary states of heton structures discussed in this paper.

The heton theory, when used within the range of its applications, adequately describes the essentially nonlinear stages in the development of purely baroclinic flows (with a zero barotropic component), which are naturally generated by thermal sources under real geophysical conditions and in laboratory experiments. The model adequately reproduces:

- the vertical and horizontal structure of geophysical fields (temperature and velocity);
- the characteristic dimensions of both individual stable vortex structures and vortex clusters (vortex ensembles);
- decay mechanisms of large vortex formations;
- the types of possible circulation regimes and the principles of their classification;
- asymptotic non-diffusion (ballistic) heat transfer laws.

Table 1. Principal stationary states of vortex structures in a two- layer fluid

Vortex structure type	**Formula and explanation**	**Figure**
Finite-core heton with a vertical axis		1a
Finite-core heton with a tilted axis		1b
Non-compensated discrete two-layer vortex — *(two-tier top)*	(3.5) — angular velocity relative to the centre with coordinates (3.7)	
Common *heton*	(3.9) — translational velocity	2
Three -vortex discrete structures		
tripole	(3.14) — angular velocity	
common roundabout	(3.15) — angular velocity relative to the central vortex ($L > L^{**}$)	3b — left
inverse roundabout	the same formula ($L < L^{**}$)	3b — right
eccentric roundabout	(3.17) — angular velocity	4
stable structure *triton*	(3.20) — dispersion equation, (3.21) — translational velocity	7, 8a
unstable triangular configuration	(3.22) — dispersion equation, ((3.23) — translational velocity	8b
Four-vortex stationary configuration *composite roundabout*		13b
von Kármán heton streets:	Translational velocity	
symmetric	(3.37)	17a, 18a, 18b
antisymmetric	(3.38)	17b, 18c, 18d

Promising directions for research into the generalization of the heton theory involve studying the interaction between vortices and large-scale flows [87], [130], [218], [84], [52], [53], [54], [36], topography [36], [45], [46], [50], [94], [125], [126], [175], [192], shore relief [45], and their interaction in closed basins, as well as problems of solute transport [81], [53]. To apply to studying the effects of differential rotation (even in the case of a homogeneous gradient - beta-plane approximation), however, would require some essential modifications being made to it, mostly because of the need to allow for the radiation of Rossby waves [76], [123], [171]. In the cases where Rossby wave radiation is suppressed (eastward heton spreading), some exact solutions can be obtained for individual hetons [62], [73], [84], [144] and von Kármán heton streets [79].

The concept of a hetonic quartet was introduced by Kizner [106] in relation to the problem of transitions in baroclinic modons [107]. A heton quartet is a two-layer ensemble of four synchronously translating quasi-geostrophic point vortices aligned perpendicularly to the axis of their translation. A hetonic quartet can also be though of as an anti-symmetric pair of hetons with specially fitted parameters, the strengths and separations of the hetons. Kizner [106] provided, a complete analysis of the nonlinear stability of hetonic quartets to antisymmetric perturbations had been provided. Of special interest are the quartets made up of overlapping hetons that are, generally, stable, but are located relatively close to the border of the stability region in the parameter space. An overlapping quartet represents a discrete model of a baroclinic modon with an overlap of the upper and lower vorticity lumps [104], [105]. A hetonic quartets of this type, being subjected to prolonged action of small perturbations, may make a transition to a pair of hetons travelling in opposite directions. After getting rid of the overlap, the stronger heton accelerates and increases its separation. In terms of

Table 2. Principal stationary states in discrete vortex structures in a three-layer fluid

Vortex structure type	**Formula and explanation**	**Figure**
Three-layer hetons:	Translational velocity	
1-modal heton with	(5.2)	28b — left (taking
tilted axis		into account footnote 11)
2-modal heton	(5.3)	28b — right
with an arc-like axis		
Rotating vortex structures	Angular velocity	
three-tier roundabout	(5.4)	
tripole in the upper or lower layer	(5.5)	
tripole in the middle layer	(5.6)	
roundabout, comprising a central	(5.7)	
vortex of the upper (lower) layer		
and satellite vortices in the middle layer		
roundabout, comprising a central	(5.8)	
vortex in the middle layer and satellite		
vortices in the upper (lower) layer		
roundabout, comprising a central	(5.9)	
vortex in the upper (lower) layer		
and satellite		
vortices in the lower (upper) layer		
top comprising vortices in the upper		
and lower layers	(5.10)	
top comprising two upper or	(5.12)	
two lower layers		
Nonmodal heton in the two upper	(5.11) — translational	
or two lower layers	velocity	

modons, this corresponds to the transition to a non-overlapping quasi-elliptical modon state [107], [108]. Kizner [106] discovered some similarity between his hetonic quartets and their transitions, on the one hand, and the finite-core hetons and their break-down considered by Sokolovskiy and Verron [186], on the other. At small separations, a finite-core heton splits up into two smaller baroclinic pairs, whereas at a greater separation, the finite-core heton evolves towards a quasi-stable state. These correspond well with Kizner's results. In fact, small separation between the vorticity patches means their considerable overlap, while a large separation makes the patches less overlapping, i. e. more similar to point-vortex hetons.

The effects of equivalent two-dimensional compressibility of the medium on heton dynamics at scales $\tilde{\lambda} \geqslant L_*$ can be taken into account by rejecting the rigid-lid approximation on the top boundary, which was used in deriving equations (2.1)–(2.2), and replacing it by the free surface condition [71]. In this limit, the barotropic mode is screened and the logarithmic Green function in (2.6) and (5.1) must be changed to $(-1/\pi)K_0(r/L_*)$, where L_* is the Oboukhov scale.

Additional effects of the emergence of cyclonic-anticyclonic asymmetry and the radiation of surface waves by hetons can be examined within the context of the theory of rotating two-layer shallow water [10], [32].

It is worth mentioning in conclusion that, although the quasi-geostrophic motions constitute a considerable part of flows of geophysical nature, the requirement for the Rossby number to be small ($\lambda \ll 1$) is not satisfied universally. In the case of intense vortices $\lambda \sim 1$, a cyclostrophic rather than geostrophic balance can take place. Solutions for localized cyclostrophic vortices are shown in [32], [75], [66], [68].

This review should provide insights into solving these problems of geophysical hydrodynamics.

Acknowledgment. We are grateful to our colleagues: V. F. Kozlov who initiated the study of the dynamics of finite-core hetons; A. V. Borisov and I. S. Mamaev who directed our attention to the study of choreographies; X. Carton, P. A. Davies, J. B. Flór, M. Galmiche, G. S. Golitsyn, V. P. Goncharov, S. K. Gulev, A. Yu. Gurulev, E. Hopfinger, T. R. Kilmatov, Z. I. Kizner, K. V. Koshel, V. V. Kozlov, V. G. Makarov, G. M. Reznik, Yu. B. Sedov, J. Sommeria, G. G. Sutyrin, E. Thivolle-Cazat, S. Valcke, V. Zeitlin, V. V. Zhmur, and V. N. Zyryanov with whom we discussed the questions considered here over several years. VMG has benefitted from continuous collaboration with his co-authors H. Borth, S. D. Danilov, A. A. Dobritsyn, T. N. Doronina, I. I. Mokhov, D. Olbers, M. V. Tevs, and T. Warncke for their creative contribution to the development of the heton theory. MAS' part of the work have been made possible owing to support by RFBR (grants № 01-05-64646, № 04-05-64367) and the management of LEGI CNRS (Grenoble). Participation of MAS and JV was supported also by INTAS/AIRBUS (grant № 04-80-7297) Investigation was conducted within the frames of the European Research Group "Regular and Chaotic Hydrodynamics".

References

[1] K. Alverson. Mechanisms for lateral exchange with oceanic convection sites. *J. Phys. Oceanogr.*, **27** (1997), 1436–1446.

[2] H. Aref. Motion of three vortices. *Phys. Fluids.*, **22** (1979), 393–400.

[3] H. Aref. Point vortex motions with a centre of symmetry. *Phys. Fluids.*, **25** (1982), 2183–2187.

[4] H. Aref. Integrable, chaotic, and turbulent vortex motion in two-dimensional flows. In: *Annual Review of Fluid Mechanics, V. 15.* Annual Reviews, Palo Alto, Calif. 1983, 345–389.

[5] H. Aref. Three-vortex motion with zero total circulation: Addendum. *J. Appl. Math. Phys. (ZAMP)*, **40** (1989), 495–500.

[6] H. Aref. A transformation of the point vortex equations. *Phys. Fluids.*, **14** (2002), 2395–2401.

[7] H. Aref, S. W. Jones, S. Mofina, I. Zawadski. Vortices, kinematics and chaos. *Physica D*, **37** (1989), 423–440.

[8] H. Aref, N. Rott, H. Thomann. Gröbli's solution of the three-vortex problem. In: *Annual Review of Fluid Mechanics, V. 24.* Annual Reviews, Palo Alto, Calif. 1992, 1–20.

[9] H. Aref. Four-vortex motion with zero total circulation and impulse. *Phys. Fluids*, **11** (1999), 3704–3715.

[10] J.-M. Baey, X. Carton. Vortex multipoles in two-layer rotating shallow-water flows. *J. Fluid Mech.*, **460** (2002), 151–175.

[11] G. K. Batchelor. *An introduction to fluid mechanics.* Cambridge University Press, 1967.

[12] L. Bauer, G. K. Morikawa. Stability of rectilinear geostrophic vortices in stationary equilibrium. *Phys. Fluids.*, **19** (1976), 929–942.

[13] S. M. Belotserkovskiy, A. S. Ginevskiy. *Modeling turbulent jets and traces based on discrete vortex method.* Fizmatlit, Moscow, 1995. (In Russian)

[14] E. S. Benilov. Instability of quasi-geostrophic vortices in a two-layer ocean with a thin upper layer. *J. Fluid Mech.*, **475** (2003), 303–331.

[15] E. S. Benilov. The effect of ageostrophy on the stability of thin oceanic vortices. *Dyn. Atmos. Oceans*, **39** (2005), 211–226.

[16] E. S. Benilov. On the stability of oceanic vortices: A solution to the problem? *Dyn. Atmos. Oceans*, **40** (2005), 133–149.

[17] E. S. Benilov, D. Broutman, E. P. Kuznetsova. On the stability of large-amplitude vortices in a continuously stratified fluid on the f-plane. *J. Fluid Mech.*, **355** (1998), 139–162.

[18] V. A. Bogomolov. Vorticity dynamics on a sphere. *Fluid Dynamics*, №6, 1977, 57–65.

[19] V. A. Bogomolov. On motion on a rotating sphere. *Izv. Atmos. Ocean. Phys.*, **21** (1985), 391–396.

[20] A. V. Borisov, I. S. Mamaev. *Poisson structures and Lie algebras in Hamiltonian mechanics.* Izd. Udm. University, Izhevsk, 1999. (In Russian)

[21] A. V. Borisov, I. S. Mamaev. Mathematical methods in the dynamics of vortex structures. In: *Fundamental and Applied Problems in Vortex Theory.* Inst. Comp. Sci., Moscow–Izhevsk, 2003, 17–178. (In Russian)

[22] A. V. Borisov, A. E. Pavlov. Dynamics and statics of vortices on a plane and a sphere. I. *Regul. Chaotic Dyn.*, **3** №1, 1998, 28–39.

[23] A. V. Borisov, V. G. Lebedev. Dynamics of three vortices on a plane and a sphere. II. General compact case. *Regul. Chaotic Dyn.*, **3** №2, 1998, 99–114.

[24] A. V. Borisov, V. G. Lebedev. Dynamics of three vortices on a plane and a sphere. III. Noncompact case. Problem of collapse and scattering. *Regul. Chaotic Dyn.*, **3** №4, 1998, 74–86.

[25] A. V. Borisov, A. V. Bolsinov, I. S. Mamaev. Lie algebras in vortex dynamics and celestial mechanics. IV. *Regul. Chaotic Dyn.*, **4** №1, 1999, 23–50.

[26] B. M. Boubnov, G. S. Golitsyn. Experimental study of convective structure in rotating fluids. *J. Fluid Mech.*, **167** (1986), 503–531.

[27] B. M. Boubnov, G. S. Golitsyn. Temperature and velocity field regimes of convective motions in a rotating plane fluid layer. *J. Fluid Mech.*, **219** (1990), 215–239.

[28] B. M. Boubnov, G. S. Golitsyn. *Convection in Rotating Fluids.* Fluid Mechanics and its Applications, V. 29. Kluwer Academic Publishers, Dordrecht, 1995.

[29] F. P. Bretherton. Critical layer instability in baroclinic flows. *Quart. J. Royal Meteorological Soc.*, **92:393** (1966), 325–334.

[30] D. Brickman. Heat flux partitioning in deep-ocean convection. *J. Phys. Oceanogr.*, **25** (1995), 2609–2623.

[31] G. F. Carnevale, R. C. Kloosterziel. Emergence and evolution of triangular vortices. *J. Fluid Mech.*, **259** (1994), 305–331.

[32] X. Carton. Hydrodynamical modelling of oceanic vortices. *Surveys in Geophys.*, **22** (2001), 179–263.

[33] X. Carton, L. Chérubin, J. Paillet, Y. Morel, A. Serpette, B. Le Cann. Meddy coupling with a deep cyclone in the Gulf of Cadiz. *J. Marine Systems*, **32** (2002), 13–42.

[34] X. J. Carton, G. R. Flierl, L. M. Polvani. The generation of tripoles from unstable axisymmetric isolated vortex structures. *Europhys. Lett.*, **9** (1989), 339–344.

[35] X. J. Carton, B. Legras. The life-cycle of tripoles in two-dimensional incompressible flows. *J. Fluid Mech.*, **267** (1994), 51–82.

[36] C. Cenedese, J. Marshall, J. A. Whitehead. A laboratory model of thermocline depth and exchange fluxes across circumpolar fronts. *J. Phys. Oceanogr.*, **34** (2004), 656–667.

[37] S.-Y. Chao, P.-T. Shaw. Close interactions between two pairs of heton-like vortices under sea ice. *J. Geophys. Res.*, **104** (1999), 23591–23605.

[38] S.-Y. Chao, P.-T. Shaw. Fision of heton-like vortices under sea ice. *J. Oceanogr.*, **55** (1999), 65–78.

[39] S.-Y. Chao, P.-T. Shaw. Slope-enhanced fission of salty hetons under sea ice. *J. Phys. Oceanogr.*, **30** (2000), 2866-2882.

[40] S.-Y. Chao, P.-T. Shaw. Heton shedding from submarine-canyon plumes in an Arctic boundary current system: sensitivity to the undercurrent. *J. Phys. Oceanogr.*, **33** (2003), 2032–2044.

[41] J. G. Charney. Numerical experiments in atmospheric hydrodynamics. In: *Proc. of Symp. in Appl. Math. 'Experimental Arithmetic High Speed Computing and Mathematics'.* Amer. Math. Soc., 1963, 289–310.

[42] A. Cui, R. Street. Large-eddy simulation of turbulent rotating convective flow development. *J. Fluid Mech.*, **447** (2001), 53-84.

[43] S. Danilov, V. Gryanik, D. Olbers. Equilibration and lateral spreading of a strip-shaped convection region. *Alfred–Wegener–Institut für Polar–und Meeresforschung*, Report №86, Marz, 1998.

[44] S. Danilov, V. Gryanik, D. Olbers. Equilibration and lateral spreading of a strip-shaped convection region. *J. Phys. Oceanogr.*, **31** (2001), 1075–1087.

[45] W. K. Dewar. Convection in small basins. *J. Phys. Oceanogr.*, **32** (2002), 2766–2788.

[46] W. K. Dewar. Baroclinic eddy interaction with isolated topography. *J. Phys. Oceanogr.*, **32** (2002), 2789–2805.

[47] M. T. DiBattista, A. J. Majda. An equilibrium statistical model for the spreading phase of open-ocean deep convection. *Proc. Natl. Acad. Sci. USA*, **96** (1999), 6009–6013.

[48] M. T. DiBattista, A. J. Majda. An equilibrium statistical theory for large-scale features of open-ocean deep convection. *J. Phys. Oceanogr.*, **30** (2000), 1325–1353.

[49] M. T. DiBattista, A. J. Majda. Equilibrium statistical predictions for baroclinic vortices: the role of angular momentum. *Theoret. Comput. Fluid Dyn.*, **14** (2001), 293–322.

[50] M. T. DiBattista, A. J. Majda, A. Marshall. A statistical theory for the 'pathiness' of open-ocean deep convection: the effect of preconditioning. *J. Phys. Oceanogr.*, **32** (2002), 599–626.

[51] S. N. Dikarev. On the effect of rotation on the convective structure in a deep homogeneous fluid. *Dokl. Akad. Nauk USSR*, **273** (1983), 718–720.

[52] T. N. Doronina. On the structure of a strong baroclinic vortex in three-dimensional shear flows. *Dokl. Akad. Nauk*, **339** (1994), 528–532.

[53] T. N. Doronina. The structure of circulation cells in intense baroclinic vortices in a current with a velocity shift and the advective transport of a solute. *Izv. Atmos. Ocean. Phys.*, **31** (1995), 223–232.

[54] T. N. Doronina. Interaction of point baroclinic vortices in quasi-geostrophic barotropic and baroclinic shearing motions. *Okeanologiya*, **37** (1997), 506–512.

[55] T. Doronina, V. Gryanik, D. Olbers, T. Warncke. A 3D heton mechanism of lateral spreading in localized convection in a rotating stratified fluid. *Alfred–Wegener–Institut für Polar–und Meeresforschung*, Report №87, Marz, 1998.

[56] B. Eckhardt. Integrable four vortex motion. *Phys. Fluids.*, **31** (1988), 2796–2801.

[57] T. Farid, A. M. Mirza, P. K. Shukla, A. Qamar. Tripolar vortices associated with toroidal ion temperature gradient modes in a magnetoplasma with sheared flows. *Phys. Plasmas*, **8** (2001), 846–849.

[58] H. J. S. Fernando, R. Chen, B. A. Ayotte. Development of a point plume in the presence of background rotation. *Phys. Fluids*, **10** (1998), 2369–2383.

[59] H. J. S. Fernando, R. Chen, D. L. Boyer. Effects of rotation on convective turbulence. *J. Fluid Mech.*, **228** (1991), 513–547.

[60] H. J. S. Fernando, D. C. Smith IV. Vortex structure in geophysical convection. *Eur. J. Mech. B/Fluids*, **20** (2001), 437–470.

[61] M. Flatau, W. H. Schubert, D. E. Stovens. The role of baroclinic processes in tropical cyclone motion: the influence of vertical tilt. *J. Atmos. Sci.*, **51** (1994), 2589–2601.

[62] G. R. Flierl. Isolated eddy models in geophysics. *Ann. Rev. Fluid Mech.*, **19** (1987), 493–530.

[63] G. R. Flierl, V. D. Larichev, J. C. McWilliams, G. M. Reznik. The dynamics of baroclinic and barotropic solitary eddies. *Dyn. Atmos. Oceans*, **5** (1980), 1–41.

[64] M. Galmiche, J. Sommeria, E. Thivolle-Cazat, J. Verron. Data assimilation applied to laboratory experiments in a rotating, stratified fluid. In: *Proceedings of the Moscow International Conference on Fluxes and Structures in Fluids.* 2001, 56–57.

[65] P. Gent, J. McWilliams. Isopycnal mixing in ocean circulation models. *J. Phys. Oceanogr.*, **20** (1990), 150–155.

[66] V. P. Goncharov, V. M. Gryanik, V. I. Pavlov. Venusian 'hot spots': Physical phenomenon and its quantification. *Phys. Rev. E*, **66** (2002), 066304-1–066304-11.

[67] V. P. Goncharov, V. I. Pavlov. *Problems of Fluid Dynamics in a Hamiltonian Description.* Izd. Mosk. Univ., Moscow, 1993. (In Russian)

[68] V. P. Goncharov, V. I. Pavlov. Cyclostrophic vortices in polar regions of rotating planets. *Nonlinear Processes in Geophys.*, **8** (2001), 301–311.

[69] R. W. Griffiths, E. J. Hopfinger. Experiments with baroclinic vortex pairs in a rotating fluid. *J. Fluid Mech.*, **173** (1986), 501–51.

[70] R. W. Griffiths, E. J. Hopfinger. Coalescing of geostrophic vortices. *J. Fluid Mech.*, **178** (1987), 73–97.

[71] V. M. Gryanik. Dynamics of singular geostrophic vortices in a two-layer model of the atmosphere (ocean). *Izv. Atmos. Ocean. Phys.*, **19** (1983), 227–240.

[72] V. M. Gryanik. Dynamics of localized vortical disturbances — 'vortex charges' in a baroclinic fluid. *Izv. Atmos. Ocean. Phys.*, **19** (1983), 467–475.

[73] V. M. Gryanik. Localized vortical disturbances — 'vortex charges' and 'vortex threads' in a baroclinic differentially rotating fluid. *Izv. Atmos. Ocean. Phys.*, **24** (1988), 1251–1261.

[74] V. M. Gryanik. Theoretical models of the dynamics of localized quasi-geostrophic vortices in the atmosphere and ocean. In: *Studying the Vortex Dynamics and Energetics of the Atmosphere and the Problems of Climate.* Gidrometeoizdat, Leningrad, 1990, 31–60. (In Russian)

[75] V. M. Gryanik. On the vortical nature of hot spots in the polar zone of the Venus atmosphere. *Dokl. Akad. Nauk*, **313** (1990), 300–305.

[76] V. M. Gryanik. Rossby wave emission and adaptation of potential vortex fields in the atmosphere (ocean). *Dokl. Akad. Nauk* , **326** (1992), 976–979.

[77] V. M. Gryanik. Vortex dynamics and turbulent lateral heat transport. In: H. Z. Baumert, J. Simpson, J. Sündermann (Eds.). *Marine Turbulence: Theory, Observations, and Models. Results of the CARTUM Project.* Cambridge University Press, 2005, 444–457.

[78] V. M. Gryanik. Vortex dynamics and β-plane turbulence. In: H. Z. Baumert, J. Simpson, J. Sündermann (Eds.). *Marine Turbulence: Theory, Observations, and Models. Results of the CARTUM Project.* Cambridge University Press, 2005, 494–510.

[79] V. M. Gryanik, H. Borth, D. Olbers. The theory of quasigeostrophic von Kármán vortex streets in two-layer fluids on beta-plane and intermittent turbulent jets. *Alfred–Wegener–Institut für Polar–und Meeresforschung*, Report №106, 2001.

[80] V. M. Gryanik, H. Borth, D. Olbers. The theory of quasigeostrophic von Kármán vortex streets in two-layer fluids on beta-plane. *J. Fluid Mech.*, **505** (2004), 23–57.

[81] V. M. Gryanik, T. N. Doronina. Advective transport of a conservative solute by baroclinic singular quasigeostrophic vortices in the atmosphere (ocean). *Izv. Atmos. Ocean. Phys.*, **26** (1990), 1011–1026.

[82] V. M. Gryanik, T. N. Doronina. Interaction between intense baroclinic quasi-geostrophic vortices in currents with a vertical and horizontal shift in velocity. *Izv. Atmos. Ocean. Phys.*, **33** (1997), 171–183.

[83] V. M. Gryanik, T. N. Doronina, I. I. Mokhov, M. V. Tevs. Changes in dimensions of atmospheric vortices under climatic changes. *Izv. Atmos. Ocean. Phys.*, **29** (1993), 596–607.

[84] V. M. Gryanik, T. N. Doronina, D. Olbers, T. H. Warncke, H. Torsten. The theory of three-dimensional hetons and vortex-dominated spreading in localized turbulent convection in a fast rotating stratified fluid. *J. Fluid Mech.*, **423** (2000), 71–125.

[85] V. M. Gryanik, M. A. Sokolovskiy, J. Verron. Dynamics of baroclinic vortices with zero total intensity (hetons). In: *Fundamental and Applied Problems in Vortex Theory.* Inst. Comp. Sci., Moscow–Izhevsk, 2003, 547–622. (In Russian)

[86] V. M. Gryanik, M. V. Tevs. Dynamics of singular geostrophic vortices in an N-layer model of the atmosphere (ocean). *Izv. Atmos. Ocean. Phys.*, **25** (1989), 243–256.

[87] V. M. Gryanik, M. V. Tevs. Dynamics of singular geostrophic vortices near critical points of currents in an N-layer model of the atmosphere (ocean). *Izv. Atmos. Ocean. Phys.*, **27** (1991), 733–745.

[88] V. M. Gryanik, M. V. Tevs. Studying the dynamics and energetics of heton interaction in linearly and exponentially stratified media. *Izv. Atmos. Ocean. Phys.*, **33** (1997), 419–433.

[89] G. J. F. van Heijst. Topography effects on vortices in a rotating fluid. *Meccanica*, **29** (1994), 431–451.

[90] G. J. F. van Heijst, R. C. Kloosterziel. Tripolar vortices in a rotating fluid. *Nature*, **338** (1989), 569–571.

[91] G. J. F. van Heijst, R. C. Kloosterziel, C. W. M. Williams. Laboratory experiments on the tripolar vortex in a rotating fluid. *J. Fluid Mech.*, **225** (1991), 301–331.

[92] K. R. Helfrich, T. M. Battisti. Experiments on baroclinic vortex shedding from hydrothermal plumes. *J. Geophys. Res.*, **96** (1991), 12511–12518.

[93] K. R. Helfrich, U. Send. Finite-amplitude evolution of two-layer geostrophic vortices. *J. Fluid Mech.*, **197** (1988), 331–348.

[94] S. Herbette, Y. Morel, M. Arhan. Erosion of a surface vortex by a seamount. *J. Phys. Oceanogr.*, **33** (2003), 1664–1679.

[95] J. S. Hesthaven, J. P. Lynov, J. J. Rasmussen, G. G. Sutyrin. Generation of tripolar vortical structures on the beta plane. *Phys. Fluids.*, **A5** (1993), 1674–1678.

[96] N. G. Hogg, H. M. Stommel. The heton, an elementary interaction between discrete baroclinic geostrophic vortices, and its implications concerning eddy heat-flow. *R. Soc. Lond.*, **A397** (1985), 1–20.

[97] N. G. Hogg, H. M. Stommel. Hetonic explosions: the breakup and spread of warm pools as explained by baroclinic point vortices. *J. Atmos. Sci.*, **42** (1985), 1465–1476.

[98] N. G. Hogg, H. M. Stommel. How currents in the upper thermocline could advect meddies deeper down. *Deep-Sea Res.*, **37** (1990), 613–623.

[99] E. J. Hopfinger, G. J. F. van Heijst. Vortices in rotating fluids. In: *Annual Review of Fluid Mechanics, V. 25.* Annual Reviews, Palo Alto, Calif. 1993, 241–289.

[100] M. Ikeda. Instability and splitting of mesoscale rings using a two-layer quasi-geostrophic model on an f-plane. *J. Phys. Oceanogr.*, **11** (1981), 987—998.

[101] G. N. Ivey, J. R. Taylor, M. J. Coates. Convectively driven mixed layer growth in a rotating, stratified fluid. *Deep-Sea Res.*, **42** (1995), 331–349.

[102] V. M. Kamenkovich, M. N. Koshlyakov, A. S. Monin. *Synoptic Vortices in the Ocean.* Gidrometeoizdat, Leningrad. 1987. (In Russian)

[103] R. Khvoles, D. Berson, Z. Kizner. The structure and evolution of elliptical barotropic modons. *J. Fluid Mech.*, **530** (2005), 1–30.

[104] Z. I. Kizner. Rossby solitons with axially symmetric baroclinic modes. *Dokl. Akad. Nauk USSR*, **275** (1984), 1495–1498.

[105] Z. I. Kizner. Solitary Rossby waves with baroclinic modes. *J. Mar. Res.*, **55** (1997), 671–685.

[106] Z. Kizner. Stability and transitions of hetonic quartets and baroclinic modons. *Phys. Fluids*, **18** (2006), 056601-1–056601-12.

[107] Z. Kizner, D. Berson, R. Khvoles. Baroclinic modon equilibria on the beta-plane: stability and transitions. *J. Fluid Mech.*, **468** (2002), 239–270.

[108] Z. Kizner, D. Berson, R. Khvoles. Noncircular baroclinic beta-plane modons: Constructing stationary solutions. *J. Fluid Mech.*, **489** (2003), 199–228.

[109] Z. Kizner, R. Khvoles. The tripole vortex: Experimental evidence and explicit solutions. *Phys. Rev.*, **E70** (2004), 016307-1–016307-4.

[110] Z. Kizner, R. Khvoles. Two variations on the theme of Lamb–Chaplygin: Supersmooth dipole and rotating multipoles. *Regul. Chaotic Dyn.*, **9** (2004), 509–518.

[111] B. A. Klinger. Baroclinic eddy generation at a sharp corner in a rotating system. *J. Geophys. Res.*, **99** (1994), 12515–12531.

[112] B. A. Klinger, J. Marshall. Regimes and scaling laws for rotating deep convection in the ocean. *Dyn. Atmos. Oceans*, **21** (1995), 227–256.

[113] N. E. Kochin, I. A. Kibel', N. V. Roze. *Theoretical Hydrodynamics. Part 1.* Fizmatgiz, Moscow, 1963. (In Russian)

[114] J. Koiller, S. P. Carvalho, R. R. Silva, L. C. G. Oliveira. On Aref's vortex motions with a symmetry centre. *Physica D*, **16** (1985), 27–61.

[115] V. F. Kozlov. Construction of a numerical model of geostrophic vortex evolution in a baroclinic fluid based on the contour dynamic method. *Izv. Atmos. Ocean. Phys.*, **21** (1985), 211–213.

[116] V. F. Kozlov. Model of interaction between elliptical vortex patches taking into account the involvement effects. *Izv. Atmos. Ocean. Phys.*, **29** (1993), 98–105.

[117] V. F. Kozlov. Geophysical hydrodynamics of vortex patches. *Marine Hidophysical Journal*, №1, 1994, 26–35.

[118] V. F. Kozlov, I. V. Mazur. On a formation model of intra-thermocline vortices in the ocean. *Meteorology & Hidrology*, №8, 1986, 83–88.

[119] V. F. Kozlov, V. G. Makarov, M. A. Sokolovskiy. A numerical model of baroclinic instability of axially symmetric vortices in a two-layer ocean. *Izv. Atmos. Ocean. Phys.*, **22** (1986), 868–874.

[120] V. V. Kozlov. *General Theory of Vortices.* Izd. Udmurt Univ., Izhevsk, 1999. (In Russian) English transl.: Encyclopaedia of Mathematical Sciences, V. 67. Springer, New York, 2003.

[121] L. G. Kurakin, V. I. Yudovich. On nonlinear stability of steady rotation of a regular vortex polygon. *Dokl. Akad. Nauk*, **384** (2002), 476–482. English transl.: *Dokl. Phys.*, **47** (2002), 465–470.

[122] L. G. Kurakin, V. I. Yudovich. The stability of stationary rotation of a regular vortex polygon. *Chaos*, **12** (2002), 574–595.

[123] M. V. Kurganskiy. On the motion of a pair of vortices on the beta-plane. In: *Studying the Vortex Dynamics and Energetics of the Atmosphere and the Problems of Climate.* Gidrometeoizdat, Leningrad, 1990, 123–130. (In Russian)

[124] M. V. Kurganskiy, M. S. Tatarskaya. Application of the notion of potential vortex in meteorology. *Izv. Atmos. Ocean. Phys.*, **23** (1987), 787–814.

[125] E. Kvaleberg, S. L. Morey, J. J. O'Brien. Frontogenesis and subsequent formation of cold filaments and eddies on an idealized shelf. *OCEANS*, 2003. www.coaps.fsu.edu/morey/GoM/kvaleberg761.pdf

[126] J. H. LaCasce. A geostrophic vortex over a slope. *J. Phys. Oceanogr.*, **28** (1998), 2362–238.

[127] G. Lamb. *Hydrodynamics*. 6th ed. Cambridge University Press, 1932.

[128] S. Legg, H. Jones, M. Visbeck. A heton perspective of baroclinic eddy transfer in localized open ocean convection. *J. Phys. Oceanogr.*, **26** (1996), 2251–2266.

[129] S. Legg, J. Marshall. A heton model of the spreading phase of open-ocean deep convection. *J. Phys. Oceanogr.*, **23** (1993), 1040–1056.

[130] S. Legg, J. Marshall. The influence of the ambient flow on the spreading of convected water masses. *J. Marine Res.*, **56** (1998), 107–139.

[131] S. Legg, J. Marshall. Temperature and salinity variability in heterogeneous oceanic convection. *J. Phys. Oceanogr.*, **30** (2000), 1188–1206.

[132] S. Legg, J. C. McWilliams. Convective modifications of a geostrophic eddy field. *J. Phys. Oceanogr.*, **31** (2001), 874–891.

[133] S. Legg, J. C. McWilliams, J. Gao. Localization of deep ocean convection by a mesoscale eddy. *J. Phys. Oceanogr.*, **28** (1998), 944–970.

[134] B. Legras, D. G. Dritschel. A comparison of the contour surgery and pseudo-spectral method. *J. Comput Phys.*, **104** (1993), 287–302.

[135] J. M. Lilly, P. B. Rhines, M. Visbeck, R. Davis, J. R. N. Lazier, F. Schott, D. Farmer. Observing deep convection in the Labrador Sea during winter 1994/95. *J. Phys. Oceanogr.*, **29** (1999), 2065–2098.

[136] C. C. Lim, A. J. Majda. Point vortex dynamics for coupled surface/interior QG and propagating heton clusters in models for ocean convection. *Geophys. Astrophys. Fluid Dyn.*, **94** (2001), 177–220.

[137] S.-J. Lin. Contour dynamics of tornado-like vortices. *J. Atmos. Sci.*, **49** (1992), 1745–1756.

[138] V. G. Makarov. Numerical modelling of formation of three-polar vortices by the contour dynamic method. *Izv. Atmos. Ocean. Phys.*, **32** (1996), 46–55.

[139] J. S. Marshall. Chaotic oscillations and breakup of quasigeostrophic vortices in the N-layer approximation. *Phys. Fluids*, **7** (1995), 983–992.

[140] J. S. Marshall, B. Parthasarathy. Tearing of an aligned vortex by a current difference in two-layer quasi-geostrophic flow. *J. Fluid Mech.*, **225** (1993), 157–182.

[141] J. Marshall, F. Schott. Open-ocean convection: observation, theory, and models. *Rev. Geophys*, **37** (1999), 1–64.

[142] R. P. Matano, E. J. Beier. On the mesoscale dynamics of the Indian/Atlantic interocean exchange. American Geophysical Union, Fall Meeting, 2002.

[143] T. Maxworthy, S. Narimousa. Unsteady, turbulent convection into a homogeneous rotating fluid, with oceanographic applications. *J. Phys. Oceanogr.*, **24** (1994), 865-887.

[144] N. R. McDonald. The interaction of two baroclinic geostrophic vortices on the β-plane. *R. Soc. Lond. Proc. Ser. A Math. Phys. Eng. Sci.*, **456** (2000), 1029–1049.

[145] J. C. McWilliams, J. B. Weiss, I. Yavneh. The vortices of homogeneous geostrophic turbulence. *J. Fluid Mech.*, **401** (1993), 1–26.

[146] S. P. Meacham, K. K. Pankratov, A. F. Shchepetkin, V. V. Zhmur. The interaction of ellipsoidal vortices with background shear flows in a stratified fluid. *Dyn. Atmos. Oceans*, **21** (1994), 167–212.

[147] V. V. Meleshko, G. J. F. van Heijst. Interaction of two-dimensional vortex structures: Point vortices, contour kinematics and stirring properties. *Chaos, Solitons & Fractals*, **4** (1994), 977–1010.

[148] V. V. Meleshko, M. Yu. Konstantinov. *Dynamics of Vortex Structures*. Naukova Dumka, Kiev, 1993.

[149] I. I. Mokhov, T. N. Doronina, V. M. Gryanik, R. R. Khairullin, L. V. Korovkina, V. E. Lagun, O. I. Mokhov, E. P. Naumov, V. K. Petukhov, A. O. Senatorsky, M. V. Tevs. Extratropical cyclones and anticyclones: Tendencies of change. In: S. Gronas, M. A. Shapiro (Eds.). *The Life of Extratropical Cyclones. V. 2*. Geophysical Institute, University of Bergen, Bergen, Norway, 1994, 56–60.

[150] I. I. Mokhov, V. M. Gryanik, T. N. Doronina, V. E. Lagun, O. I. Mokhov, E. P. Naumov, V. K. Petukhov, M. V. Tevs, R. R. Khairullin. Vortex activity in the atmosphere: tendencies of changes. Institute of Atmospheric Physics of RAS, Moscow. Preprint №2, 1993.

[151] A. S. Monin. *Weather Forecast As a Physical Problem*. Nauka, Moscow, 1969.

[152] Y. G. Morel, X. J. Carton. Multipolar vortices in two-dimensional incompressible flows. *J. Fluid Mech.*, **267** (1994), 23–51.

[153] Y. Morel, J. McWilliams. Evolution of isolated interior vortices in the ocean. *J. Phys. Oceanogr.*, **27** (1997), 727–748.

[154] Y. Morel, J. McWilliams. Effects of isopycnal and diapycnal mixing on the stability of oceanic currents. *J. Phys. Oceanogr.*, **31** (2001), 2280–2296.

[155] G. K. Morikawa, E. V. Swenson. Interacting motion of rectilinear geostrophic vortices. *Phys. Fluids*, **14** (1971), 1058–1073.

[156] S. Narimousa. Turbulent convection into a linear stratified fluid: the generation of 'subsurface anticyclones'. *J. Fluid Mech.*, **354** (1998), 101–121.

[157] P. K. Newton. *The N-Vortex Problem: Analytical Techniques*. Applied Mathematical Sciences, V. 145. Springer, Berlin, 2001.

[158] E. A. Novikov. Dynamics and statistics of a vortex system. *Soviet Phys. JETP*, **68** (1975), 1868–1882.

[159] E. A. Novikov, Yu. B. Sedov. Stochastic properties of a four-vortex system. *Soviet Phys. JETP*, **75** (1978), 868–876.

[160] D. Olbers, J.-O. Wolff, C. Volker. Eddy fluxes and second-order moment balances for non-homogeneous quasigeostrophic turbulence in wind-driven zonal flows. *J. Phys. Oceanogr.*, **30** (2000), 1645–1668.

[161] A. Okamoto, K. Hara, K. Nagaoka, S. Yoshimura, J. Vranješ, M. Kono, M. Y. Tanaka. Experimental observation of a tripolar vortex in a plasma. *Phys. Plasmas*, **10** (2003), 2211–2216.

[162] P. Orlandi, G. F. van Heijst. Numerical simulation of tripolar vortices in 2D flow. *Fluid Dyn. Res.*, **9** (1992), 179–206.

[163] P. Orlandi, G. F. Carnevale. Evolution of isolated vortices in a rotating fluid of finite depth. *J. Fluid Mech.*, **381** (1999), 239–269.

[164] J. Paillet, B. Le Cann, X. Carton, Y. Morel, A. Serpette. Dynamics and evolution of a northern meddy. *J. Phys. Oceanogr.*, **32** (2002), 55–79.

[165] L.-L. Pan. Observed positive feedback the NOA and North Atlantic SSTA tripole. *Geophys. Res. Lett.*, **32** (2005), L06707, 1-4.

[166] J. Pedlosky. The instability of continuous heton clouds. *J. Atmos. Sci.*, **42** (1985), 1477–1486.

[167] J. Pedlosky. Geophysical Fluid Dynamics. 2nd ed. Springer, New York, 1987.

[168] H. Poincaré. *Théorie des tourbillons*. Gauthier-Villars, Paris, 1893.

[169] J. M. Pringle. Cross-shelf eddy heat transport in a wind-free coastal ocean undergoing winter time cooling. *J. Jeophys. Res.*, **106** (2001), 2589–2604.

[170] D. I. Pullin. Contour dynamics method. *Annu. Rev. Fluid Mech.*, **24** (1992), 89–115.

[171] G. M. Reznik, R. H. J. Grimshaw, K. Sriskanderejan. On basic mechanisms governing two-layer vortices on a beta-plane. *Geophys. Astrophys. Fluid Dyn.*, **86** (1997), 1–42.

[172] N. Rott. Three-vortex motion with zero total circulation. *J. Appl. Math. Phys. (ZAMP)*, **40** (1989), 473–494.

[173] N. Rott. Constrained three- and four-vortex problems. *Phys. Fluids*, **2** (1990), 1477–1480.

[174] P. G. Saffman. *Vortex Dynamics*. Cambridge University Press, 1992.

[175] N. Serra, S. Sadoux, I. Ambar, D. Renouard. Observations and laboratory modeling of meddy generation at cape St. Vincent. *J. Phys. Oceanogr.*, **32** (2002), 3–25.

[176] T. G. Shepherd. Symmetries, conservation laws, and Hamiltonian structure in geophysical fluid dynamics. *Advances in Geophys.*, **32** (1990), 287–338.

[177] K. Shimada, A. Kubokawa. Nonlinear evolution of linearly unstable barotropic boundary current. *J. Phys. Oceanogr.*, **27** (1997), 1326–1348.

[178] C. Simó. New families of solutions to the N-body problems. In: *Proc. European Congress of Mathematics, Vol. I (Barcelona, 2000)*. Progr. Math., V. 201. Birkhäuser, Basel, 2000, 101–115.

[179] D. A. Smeed. Baroclinic instability of three-layer flows. Part 1. Linear stability. *J. Fluid Mech.*, **194** (1988), 217–231.

[180] D. A. Smeed. Baroclinic instability of three-layer flows. Part 2. Experiments with eddies. *J. Fluid Mech.*, **194** (1988), 233–259.

[181] M. A. Sokolovskiy. On the head-on collision of distributed hetons. *Dokl. Akad. Nauk USSR*, **306** (1989), 198–202. English transl.: *Dokl. Phys.*, **306** (1989), 215–217.

[182] M. A. Sokolovskiy. Numerical modelling of interaction between distributed hetons at head-on collision. In: *Contour dynamics method in oceanological studies*. Pacific Oceanological Institute. Far-East Division of RAS, Vladivostok, 199, 40–57. (In Russian)

[183] M. A. Sokolovskiy. Modeling three-layer vortex motions in the ocean by the contour dynamics method. *Izv. Atmos. Ocean. Phys.*, **27** (1991), 550–562.

[184] M. A. Sokolovskiy. Stability of an axisymmetric three-layer vortex. *Izv. Atmos. Ocean. Phys.*, **33** (1997), 16–26.

[185] M. A. Sokolovskiy. Stability analysis of the axisymmetric three-layered vortex using contour dynamics method. *Comput. Fluid Dyn. Journal.*, **6** (1997), 133–156.

[186] M. A. Sokolovskiy, J. Verron. Finite-core hetons: Stability and interactions. *J. Fluid Mech.*, **423** (2000), 127–154.

[187] M. A. Sokolovskiy, J. Verron. Four-vortex motion in the two layer approximation: Integrable case. *Regul. Chaotic Dyn.*, **5** (2000), 413–436.

[188] M. A. Sokolovskiy, J. Verron. New stationary solutions of the three-vortex problem in a two-layer fluid. *Dokl. Akad. Nauk*, **383** (2002), 61–66. English transl.: *Dokl. Phys.*, **47** (2002), 233–237 .

[189] M. A. Sokolovskiy, J. Verron. Dynamics of the triangular two-layer vortex structures with zero total intensity. *Regul. Chaotic Dyn.*, **7** (2002), 435–472.

[190] M. A. Sokolovskiy, J. Verron. Dynamics of the three vortices in a two-layer rotating fluid. *Regul. Chaotic Dyn.*, **9** (2004), 417–438.

[191] M. A. Sokolovskiy, J. Verron. Some properties of motion of $A + 1$ vortices in a two-layer rotating fluid. *Russian Scientific Journal of Nonlinear Dynamics*, **2** (2006), 27–54. (In Russian)

[192] M. A. Sokolovskiy, J. Verron, I. M. Vagina. Effect of a submerged small-height obstacle on the dynamics of a distributed heton. *Izv. Atmos. Ocean. Phys.*, **37** (2001), 131–143.

[193] M. A. Spall, D. C. Chapman. On the efficiency of baroclinic eddy heat transport across narrow fronts. *J. Phys. Oceanogr.*, **28** (1998), 2275–2287.

[194] E. L. Steffen, E. A. D'Asaro. Deep convection in the Labrador Sea as observed by Lagrangian floats. *J. Phys. Oceanogr.*, **32** (2002), 475–492.

[195] M. E. Stern. Minimal properties of planetary eddies. *J. Marine Res.*, **33** (1975), 1–13.

[196] F. Straneo, M. Kawase. Comparisons of localized convection due to localized forcing and to preconditioning. *J. Phys. Oceanogr.*, **29** (1999), 55–68.

[197] G. G. Sutyrin, J. McWilliams, R. Saravanan. Corotating stationary states and vertical alignment of geostrophic vortices with thin core. *J. Fluid Mech.*, **357** (1998), 321–349.

[198] J. Takahashi, A. Masuda. Mechanism of southward translation of meddies. *J. Oceanography.*, **54** (1998), 669–680.

[199] M. V. Tevs. A kinematic study of the vertical structure of tropic cyclones based on an N-level quasi-geostrophic atmospheric model. *Izv. Atmos. Ocean. Phys.*, **35** (1999), 481–486.

[200] E. Thivolle-Cazat, J. Sommeria, M. Galmiche, J. Verron. An experimental investigation of heton instability in a rotating, two-layer fluid. In: *Proceedings of the Moscow International Conference on Fluxes and Structures in Fluids.* 2001, 205-206.

[201] E. Thivolle-Cazat, J. Sommeria, M. Galmiche. Baroclinic instability of two-layer vortices in laboratory experiments. *J. Fluid Mech.*, **544** (2005), 69–97.

[202] A. M. Treguier, O. Boebel, B. Barnier, G. Madec. Agulhas eddy fluxes in a $1/6^\circ$Atlantic model. *Deep-Sea Res. II*, **50** (2000), 251–280.

[203] S. Valcke, J. Verron. On interactions between two finite-core hetons. *Phys. Fluids*, **A5** (1993), 2058–2060.

[204] S. Valcke, J. Verron. Interaction of baroclinic isolated vortices: The dominant effect of shielding. *J. Phys. Oceanogr.*, **23** (1993), 1346–1362.

[205] S. Valcke, J. Verron. Cyclon-anticyclon asymmetry in the merging process. *Dyn. Atmos. Oceans.*, **24** (1996), 227–236.

[206] F. Vandermeirsch, Y. Morel, G. Sutyrin. The net advective effect of a vertically sheared current on a coherent vortex. *J. Phys. Oceanogr.*, **31** (2001), 2210-2225.

[207] F. Vandermeirsch, Y. Morel, G. Sutyrin. Resistance of a coherent vortex to a vertical shear. *J. Phys. Oceanogr.*, **32** (2002), 3089-3100.

[208] O. U. Velasco Fuentes, G. J. F. van Heijst, N. P. M. van Lipzing. Unsteady behaviour of a topography-modulated tripole. *J. Fluid Mech.*, **307** (1996), 11–41.

[209] J. Verron, E. J. Hopfinger, J. C. McWilliams. Sensitivity to initial conditions in the merging of two-layer baroclinic vortices. *Phys. Fluids.*, **A2** (1990), 886–889.

[210] J. Verron, S. Valcke. Scale-dependent merging of baroclinic vortices. *J. Fluid Mech.*, **264** (1994), 81–106.

[211] R. Verzicco, P. Orlandi. A finite-difference scheme for three-dimensional incompressible flow in cylindrical coordinates. *J. Comput. Phys.*, **123** (1996), 402–414.

[212] J. Vranješ. Tripolar vortex in plasma flow. *Planetary and Space Sci.*, **47** (1999), 1531–1535.

[213] J. Vranješ, G. Marić, P. K. Shukla. Tripolar vortices and vortex chains in dusty plasma. *Phys. Lett. A*, **258** (1999), 317–322.

[214] J. Vranješ, P. K. Shukla, M. Kono, S. Poedts. Linear and nonlinear electrostatic modes in a nonuniform magnetized electron plasma. *Phys. Plasmas*, **8** (2001), 3165–3176.

[215] J. Vranješ, L. Stenflo, P. K. Shukla. Tripolar vortices and chains in a shallow atmosphere. *Phys. Lett. A*, **267** (2000), 184–187.

[216] J. Vranješ, A. Okamoto, S. Yoshimura, S. Poedts, M. Kono, M. Y. Tanaka. Analytical description of a neutral-induces tripole vortex in a plasma. *Phys. Rev. Let.*, **86** (2002), 265002-1–265002-4.

[217] D. Walsh, L. J. Pratt. The interaction of a pair of point potential vortices in uniform shear. *Dyn. Atmos. Oceans*, **22** (1995), 135–160.

[218] J. A. Whitehead, J. Marshall, G. E. Hufford. ocalized convection in a rotating stratified fluid. *J. Geophys. Res.*, **101** (1996), 25705–25721.

[219] W. R. Young. Some interactions between small numbers of baroclinic, geostrophic vortices. *Geophys. Astrophys. Fluid Dyn.*, **33** (1985), 35–61.

[220] N. J. Zabusky, M. H. Hughes, K. V. Roberts. Contour dynamics for the Euler equations in two dimensions. *J. Comput. Phys.*, **30** (1979), 96–106.

[221] V. V. Zhmur, K. K. Pankratov. Dynamics of a semi-ellipsoidal near-surface vortex in a heterogeneous current. *Okeanologiya*, **29** (1989), 205–211.

[222] V. V. Zhmur, K. K. Pankratov. Long-range interaction of an ensemble of quasi-geostrophic vortices. Hamiltonian formulation. *Izv. Atmos. Ocean. Phys.*, **26** (1990), 972–981.

[223] V. V. Zhmur, A. F. Shchepetkin. Evolution of an ellipsoidal vortex in a stratified ocean in the f-plane approximation. *Izv. Atmos. Ocean. Phys.*, **27** (1991), 492–503.

[224] V. V. Zhmur, A. F. Shchepetkin. Interaction between two quasi-geostrophic baroclinic vortices: a tendency toward approaching and merging. *Izv. Atmos. Ocean. Phys.*, **28** (1992), 538–551.

[225] S. L. Ziglin. Non-integrability of the four point vortex motion problem. *Dokl. Akad. Nauk SSSR*, **250** (1980), 1296–1300.